ADRIANA MIRALLES SCHLEDER

Quantitative dispersion analysis of leakages of flammable and/or toxic substances on environments with barriers or semi-confined

São Paulo
2015

ADRIANA MIRALLES SCHLEDER

Quantitative dispersion analysis of leakages of flammable and/or toxic substances on environments with barriers or semi-confined

A dissertation submitted in partial fulfilment of the requirements for the degree of DOCTOR OF PHILOSOPHY (PhD) for the Polytechnic School of University of São Paulo and the Universitat Politècnica de Catalunya.

USP concentration area:
Naval Architecture and Ocean Engineering
UPC Doctoral Program:
Chemical Processes Engineering

Supervisors:
Dr. Prof. Marcelo Ramos Martins
Dr. Prof. Elsa Pastor Ferrer

São Paulo
2015

Acknowledgements

First, I would like to express my deep gratitude to my supervisors Professors Marcelo Ramos Martins and Elsa Pastor Ferrer, both worked very hard to make this thesis and many other projects possible in a short time. Prof. Marcelo is more than a supervisor, he is a valuable friend over so many years of guidance, patience and dedication. Prof. Elsa, my other dear supervisor, became much more than a supervisor turned into a true friend. I have had the luck of having two supervisors and finding a friend in each one. Thank you so much my friends.

To Professor Eulàlia Planas Cuchi who opened the doors of CERTEC at UPC for me and this way allowed me to spend one of the best periods of my life in Barcelona. I express my sincerest gratitude at both academic and personal levels.

I would also like to express my deep appreciation to Joaquim Rocha dos Santos for constant support.

To Professor Moyses Szajnbok for always having a word of encouragement to offer.

To Professors Paulo Fernando Ferreira Frutuoso e Melo and Carlos Krieger Filho Guenther who provided valuable guidance throughout the development of this study.

To Professors Gilberto FM Souza, Enrique Andrés López Droguett and Joaquim Casal Fàbrega.

To all my friends at LabRisco and at CERTEC, who made this journey so much more enjoyable. Especially to Diana Tarragó, Oriol Rios and Miguel Muñoz for their help and expertise during the design and performance of the field tests and during all the time that I spent at CERTEC.

My sincere thanks to dear Lânia Camilo de Oliveira and dear Irene Perez who helped me so much in the execution of all procedures required during this period. I could not do it without their help.

I also wish to thank the personnel of Can Padró Security and Safety training site where the field tests were conducted.

And most important I would like to express my deepest gratitude to my brothers, who have been with me and supported me in every minute.

To the National Council for Scientific and Technological Development - Brazil CNPq, and to the Program for Development of Human Resources (PRH19) from Petrobras and Brazilian National Petroleum, Natural Gas and Biofuels Agency (ANP) by the financial support.

To the São Paulo Research Foundation (FAPESP), by the financial support (R&D project grant 2013/18218-2).

Abstract

With the industrial and technological development of the present-day society, the presence of flammable and toxic substances has increased in a growing number of activities. Dispersion of hazardous gas releases occurring in transportation or storage installations represent a major threat to health and environment. Therefore, forecasting the behaviour of a flammable or toxic cloud is a critical challenge in quantitative risk analysis. The main aim of this dissertation has been to provide new insights that can help technological risks analysts when dealing with complex dispersion modelling problems, particularly those problems involving dispersion scenarios with barriers or semi-confined.

A literature survey has shown that, traditionally, empirical and integral models have been used to analyse dispersion of toxic/flammable substances, providing fast estimations and usually reliable results when describing simple scenarios (e.g. unobstructed gas flows over flat terrain). In recent years, however, the use of CFD tools for simulating dispersion accidents has significantly increased, as they allow modelling more complicated gas dispersion scenarios, like those occurring in complex topographies, semi-confined spaces or with the presence of physical barriers. Among all the available CFD tools, FLACS® software is envisaged to have high performance when simulating dispersion scenarios, but, as other codes alike, still needs to be fully validated.

This work contributes to the validation of FLACS software for dispersion analysis. After a literature review on historical field tests, some of them have been selected to undertake a preliminary FLACS performance examination, inspecting all possible sources of uncertainties in terms of reproducibility capacity, grid dependence and sensitivity analysis of input variables and simulation parameters. The main outcomes of preliminary FLACS investigations have been shaped as practical guiding principles to be used by risk analysts when performing dispersion analysis with the presence of barriers using CFD tools.

Although the literature survey has shown some experimental data available, none of the works include detailed exercises giving new insights of how to perform accurate CFD simulations nor giving precise rates of FLACS performance. Therefore, new experiments have been performed in order to offer new sets of cloud dispersion data for comprehensive validation studies. Propane cloud dispersion field tests (unobstructed and with the presence of

a fence obstructing the flow) have been designed and undertaken at Can Padró Security and Safety training site (Barcelona) by which intensive data on concentration has been acquired. Four tests were performed, consisting on releases up to 0.5 kg/s of propane during 40 seconds in a discharge area of 700 m^2.

The field tests have contributed to the reassessment of the critical points raised in the guiding principles and have provided experimental data to be used by the international community for dispersion studies and models validation exercises.

FLACS software has been challenged against the experimental data collected during the field tests. In general terms, the CFD-based simulator has shown good performance when simulating cloud concentration. FLACS reproduces successfully the presence of complex geometry and its effects on cloud dispersion, showing realistic concentration decreases due to cloud dispersion obstruction by the existence of a fence. However, simulated clouds have not represented the whole complex accumulation dynamics due to wind variation, since they have diluted faster than experimental clouds.

Keywords: dispersion, dense gas, field tests, computational fluid dynamics, FLACS software.

Resumo

Com o atual desenvolvimento industrial e tecnológico da sociedade, a presença de substâncias inflamáveis e/ou tóxicas aumentou significativamente em um grande número de atividades. A possível dispersão de gases perigosos em instalações de armazenamento ou em operações de transporte representam uma grande ameaça à saúde e ao meio ambiente. Portanto, a caracterização de uma nuvem inflamável e/ou tóxica é um ponto crítico na análise quantitativa de riscos. O objetivo principal desta tese foi fornecer novas perspectivas que pudessem auxiliar analistas de risco envolvidos na análise de dispersões em cenários complexos, por exemplo, cenários com barreiras ou semi-confinados.

A revisão bibliográfica mostrou que, tradicionalmente, modelos empíricos e integrais são usados na análise de dispersão de substâncias tóxicas / inflamáveis, fornecendo estimativas rápidas e geralmente confiáveis ao descrever cenários simples (por exemplo, dispersão em ambientes sem obstruções sobre terreno plano). No entanto, recentemente, o uso de ferramentas de CFD para simular dispersões aumentou de forma significativa. Estas ferramentas permitem modelar cenários mais complexos, como os que ocorrem em espaços semi-confinados ou com a presença de barreiras físicas. Entre todas as ferramentas CFD disponíveis, consta na bibliografia que o software FLACS® tem bom desempenho na simulação destes cenários. Porém, como outras ferramentas similares, ainda precisa ser totalmente validado.

Após a revisão bibliográfica sobre testes de campo já executados ao longo dos anos, alguns testes foram selecionados para realização de um exame preliminar de desempenho da ferramenta CFD utilizado neste estudo. Foram investigadas as possíveis fontes de incertezas em termos de capacidade de reprodutibilidade, de dependência de malha e análise de sensibilidade das variáveis de entrada e parâmetros de simulação. Os principais resultados desta fase foram moldados como princípios práticos a serem utilizados por analistas de risco ao realizar análise de dispersão com a presença de barreiras utilizando ferramentas CFD.

Embora a revisão bibliográfica tenha mostrado alguns dados experimentais disponíveis na literatura, nenhuma das fontes encontradas incluem estudos detalhados sobre como realizar simulações de CFD precisas nem fornecem indicadores precisos de desempenho. Portanto, novos testes de campo foram realizados a fim de oferecer novos dados para estudos de validação mais abrangentes. Testes de campo de dispersão de nuvem de propano (com e sem

a presença de barreiras obstruindo o fluxo) foram realizados no campo de treinamento da empresa Can Padró Segurança e Proteção (em Barcelona). Quatro testes foram realizados, consistindo em liberações de propano com vazões de até 0,5 kg/s, com duração de 40 segundos em uma área de descarga de 700 m^2. Os testes de campo contribuíram para a reavaliação dos pontos críticos mapeados durante as primeiras fases deste estudo e forneceram dados experimentais para serem utilizados pela comunidade internacional no estudo de dispersão e validação de modelos.

Simulações feitas utilizando-se a ferramenta CFD foram comparadas com os dados experimentais obtidos nos testes de campo. Em termos gerais, o simulador mostrou bom desempenho em relação às taxas de concentração da nuvem. O simulador reproduziu com sucesso a geometria complexa e seus efeitos sobre a dispersão da nuvem, mostrando claramente o efeito da barreira na distribuição das concentrações. No entanto, as simulações não foram capazes de representar toda a dinâmica da dispersão no que concerne aos efeitos da variação do vento, uma vez que as nuvens simuladas diluíram mais rapidamente do que nuvens experimentais.

Palavras chaves: dispersão, gás denso, testes de campo, dinâmica dos fluidos computacional, FLACS software.

Resum

Amb el desenvolupament industrial i tecnològic de la societat actual, la presència de productes tòxics i inflamables s'ha vist incrementada àmpliament en diferents sectors. La dispersió de fuites de substàncies perilloses que poden tenir lloc durant el transport o emmagatzematge d'aquestes, pot representar un risc important per a les persones i pel medi ambient. Per això, poder predir el comportament d'un núvol tòxic o inflamable representa un dels reptes més importants de l'anàlisi quantitativa del risc. El principal objectiu d'aquesta tesi és el d'aportar nous coneixements que siguin d'interès pels analistes de risc tecnològic a l'hora d'enfrontar-se a problemes de modelització dispersió de certa complexitat, com ara aquells que ocorren en escenaris semi-confinats o amb presència de barreres.

La revisió bibliogràfica ha permès detectar que, tradicionalment, els models que més s'han emprat per analitzar la dispersió de fuites han estat els de naturalesa empírica i integral, ja que aquests poden donar bones prediccions i de manera més àgil en escenaris senzills sense obstruccions i en terreny pla. Tanmateix, en els darrers anys, l'ús d'eines CFD (Computational Fluid Dynamics) per a simular la dispersió accidental s'ha vist incrementat, ja que aquests programaris permeten modelitzar escenaris més complexos, pel que fa a la topografia o a la presència d'elements que puguin obstruir el flux de material. D'entre totes les eines CFD disponibles, el programari FLACS® és el que mostra més potencial a l'hora de simular aquesta tipologia d'escenaris, però, com altres eines de la seva tipologia, encara requereix estudis complerts de validació.

Aquesta tesi contribueix a la validació de FLACS per a realitzar anàlisis de dispersió. Després de revisar amb cura els estudis experimentals de la bibliografia, alguns d'ells han estat seleccionats per a dur a terme una avaluació inicial de les prestacions de FLACS, en la que s'han investigat totes les possibles fonts d'incertesa que poden aparèixer en les simulacions. Se n'ha estudiat la reproductibilitat, la dependència del domini i mida de cel·les i la sensibilitat de la concentració a variacions en les variables d'entrada i en els paràmetres de simulació. Els principals resultats d'aquesta anàlisi preliminar s'han presentat en forma de "principis guia" que podran ser utilitzats per analistes de risc per tal que puguin simular de manera acurada escenaris complexes de dispersió amb l'eina FLACS o amb d'altres programaris similars.

Tot i que a la bibliografia hi ha algunes dades experimentals disponibles, cap dels treballs inclou exercicis de validació suficientment complets. Tampoc s'hi inclou informació sobre com cal plantejar adequadament els escenaris de simulació ni tampoc s'hi troben valoracions quantitatives de la fiabilitat de FLACS. Per aquest motiu, en el marc d'aquesta tesi, s'ha dut a terme experiments per tal de tenir noves dades que permetin realitzar estudis de validació complets. Les proves han consistit en fuites de propà (lliures i amb obstruccions) i s'han dut a terme al centre de seguretat Can Padró (Sant Vicenç de Castellet, Barcelona). Amb aquests experiments s'ha pogut obtenir una gran quantitat de dades de concentració dels núvols experimentals. S'han dut a terme un total de 4 proves, amb cabals de 0.5 kg/s en una àrea de descàrrega de 700 m2.

Les prestacions de FLACS ha estat provades tot simulant les proves experimentals. A nivell general, el programari ha tingut un bon rendiment a l'hora de simular la concentració dels núvols de propà. A més, ha pogut reproduir de manera adequada la presència d'una obstrucció i els seus efectes en la dispersió, donant resultats de descens de concentració realistes. Tanmateix, els núvols simulats no han representat en la seva totalitat la dinàmica d'acumulació dels experiments reals degut a la gran variabilitat del vent i han mostrat temps de dilució inferiors als reals.

Paraules clau: dispersió, gas dens, proves de camp, dinàmica de fluids computacional, FLACS software

Figures list

Tables List

Nomenclature

Roman letters

u_*	square root of the shear stress divided by the density of air at the surface
H_0	sensible heat flux
c_p	specific heat
T_a	near-surface absolute temperature of the air
g	gravitational acceleration
L	Monin-Obukhov length
z_0	surface roughness
z_s	constant depending on the Pasquill stability class according to Table 2
L_s	constant depending on the Pasquill stability class according to Table 2
G_0	turbulence contribution due to subgrid obstructions
f_i	parameter of friction forces depending on subgrid objects
u_i	Mean velocity (i^{th} component, vector)
$F_{0,i}$	resistance due to sub-grid obstructions
$F_{w,i}$	resistance due to walls
p	pressure
h	enthalpy
μ_{eff}	effective viscosity
$\dot{Q}$	heat rate
V	volume
R_{fuel}	fuel reaction rate
k	kinetic energy
G	rate of turbulence
P_k	turbulent kinetic energy

P_ε	production of dissipation
G_s	flow shear stresses
G_w	wall shear stresses,
G_b	buoyancy force
G_o	turbulence due to subgrid objects
R_f	buoyancy term
y_{cv}	distance from the wall point to the wall
y^+	dimensionless wall distance
y	Wall distance
I_T	relative turbulence intensity
l_{LT}	turbulence length scale
U_0	mean flow velocity
z_d	canopy height
z_0	roughness length
u^*	friction velocity
z_{ref}	reference height for wind velocity

Greek letters

κ	Von Karman constant (0.4)
β_v	volume porosity
β_i	area porosity in the ith direction
ρ	density
σ_{ij}	stress tensor
μ_{eff}	effective viscosity
Υ_{fuel}	mass fraction

ξ	fraction of the mixture
k	kinetic energy
ε	dissipation rate
σ	Prandtl-Schmidt number
μ	substance viscosity
μ_t	turbulent viscosity
δ_{ij}	Kronecker delta function
τ_w	wall shear stress

Subscripts

a	air
o	subgrid
v	volume
f	fluid
s	Solid
i	spatial index
w	wall
eff	effective
h	enthalpy
ξ	fraction of mixture
d	drag
b	buoyancy
T	turbulence

Contents

1 INTRODUCTION

In the present day society, with industrial and technological development, the presence of flammable or toxic substances can be found in an increasing number of activities. Flammable substances are used as energy sources, toxic substances are used in a huge number of industrial processes, and often flammable and toxic substances are present in the same processes. Although these substances are essential nowadays, there are risks involved in their manipulation, storage and transportation that should be controlled whenever possible.

Large amounts of these substances, specially fuels, are transported from their production areas to storage areas (onshore or offshore) or directly to demand areas by ships and then offloaded; thus a significant percentage of the risks associated to flammable and/or toxic materials are in maritime environment, such as transport ships, offshore production plants, port terminals and offshore terminals. It has to be noted that most of the accidents involving leakages take place in scenarios with complex geometry like those found in the offshore industry.

The currently accepted definition of risk is the result of the frequency of occurrence and of the consequences generated by an undesired event. Risk reduction is achieved by reducing the frequency of undesired events and by the mitigation of consequences. The consequences analysis intends to define the extent and nature of the effects caused by undesired events and thus quantifies the damage caused by such events. In the case of leaking flammable and/or toxic materials, effects are analysed for explosions, fires and toxicity. The consequences of the undesired events can cause personal injury (physical or psychological and can affect both people involved in the industrial operations and also external population), assets damage (usually destruction of equipment and building) and environmental damage (release of hazardous substances into the atmosphere, into the soil or into the water) As such, these consequences usually imply huge economic losses and quite often lead to other indirect losses such as damage to company image.

1.1 Effects and consequence analysis of flammable or toxic leakages

The consequence analysis is used to define the extent and nature of effects caused by undesired events on individuals, buildings, equipment and the environment; and thus

quantifies the damage caused by such events. For the case of leaking flammable and/or toxic materials, consequences are analysed for explosions, fires and toxicity.

When a flammable substance is released from a storage tank or pipeline, a liquid pool may form. As the pool forms, some of the liquid will evaporate, disperse, and if the vapour cloud finds an ignition source while its concentration is between the lower and upper flammability limits (LFL and UFL), a flash fire will occur. Moreover, the flame can travel back to the spill, resulting in a pool fire. A pool fire involves burning of the vapour above the liquid pool as it evaporates from the pool and mixes with air. This sequence is described by Pitblado, Baik and Raghunathan (2006). In case of flash fire, the potential to injure individuals is restricted within the range of the ignited gas cloud and, for pool fire, the potential for fatalities is due to the exposure to heat radiation. If the flammable substance is pressurized, the discharge will take place in form of a jet and if there is an immediate ignition a jet fire may occur. As in the case of the pool fire, the potential for fatalities will be due to the exposure to heat radiation.

Furthermore, in specific conditions, the release of a flammable substance can cause an explosion; it occurs when the cloud ignites in presence of turbulence. The turbulence may be generated by the release conditions or by the presence of obstacles (like congested or semi confined areas); it modifies the flame geometry that causes the increase of the flame area; this change causes the increase of the burning rate and, consequently, the increase of the flame propagation speed, which can cause a blast. The potential for fatalities is in this case due to the exposure to overpressure.

To perform the consequences analysis of leakage of flammable and/or toxic substances, the first step is to model the effects of the undesired event. As presented by Casal (2008), these effects are estimated by mathematical models that describe the phenomenon and provide predictions for the thermal radiation emitted by a fire, the peak overpressures from an explosion, the trajectory of fragments or the concentration in the dispersion of a released material.

Usually, to evaluate the effects of a leakage several phenomena have to be modelled: the discharge of the substance, the pool spreading and vaporization (if the pool occurs), the cloud formation and dispersion, the radiation emitted by the fires, the shock wave of blasts, etc.

This study is mainly focused on the cloud formation and dispersion, i.e. the evolution and the features of the cloud, such as concentration, temperature, velocity and dimensions as

function of time and position. In the case of flammable substances, modelling the cloud formation and dispersion allows predicting the area where a fire or explosion may occur and the quantity of flammable material present in the area; in the case of toxic substance, it allows to predict the concentration in time and space and thus the toxicity levels.

1.2 Cloud formation and dispersion: theoretical framework

The initial step that has to be considered when modelling a cloud of any toxic/flammable substance is the estimation of the amount of material involved in the release and its release rate by means of appropriate source term models. Following, dispersion phenomena have to be taken into account in order to study the evolution of the cloud and come up with key variables for consequence analysis, like the concentration variation with time and space.

Modelling cloud formation and dispersion has inherently huge complexity. It has to be highlighted that the underlying problem is related to fluid dynamics, where substances of different properties, complex geometries and atmospheric characteristics converge all together.

As reported by CCPS (1995), to evaluate the analysis of an accidental release it is necessary to define the governing conditions of the discharge scenario and environment; the items that can define these conditions are source information, environmental conditions, release types, possible source scenarios and possible dispersion mechanisms. The release is usually described by separating the region analysed in three sections: first the release section, where the release is almost independent of the environment conditions (the features of the source term define this region which can be quite small or even not exist depending on the release conditions), next the intermediary section where both source and environment conditions are important in modelling and, the last section, where environmental conditions dominate the process of dispersion. The next sections present the source terms and the formation and dispersion of the cloud formed.

1.2.1 Source term modelling

As reported by Casal (2008), the accidents usually start with a loss of containment and the released material is often a gas, a liquid or both, i.e. a two-phase flow. These releases can be continuous for a period (i.e. a hole in a tank or in a pipe) or instantaneous (i.e. a catastrophic

tank rupture). In continuous releases, if the material released is pressurized, a jet is formed; additionally, if the material released is a liquid, a pool may form and will evapourate contributing to the cloud formation. For continuous releases it is necessary to estimate the mass flow rate and the total amount released or the release time. In instantaneous releases, if the material released is gas, an instantaneous gas cloud (usually called a puff in the literature) is formed and, if the material released has a fraction of liquid, a pool may also appear.

In both cases, during the release, the material interacts with the immediate surroundings and this interaction affects directly the form that the material enters the ambient; the released material can form a pool, disperse or be ignited immediately (TNO, 2005). The features of the release are controlled essentially by the ambient conditions and by the features of the material before the release (state, pressure, temperature, etc.).

Casal (2008) and CCPS (1995) present detailed data about physical aspects of the source terms and TNO (2005) and CCPS (1998) present models available on the literature to treat source terms. After evaluating the discharge of the substance, the pool spreading and vaporization (if the pool occurs) and the cloud formation according to the source term, it is then possible to evaluate the cloud dispersion.

1.2.2 Dispersion modelling

The cloud dispersion process depends on the density of the cloud substance, the atmospheric conditions and the features of the source term. If the substance released has a density higher than air upon release, the first stage of the dispersion will occur as dense gas and when the cloud dilutes enough equalling its density to the air's, the dispersion will occur as passive dispersion. In the dense gas dispersion the cloud will undertake descending movements until it will reach the ground and then spread radially under influence of the gravitational forces, thus the dense cloud will have the horizontal dimension greater that the vertical dimension. The vertical dimension will be higher in the extremities of the cloud due to the air resistance (TNO, 2005) as presented in Figure 1. After this stage, when the cloud density is similar to the air density, passive dispersion will occur, which will be governed by the atmospheric conditions, mainly by wind and atmospheric stability (TNO, 2005).

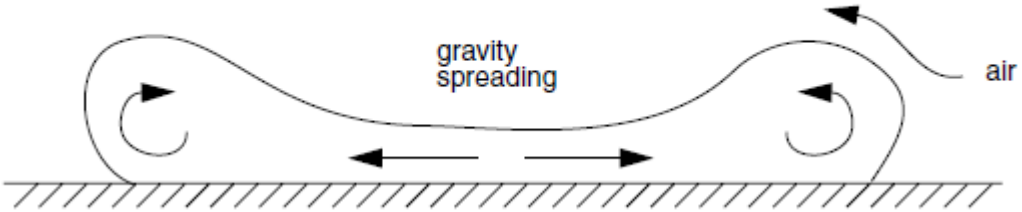

Figure 1 - Gravity spreading of a dense gas cloud
Source: TNO (2005)

The atmospheric instability is due to the wind flow and the air displacement between different layers due to the temperature difference between these layers. This instability causes turbulence. Turbulence generates eddies of different sizes; eddies smaller than the cloud disperse the cloud and increase the cloud size (there is no effect on position of the cloud), eddies much bigger than the cloud merely move the cloud (there is no effect on form neither on size) and eddies with the same size of the cloud change the cloud form and increase its contour (TNO, 2005).

Finally, there is the source term influence in the dispersion process; the clouds may be formed from an area or volume source (like a pool) or formed from a jet. When the material is released with a high velocity compared to velocities in the ambient air a jet is formed; in this case the jet length will depend on the features of the jet itself and the difference between the jet and the air velocity will cause the spreading of the jet sideways. The velocity of the jet reduces as moving away from the release point and when it matches the air velocity, the dense gas dispersion takes place (if the density of the substance released is higher than the air). Finally, the passive dispersion occurs when the dense gas cloud dilutes or just after the jet if the density of the released material is equal or lower than air density.

Atmospheric stability

As mentioned in the previous section, the air displacement between different layers and the wind flow cause atmospheric instability that facilitates the cloud dilution; thus, the cloud concentration will be lower in unstable conditions.

When an air portion moves from surface upwards it expands as pressure decreases and then the temperature decreases. If after the expansion, the air portion has the same temperature as

its surroundings the atmospheric condition will be neutral; if its temperature is lower than its surroundings the atmospheric condition will be stable and the portion will be forced downwards; and if its temperature is higher than its surroundings the atmospheric condition will be unstable and the portion will be forced upwards (TNO, 2005 and Casal, 2008).

When the atmospheric condition is unstable, there is a heat flux from the ground surface upwards and when it is stable there is a heat flux downwards; as presented by (TNO, 2005), the stability condition of the atmospheric layer above the earth's surface is defined by the ratio of the turbulence generated by the temperature gradient and the turbulence generated by the wind shear at the surface; this ratio may be expressed by the Monin-Obukhov length, which is defined as:

$$L = \frac{-\rho_a c_p T_a u_*^3}{\kappa g H_0} \quad (1)$$

where:

u_* : is the square root of the shear stress divided by the density of air at the surface;

H_0: is the sensible heat flux;

ρ_a : is the air density;

c_p: is the specific heat;

T_a: is the near-surface absolute temperature of the air;

κ: is the von Karman constant (0.4) and g the gravitational acceleration.

The Monin-Obukhov length may be interpreted as the height above the ground where the turbulence generated by wind is equal to the turbulence generated by the temperature gradient. This equilibrium does not occur in unstable conditions, thus:

$L > 0$ stable condition ($H_0 < 0$)

$L < 0$ unstable condition ($H_0 > 0$)

$L = \infty$ neutral condition ($H_0 = 0$)

The atmospheric conditions are also frequently classified by qualitative methods been the most common the Pasquill method, which classified the stability condition in classes from A to F as showed in Table 1 (Pasquill, 1961).

Table 1 - Pasquill Stability

Stability class	Description
A	Extremely unstable condition
B	Moderately unstable condition
C	Slightly unstable condition
D	Neutral condition
E	Slightly stable condition
F	Moderately stable condition

The Pasquill classes and the Monin-Obukhov length can be related as presented in TNO (2005), in which the Monin-Obukhov length is calculated from de Pasquill stability as:

$$\frac{1}{L} = \frac{1}{L_s} log_{10}\left(\frac{z_0}{z_s}\right) \quad (2)$$

where:

z_0 is the surface roughness;

z_s is a constant depending on the Pasquill stability class according to Table 2;

L_s is a constant depending on the Pasquill stability class according to Table 2;

According to TNO (2005), if the surface roughness is higher than 0.5 m, the Monin-Obukhov length calculated for roughness equal to 0.5 m should be used.

Hsu (1992) proposed a similar method to establish the relation between the Monin-Obukhov length and the Pasquill stability classes for dispersions over sea. Figure 2 presents this relation; the stability class depends on the wind speed at 10 m height and the temperature difference between the sea and the air.

Table 2 - Calculation of Monin-Obukhov length from Pasquill stability.
Source: TNO (2005)

Stability class	L_s (m)	z_s (m)
A	33.162	1117
B	32.258	11.46
C	51.787	1.324
D	∞	NA
E	-48.330	1.262
F	-31.325	19.36

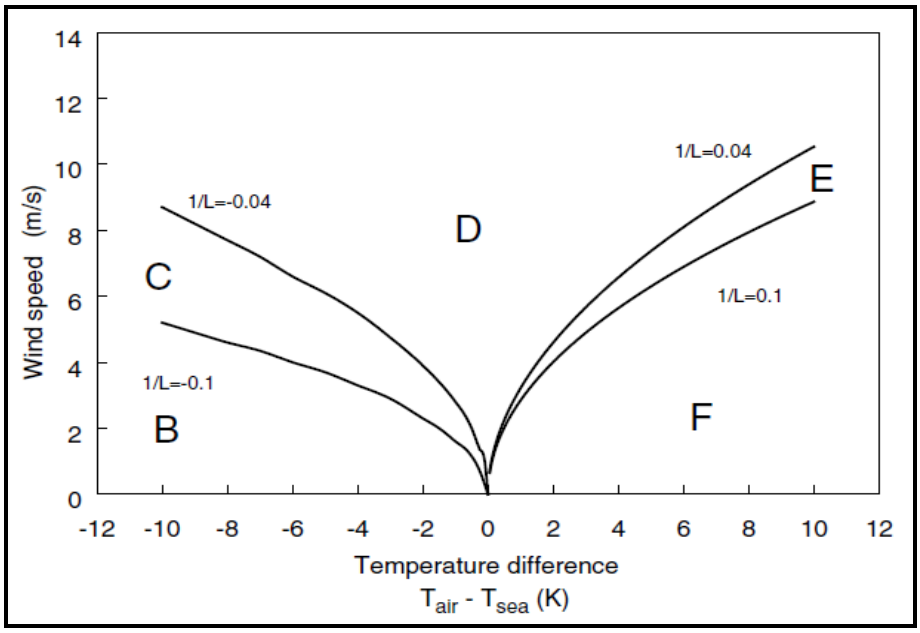

Figure 2 - Pasquill stability classes and Monin-Obukhov length for dispersions over sea.
Source: TNO (2005)

Although the Pasquill method and the methods to calculate the Monin-Obukhov length from the Pasquill stability are used extensively, both Hanna et al. (1982) as well as TNO (2005) warn about the restrictions of the qualitative methods; Hanna et al. (1982) reminds that this scheme should not be used, for example, in problems that involve complex geometry, effective height releases above 100 m and others; and TNO (2005) reminds that at the European Workshop - Objectives for Next Generation of Practical Short-Range Atmospheric

Dispersion Models held on May 1992, it was agreed that models should use schemes using quantifications of physical parameters of the boundary layer.

The study of the transportation and dilution process of a toxic/flammable cloud is generally performed by means of mathematical models, which main outputs are the concentration at any location surrounding the release, as a function of time. In the following chapter a literature survey of the most significant models is presented.

1.3 Rationale of research

In order to perform the consequence analysis of flammable or toxic releases, there is not a unique method to obtain the solution of the set of equations that model the physical phenomena. Traditionally, empirical and semi-empirical models have been used providing fast dispersion estimations and usually reliable results when describing unobstructed gas flow over flat terrain. However, it is recognized that these models provide unreliable results when applied to complex topographies (Mazzoldi et al., 2008). The use of these models implies that no geometry complexity of the scenario evaluated is taken into account, since these models are not able to do so. Nowadays, it is still not unusual, the inappropriate use of these models to asses scenarios in which the geometrical configuration of the scenario (such as a barrier) may have significant influence.

An example of this issue is the use of semi-empirical models to evaluate the dispersion in environments with some degree of confinement. This may produce inaccurate results, since the models will probably underestimate the concentrations in the near field and overestimate the concentrations in the far field, since they are not able to model the effect of the partial confinement that slows the dispersion.

With the computational advances, physical models implemented in Computational Fluid Dynamics (CFD) tools are already being used for short and medium range gas dispersion scenarios over terrains with some degree of complexity. However, most of the tools are still under performance validation processes.

A major problem in risk analysis is the variability in outcomes that can be obtained depending on the tool and the criteria used. According to Pasman et al. (2009), the factor that results in the greatest impact to uncertainty is related to the analyst judgment during the scenario definition and the selection of the model used to perform the analysis. Additionally,

it is important to note that the process of analysis is intrinsically related to the software in which the models are implemented; thus, in order to obtain reliable and reproducible outcomes, these programs should be verifiable, robust and validated against experimental/real data.

Regarding dispersion analysis, one can cite two studies linked with this issue; the first one, a study reported by Amendola et al. (1992) which describes a project of the European Community to gather the state of the art of the chemical risk analysis; and the second one, presented by Lauridsen et al. (2002) which describes a similar study performed ten years later. In the first study, the same scenario (an ammonia storage facility) was analysed by eleven different teams of specialists. Among other results, the concentration (in a specific point and time) of the cloud formed by an ammonia release estimated by these teams varied by twelve orders of magnitude; and excluding the two extreme values, by two orders of magnitude. In the second one, in which seven teams assessed a similar scenario (an ammonia plant with loading and unloading operations) the results for concentration varied by three orders of magnitude. These two exercises show that the results may vary significantly as a function of the decisions of the analysers and of the tools used; when using CFD this issue is even more critical due to the large amount of decisions that should be taken by the users on the initial conditions and simulation parameters.

Lauridsen et al. (2002) claimed that the factors that contribute most to variability in consequence analysis are the definition of the scenario, the choice of the model for dispersion, differences in dispersion calculation codes and analyst conservatism or judgment.

Within this context, this dissertation aims at providing new insights that can help technological risks analysts when dealing with complex dispersion modelling problems. Particularly, it is focused on dispersion scenarios with barriers or semi-confined and seeks to identify the most critical points when modelling this type of events, especially by means of CFD tools.

Furthermore, this work will contribute to the dissemination of the culture of risk assessment in strategic sectors of Brazil, such as the marine industry and the oil and gas industry. It has to be highlighted that while the concern for the assessment and management of risks associated with industrial activities is increasingly gaining importance worldwide, and some regulations and standards for risk assessment have been proposed (Seveso directives of

the European Parliament in the European Union (Seveso II, 2003), guidelines for chemical process quantitative risk analysis of CCPS in the United States (CCPS, 2000), etc.) in Brazil there are still no clear guidelines of how to deal with technological risks. It is hence an urgency for Brazil to overcome this problem and the outcomes of this work will represent a contribution in this sense.

1.4 Goals

1.4.1 Main goal

The goal of this study is to map critical points in quantitative dispersion analysis of leakages of flammable and/or toxic substances on realistic environments with barriers, for example, in offshore production units or in refineries.

1.4.2 Secondary goals

1. To investigate the applicability and limitations of dispersion models available in the literature for scenarios implying complex geometries.

2. To contribute to the validation of a CFD tool for dispersion analysis.

3. To undertake field tests in order to offer new sets of cloud dispersion data *i)* to complement the quantitative analysis performed in this study *ii)* to be used by the international community for models validation purposes;

4. To contribute to the dissemination of the culture of risk assessment and management in strategic sectors of Brazil.

1.5 Thesis structure

This dissertation is structured into six chapters. The first one is an introductory chapter in which a general overview of the subject treated in this work is provided. The research objectives of this study and the structure of the thesis are also presented.

Chapter 2 includes a succinct literature survey of the most significant dispersion models. It highlights the key features of empirical, integral and physical mathematical models and reviews the most compelling simulation tools in which these models are implemented.

In Chapter 3, the CFD model selected to perform the study (FLACS) is investigated. A detailed description of the model is firstly presented. Then, FLACS validation is tackled, considering the following aspects: first, a survey on experimental data available for validation is detailed; next, literature on already existing validation studies is reviewed and finally, the first attempt to assess FLACS performance within the work at hand is presented. The third part of the chapter includes a reproducibility, grid dependence and sensitivity analysis study performed within the work at hand. Chapter 3 ends summarizing some guiding principles which are of interest when modelling dispersion with a CFD tool.

Chapter 4 is devoted to the propane cloud dispersion field tests performed in Can Padró security and safety training site (Sant Vicenç de Castellet, Barcelona) during July 2014. The preliminary design, the final set-up and the data obtained during the tests are detailed.

In Chapter 5 the main results found when challenging the CFD tool (FLACS) against two experimental data of Can Padró tests (one test with a physical obstruction and one unobstructed test) are presented and discussed.

Finally, Chapter 6 presents the conclusions of this thesis, including some recommendations for future work.

2 LITERATURE SURVEY ON DISPERSION MODELLING

The dispersion models are typically classified as models that treat clouds formed by substances with densities higher than the air or models that treat clouds formed by substances with densities equal or lower than the air. Furthermore, these models are subdivided in models that treat clouds formed from an area or volume as source term and models that treat clouds formed from a jet. There are different approaches to model cloud dispersion in terms of the nature of equations developed: empirical, integral (or semi-empirical) and fully physical. Empirical models are based entirely in experimental data and integral models use differential or integral equations to model the physic phenomena including empirical coefficients to calibrate these equations. Both approaches (empirical and integral) have been traditionally used in cloud dispersion modelling. However, in recent years due to the computational advances the use of fully physical models using CFD tools has increased. In this chapter, a literature survey of the most significant dispersion models is firstly presented focusing on the advantages and disadvantages of each one, and following, the most compelling simulation tools in which these models are implemented are also reviewed.

2.1 Empirical Models

The empirical models are based entirely on experimental data, i.e. the set of equations forming the model is developed based on empirical correlations. These models provide fast results and are easy to implement, however, they are not comprehensive as integral and physical models. As mentioned previously, the models are divided in models to evaluate dense gas dispersion or dispersion of substances with densities equal or lower than the air; and each one may present a jet or an area (or volume) as source term. Among the empirical models, the following models are reviewed: *i)* the model proposed by Britter and McQuaid (1988) to evaluate the dispersion of dense clouds without the presence of jet; *ii)* the Gaussian Plume Model (GPM) to evaluate the dispersion of passive clouds without the presence of jet; *iii)* the model proposed by Turner (1970), that is a modified version of the GPM used to evaluate dispersions of substances less dense than air without the presence of jet; *iv)* the model proposed by Chen and Rodi (1980) to evaluate dispersion of substances more or less denser than air, with jet in uniform quiescent atmosphere; and *v)* the Briggs (1969) model for clouds formed by jets with crosswind and formed by substances less dense than air.

2.1.1 The Britter and McQuaid (1988) model

The model proposed by Britter and McQuaid (1988) consists of empirical correlations between a set of independent variables that describe the dense cloud dispersion of an instantaneous or continuous releases without jet (TNO, 2005). The model presents a set of monograms that represent the concentration decay of the dense cloud as function of the release point distance; these monograms were developed from experimental data from field, laboratory and wind tunnel tests. One important issue is that the experimental tests used to develop this monograms are test of releases over flat terrain and the model does not present any treatment for releases in terrains with any degree of complexities.

The model is widely accepted and is considered a fundamental reference for dispersion of dense gas clouds; it is especially useful for calculations with an indicative purpose, as a preliminary analysis. However, to perform more comprehensive analysis others models should be used.

2.1.2 Gaussian plume modelling

This type of dispersion modelling is generally recommended to evaluate passive cloud dispersion over flat and uniform terrain of instantaneous or continuous releases without the presence of jets and has its origin on the general equations proposed by Pasquill (1961) and Gifford (1961). In this sense, it has to be highlighted the Gaussian Plume Model (GPM) described by TNO (2005). It consists of a set of formulas developed to estimate the concentration as function of the release rate, wind velocity, mass released and dispersion parameters (which are defined from experimental data). It is based on the fact that assuming homogenous turbulence and wind speed, the concentration distribution of a cloud spreading in all directions becomes Gaussian in shape.

The GPM model is widely used to evaluate passive dispersion and is applicable for dispersion over flat terrain. However, it should not be used to evaluate periods longer than 3 hours, since it is not capable to consider changes in the atmospheric conditions that may occur frequently during the day.

2.1.3 The Turner (1970) model

The model proposed by Turner (1970) is a modified version of the traditional GPM model that evaluates a continuous source with a Gaussian plume distribution with emphasis in the first hour of dispersion, since it does not take into account measurements of turbulence or changes in the atmospheric conditions. It is recommended only to passive dispersions without the presence of jet over flat terrains and near the surface (i.e. from the surface to about 20 m height).

The set of equations implemented in this model is based in the assumption that the release duration should be equal or greater than the travel time to the downwind position under consideration, the material should be a stable gas or aerosol and the plume is distributed normally in both the cross wind and vertical directions (Turner, 1970).

The most significant difference between the traditional GPM model and this modified version consists on the fact that a gradient of wind velocity is added to the original formulation to estimate the concentration (Reynolds, 1992).

2.1.4 The Chen and Rodi (1980) model

The model proposed by Chen and Rodi (1980) evaluates the dispersion from clouds formed by vertical jets if the released substance is denser than air or by jets of any direction if the released substance is less dense than air. The model predicts a uniform quiescent atmosphere (without wind) and the release velocity has to be less than one third of the velocity of sound under ambient pressure (TNO, 2005).

This model is also based on empirical data; it is made of empirical equations that estimate the concentration and the velocity of the centre of the jet as a function of the release point distance, and from these equations the limits and mass of the cloud can be inferred. This model is simple to implement however it is applicable to a very specific scenario.

2.1.5 The Briggs (1969) model

In contrast with the Chen and Rodi (1980) approach, Briggs (1969) developed a model to evaluate the dispersion of passive plumes formed by a vertical jet or by a release without jet in presence of crosswind. In this model, it is considered that the wind generates a pressure field

on the jet, which deflects the jet. Based on empirical data, the model first estimates the cloud height as function of the release point distance in downwind direction; next, it estimates the maximum height and the position and radius of the cloud at the moment that the cloud reaches its maximum vertical position; and finally, considering the concentration distribution uniform, it estimates the concentration as a function of the cloud radius. From this stage, then others models can be used to evaluate the passive cloud dispersion. As in the previous case, its implementation is simple but its applicability is very restricted.

2.2 Integral models

The integral models are models that use differential or integral equations to model the physical principles which describe the variables of interest in a rather simple way; they include coefficients defined by empirical data in order to solve these equations.

In this section the following models are summarized: Havens and Spicer (1985) model, the models proposed by Zeman (1982) and by Hoot, Meroney and Peterka (1973) and the Unified Dispersion Model (UDM) developed by Haper (2009).

2.2.1 Havens and Spicer (1985) model

As reported by Reynolds (1992), the model proposed by Havens and Spicer (1985) treats specifically dense cloud dispersions formed by a continuous release, without the presence of jet and it does not take into account crosswind. The dispersion is described by a set of integral equations for mass, energy, cloud dimensions and cloud velocity; from these equations the concentration profile of the cloud can be estimated. It also has a certain empirical component to set several dispersion parameters.

This model does not treat in detail the source term. It is assumed that the release comes from a circular area (a pool formed by a leakage from a pipe or a tank); then it is assumed that the gas will spread around this area forming a secondary source. The size and amount of material in the secondary source is computed by a mass balance and a rectangular source term (a third source) is estimated in order to evaluate the dispersion model. It is a model that provides fast results; however, it should be used only for dense gas dispersions over flat terrain and does not take into account jet features as source terms.

2.2.2 The Zeman (1982) model

Zeman (1982) proposes a shallow layer model to evaluate dense gas dispersion in the presence of wind; in a shallow layer model a grounded cloud is assumed in which the features of the cloud are averaged over the cloud volume. As in previous models, a set of integral equations for mass, energy, cloud dimensions and cloud velocity are used to estimate the concentration of the cloud. Data of laboratory and field tests were used in order to define several constants present in the equations.

This model treats dense gas dispersion over flat terrain of clouds formed by instantaneous releases or horizontal jets; however, it does not treat passive clouds or any cloud formed by vertical jets. Additionally, the coefficients present in the formulae were defined using experimental data involving natural gas and they are not validated for others substances.

2.2.3 The Hoot, Meroney and Peterka (1973) model

The model proposed by Hoot, Meroney and Peterka (1973) evaluates the dispersion of dense clouds formed by vertical jets submitted to lateral wind; it is one of the simplest integral models. This model divides the cloud path in regions and then obtains in each region analytical solutions for the conservation equations (Figure 3 presents the development phases of the dispersion considered in this model). Hoot, Meroney and Peterka (1973) specified the values of the empirical constants by a comparison of the model results with wind-tunnel experiments (TNO, 2005).

In contrast with the Havens and Spicer approach, this model takes into account the effects of the transversal wind during the release and therefore it is recommended to evaluate the dispersion near the source term (Reynolds, 1992).However, it does not take into account the air entrainment due to atmospheric turbulence and therefore it is not appropriate to evaluate far field dispersion. TNO (2005) suggests evaluating the dispersion of a dense cloud formed by a vertical jet in the presence of crosswind coupling both the model proposed by Hoot, Meroney and Peterka (1973) in the near field and the model of Zeman (1982) in the far field.

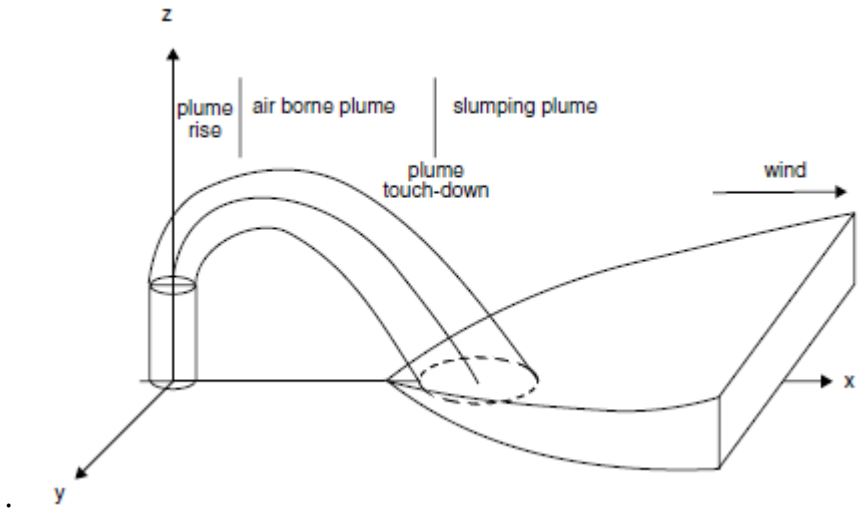

Figure 3 - The development phases of lofted plumes.

Source: TNO (2005)

2.2.4 The Unified Dispersion Model (UDM) by Haper (2009)

The Unified Dispersion Model (UDM) presented by Haper (2009) is a generic integral model that simulates the dispersion of clouds of any density over flat terrain. The UDM model can be used to simulate the dispersion of a cloud that results from an instantaneous, continuous or a finite duration release with or without the presence of a jet and without the presence of crosswind.

This model evaluates the cloud features as a function of the release point distance in downwind direction. It describes the cloud by a set of differential equations for conservation of mass, conservation of momentum, relation between cloud speed and cloud position, heat transfer, water vapour transfer and cloud spreading in crosswind direction. Empirical correlations obtained by wind-tunnel tests are used to approximate the concentration distribution to a Gaussian profile in the far field (Witlox, Holt, & Veritas, 1999).

The UDM model is a comprehensive model, the equations used allow modelling the transition of a dense cloud to a passive cloud and modelling the clouds formed by any source term. With this tool it is not need to used coupled models to evaluate the different dispersion phases what is a significant advantage over the others previously presented.

2.3 Physical models

The physical aspects of any fluid flow are governed by three principles: mass is conserved, Newton's second law is fulfilled (also referred as momentum equation), and energy is conserved. In the physical models, these principles are expressed in integral equations or partial differential equations being the most common form the Navier-Stokes equations for viscous flows and the Euler equations for inviscid flows (flows in which the dissipative and transport phenomena of viscosity, mass diffusion and thermal conductivity can be neglected).

These physical models are the ones implemented in Computational Fluid Dynamic (CFD) tools and are usually referred just as CFD models. The CFD tools transform the governing equations of the fundamental physical principles of fluid flow in discretized algebraic forms, which are solved to find the flow field values in time and/or space (Anderson, 1995). The results obtained by CFD are a set of numerical values which represent the flow field properties at selected discrete points in time and/or space.

The physical models find the flow field values in time and/or space and from these values the features of the cloud, such as the concentration, can be estimated. They are comprehensive models that allow modelling dense or passive clouds formed by any type of source term. Additionally, the physical models allow taking into account the scenarios complexities such as barriers or semi-confined spaces.

Some commercial CFD software tools are CFX, FLACS, FLUENT and PANACHE. Some of them have models for general purposes (such as Fluent or CFX) whereas others have specific models that have been developed for particular phenomenon, like dispersion, fires or explosions (such as FLACS).

2.4 Simulation tools for cloud dispersion analysis

The need for using the models for cloud dispersion prediction in a practical way led private and public companies to create software to simulate vapour cloud scenarios. This development is the result of a technological and modern approach to safety studies and help risk analysts to have faster and more complete outcomes. Next, a brief list of the most known simulation systems is summarized which are mainly based on the mathematical models reviewed.

2.4.1 SLAB® – (An atmospheric dispersion model for denser than air releases), Lakes Environmental Software

As reported in TNO (2005) the model resolved in SLAB is based on the concepts presented by Zeman (1982) and its computer implementation is reported by Ermak (1990). It is recommended to evaluate the dispersion of clouds that have a horizontal or vertical jet or an area (or volume) as source term. This model is more appropriate for denser-than-air clouds.

The SLAB model describes the cloud concentration by a set of conservation equations for mass, energy and momentum for one dimension; from these equations the dimensions and the height of the cloud are estimated; then the model assumes that the concentration distribution is Gaussian in all directions. To evaluate clouds formed by vertical jets in the presence of crosswind, the SLAB model specifically uses the model proposed by Hoot, Meroney and Peterka (Hoot, Meroney and Peterka, 1973) as submodel, since the model proposed by Zeman (1982) does not take into account the effects of the transversal wind during the release (TNO, 2005).

2.4.2 ALOHA® (Areal Locations of Hazardous Atmospheres), United States Environmental Protection Agency (EPA)

As presented by Reynolds (1992), ALOHA is a computer program based on the model proposed by Turner (1970), a modified version of the GPM that represents a continuous source with a Gaussian plume distribution; however, it evolved over the years and nowadays it is capable of modelling the dispersion of dense and passive clouds and some specific scenarios of jet releases. ALOHA uses the model proposed by Turner (1970) to model passive dispersions, uses a modified version of the model proposed by Havens and Spicer (1985) to model dense dispersions (known as the DEGADIS model) and uses in house modelling based in studies performed during the 70s and 80s to model dispersions formed by jets without the presence of crosswind (Reynolds, 1992).

Another two relevant issues are that ALOHA does not evaluate the dispersion in the near field (the cloud dispersion is evaluated at least 10 m apart from the release source) and the model assumes flat terrain. Furthermore, Reynolds (1992) reports that ALOHA was developed to calculate and display a cloud footprint in a rather short time to be used in emergency situations, and should be used to initial conservative screening of the potential

threat area of an accident. ALOHA does not provide reliable estimations of cloud concentration when the following conditions exist: very low wind speeds, very stable conditions, concentration patchiness near the source, wind shifts and terrain steering effects and distances greater than 10 km.

2.4.3 Phast® (Process Hazard Analysis Software Tool), Det Norske Veritas Software

Phast is one of the best-validated consequence codes, with several validations for each model implemented (Pitblado, Baik, & Raghunathan, 2006). The program does not model only dispersions, but also the combination of several events, in which there is no immediate ignition, as a combination of spillage (leak), pool formation and evaporation, dispersion cloud and fires.

Phast evaluates cloud dispersions according to the UDM model proposed by Haper (2009). It can be used to simulate the cloud dispersion formed by instantaneous, continuous or a finite duration releases, with or without the presence of a jet, without the presence of crosswind and with or without pool formation. This model is capable of modelling the transition of the dense cloud to passive cloud and clouds formed by any term source; however, it does not take into account any complexity in the terrain.

2.4.4 FLACS® (FLame ACceleration Simulator), GexCon AS

FLACS is a CFD tool that was specifically developed for consequences modelling (GexCon AS, 2013). It was originally developed for explosion prediction for the offshore industry and nowadays it is capable of modelling passive and dense dispersions as well as fires and explosions. FLACS uses conservation equations for mass, energy, and momentum. It solves Reynolds Averaged Navier-Stokes (RANS) equations based on the standard k-ε model of Launder & Spalding (1974). According to HSE (2013), RANS approach is widely accept and documented; it is based on the concept of separating the fluid velocity components and scalar quantities (pressure, temperature, concentration) into mean and fluctuating components, then transport equations are used to evaluate the model. The standard $k-\varepsilon$ model of Launder & Spalding (1974) presents a turbulence model based in two turbulence quantities: the turbulent kinetic energy k and its dissipation rate ε; the magnitudes of these two variables are calculated from transport equations and solved simultaneously with those governing the mean

flow behavior (Launder & Spalding 1974). Additionally, as reported by Dharmavaram et al. (2005), FLACS implemented a modification on the standard model to estimate the turbulent kinetic energy and dissipation rate based on Pasquill stability classes or Monin–Obukhov length.

Furthermore, FLACS is one of the tools that allow taking into account the geometrical complexities in a more user-friendly way (Dharmavaram et al. 2005).

2.4.5 FLUENT® - Ansys Inc.

As presented by Riddle et al. (2004), FLUENT is a comprehensive generic code, which may be used to model a wide range of physical phenomena involving flows. In dispersion modelling it is able to model passive and dense dispersions, coming from any source term. The FLUENT code solves a set of equations for conservation of mass, momentum, energy, turbulence, pressure and concentration. Moreover, it provides ten different turbulence models which should be chosen according to the features of the flow analysed (Ansys Inc, 2011).

Although this is a comprehensive code that is capable of modelling a wide range of physical phenomena, it has to be highlighted that modelling a particular specific phenomenon (like cloud dispersion, for instance) is a rather laborious work with FLUENT, because of the huge number of parameters need to be set.

2.4.6 CFX® (Computational fluid dynamics software), Ansys Inc.

CFX like FLUENT is a code for general purposes. CFX uses the RANS equations like FLACS and is based on the finite volume method for the conversion of partial differential equations and auxiliary boundary conditions into a discrete system of equations. CFX uses the Boussinesq model to predict the turbulence inside the cloud as function of the thermal expansivity (Cormier, Ruifeng, Yun, Zhang, & Mannan, 2009). Like FLUENT, CFX is a comprehensive code that is able to model a wide range of physical phenomena. However, to parametrize a full dispersion scenario can be also rather arduous.

2.4.7 Fluidyn-PANACHE® (Fluid dynamics–PANACHE), Transoft International

Fluidyn-PANACHE was developed to model atmospheric flows in short and medium range scales, and as such it is not recommended for dispersions in the far field. It allows

modelling passive and dense dispersions. Fluidyn-PANACHE uses conservation equations for mass, energy, and momentum. The conservation equations are solved in three dimensional space and in time (Mazzoldi et al., 2011). It has two turbulence models implemented; the $k-\varepsilon$ model of Launder & Spalding (1974) present also in previously reported CFD models and the $k-l$ model, in which the magnitudes of two turbulence quantities are the turbulent kinetic energy k and a function of the Monin-Obukhov length l.

2.5 Main outcomes of the literature survey

Given the previous review, when a technological risk analyst has to perform cloud dispersion calculations, he/she has several options, starting from using *i)* analytical methods (i.e. nomograms, or models of quite simple formulation), *ii)* simulation software in which a combination of empirical and integral tools are implemented, or *iii)* CFD codes which run fully physical models. It is evident that analytical methods are easier to use than software tools based on empirical and semi-empirical models, and, at the same time, it is also easier to work with this later software rather than with more complex CFD codes.

According to the literature survey, Table 3 presents a summary of these options, gathering the key information to be considered when making the choice of the most suitable system to analyse cloud dispersion. The selection of one tool or another has to be based on the characteristics of the scenario to be studied (i.e. source term, meteorological conditions and geometrical configuration of the scenario where the release takes place), the degree of accuracy required, and the computational capacity available.

The empirical and integral models usually provide reliable and fast results for dispersions in specific scenarios mostly over flat terrain; however, they present limitations when used to model dispersions over terrain with barriers or semi-confined, like the offshore production units, refineries or industrial plants. Complex geometry may create turbulence and affect the dispersion of the cloud, being us such an important aspect to be considered when performing consequences analysis of leaks of hazard substances in scenarios like the ones mentioned above.

Table 3 - Models and tools for dispersion analysis

Type of tool	Models	Model type	Type of source term	Scenario	Key points
Set of monograms	Britter and McQuaid (1988)	Empirical	Instantaneous or continuous releases /no jet	Dense cloud dispersion over flat terrain	Not recommended to terrains with any degree of complexities
Formulae "GPM"	Gaussian Plume Model (TNO, 2005)	Empirical	Instantaneous or continuous releases / no jet	Passive cloud dispersion over flat terrain	Not recommended to terrains with any degree of complexities It should not be used to evaluate periods longer than 3 hours
Formulae "Briggs"	Briggs(1969)	Empirical	Continuous releases/ Vertical jet /crosswind	Dense cloud dispersion over flat terrain	It should not be used to evaluate passive clouds
Formulae "Chen and Rodi"	Chen and Rodi (TNO, 2005)	Empirical	Vertical jet in quiescent atmosphere	Dense cloud dispersion over flat terrain	Not recommended to terrains with any degree of complexities The release velocity should be less than one third of the velocity of sound under ambient pressure
SLAB software	Zeman (1982) Hoot, Meroney and Peterka (1973) Ermak (1990)	Integral	Horizontal or vertical jet or an area (or volume) /crosswind	Dense and passive cloud dispersion over flat terrain	Not recommended to terrains with any degree of complexities It should not be used to evaluate far field dispersion
ALOHA software	Turner (1970) Havens and Spicer (1985)	Integral	Horizontal or vertical jet / no crosswind	Dense and passive cloud dispersion over flat terrain	It does not evaluate the dispersion in the near field It was developed to calculate and display a cloud footprint in short time
Phast Risk software	UDM(Haper, 2009)	Integral	Instantaneous or continuous / jet in any direction / no crosswind	Dense and passive cloud dispersion over flat terrain	It is a comprehensive model, the equations used allow modelling the transition of the dense cloud to passive cloud

Type of tool	Models	Model type	Type of source term	Scenario	Key points
FLACS-(CFD)-software	RANS equations based on the standard k-ε model (GexCon AS, 2013)	Physical	Instantaneous or continuous releases jet / crosswind	Dense and passive cloud dispersion / terrain complexities	Obstacles such as pipes are represented as area and volume porosity in the geometry It is a specific model to evaluate dispersions and explosions
FLUENT (CFD) software	RANS equations and ten different turbulence models (Riddle et al., 2004)	Physical	Instantaneous or continuous releases jet / crosswind	Dense and passive cloud dispersion / terrain complexities	It is a comprehensive code that is capable to model a wide range of physical phenomena; however, modelling specific phenomenon is a laborious work
CFX (CFD) software	RANS equations and Boussinesq model to predict the turbulence (Cormier, Ruifeng, Yun, Zhang, & Mannan, 2009)	Physical	Instantaneous or continuous releases jet /crosswind	Dense and passive cloud dispersion / terrain complexities	It is a comprehensive code that is capable to model a wide range of physical phenomena; however, modelling specific phenomenon is a laborious work
FLUIDYN (CFD) software	RANS equations based on the standard k-ε model or based on k-l model (Mazzoldi et al., 2011)	Physical	Instantaneous or continuous releases jet / crosswind	Dense and passive cloud dispersion in short and medium range scales	It is not recommended for far field dispersions

The empirical and integral models treat terrain complexities by using a surface roughness parameter, which is a very imprecise approximation and is not suitable when local arrangement has barriers or present some degree of confinement. Predictions performed by empirical and the integral methods tend to overestimate the impacts in the far field and underestimate the impacts in the near field (Mazzold et al., 2008).

Although the CFD tools need more computational time, they allow taking into account the scenario complexities such as barriers or semi-confined spaces, and hence they are more suitable to model dispersion when a realistic/complex scenario has to be considered.

CFD tools have proven to be promising to perform consequences analysis in environments with complex geometry (Hanlin, 2006); however, there are still challenges to overcome. As shown by Plasmans et al. (2012), previous studies have showed that large differences may arise between the results when different tools and different CFD analysts to assess the same scenario are considered. The results of CDF simulations can be very sensitive to the wide range of computational parameters that must be set by the analyst (Plasmans et al., 2012); for a typical simulation, the user needs to select the variables of interest, the turbulence models to be used, the computational domain and mesh, the boundary conditions, the discretization methods and convergence criteria among others. During the last decades, sensitivity tests, verification and validation studies have been conducted to verify the influence of these parameters in computational simulations (Duijm et al., 1996; Ivings et al., 2007; Coldrick et al., 2009), but clear guidelines of how to appropriately set all these parameters to perform a reliable consequence analysis using CFD are still missing. Finally, it has to be noted that among the available CFD tools, there are some that have specific models for dispersion analysis implemented, whereas some others have a more general focus, which make their use more complicated when applied to study consequences of leakages of toxic/flammable substances.

Given the above-mentioned key issues to be initially considered when planning a cloud dispersion modelling study in complex environments, the main finding that arises from all of them is that FLACS software shall theoretically be the most appropriate tool to be used. It is a CFD tool that has specific models for consequence analysis, which shall allow the representation of physical barriers present into the dispersion path. Moreover, it has also coupled models to perform fire and explosions analysis which can be of interest when aiming to study secondary events that may take place in a cloud being dispersed when an ignition source is present. However, FLACS CFD software, as other codes alike, still needs to be fully validated. Furthermore, detailed recommendations of how to perform trustworthy dispersion analysis are lacking.

Thus, considering the goals exposed in section 1.4, FLACS is the selected CFD simulation tool to be used in this study. Next chapter includes a detailed description of its modelling structure followed by a preliminary validation exercise using historical data.

3 FLACS CFD SOFTWARE: DESCRIPTION AND PRELIMINARY VALIDATION ATTEMPTS

FLACS simulation CFD code is the tool selected in this study to provide new insights in cloud dispersion simulation. It is envisaged to have high performance when used for quantitative consequence analysis, but, as many other CFD codes, it is still subject to a validation process. In this chapter a detailed description of the code in terms of models implemented, geometry representation and numerical discretization schemes is first included. Following, a literature survey on already existing FLACS validation attempts is undertaken, and next, FLACS performance is deeply investigated using historical data. The conclusions of this chapter are shaped as preliminary guidelines for the correct use of CFD, and particularly of FLACS software, when used to undertake dispersion analysis of scenarios with some geometrical complexity.

3.1 FLACS simulation approach: models, numerical resolution and key variables

FLACS solves RANS equations based on the standard $k-\varepsilon$ model of Launder & Spalding (1974). It solves conservation equations for mass, mass fraction of species, energy and momentum using a finite volume method on a 3-D Cartesian grid, where complex geometries are represented by a porosity concept.

In this section first the geometry representation is explored; next the governing equations and turbulence are described; following, the boundary conditions and numerical schemes implemented on FLACS are detailed; and finally, input and output variables necessary to evaluate cloud dispersions using FLACS are summarized. Moreover, fundamental aspects of CFD modelling are gathered in Appendix A.

3.1.1 Geometry and grid representation

In order to solve the physics of the flow field, it is necessary to divide the flow domain in small subdomains, which implies the generation of a grid (or mesh) of cells also defined as control volumes. The geometry and size of these cells coupled with the numerical method used to solve the equations are crucial aspects when evaluating the accuracy and the

resolution time of a simulation. As presented by Thompson et al. (2010), in any CFD simulation grid cells must be sufficiently small to provide an accurate numerical approximation, but they cannot be so tiny in size that the solution is impractical to obtain. Thus, in most CFD tools, the mesh is refined in the regions of interest as around the main obstacles affecting the cloud dispersion and nearby the source terms (micro grid) and is smoothly increased to the prevailing grid (macro grid).

Generally, CFD meshes can be structured, meaning that the lines are based on coordinate directions, or unstructured i.e. with no relation with coordinate directions; in the first case the mesh consists of quadrilateral cells in 2D, or hexahedral cells in 3D, and the unstructured mesh usually consists of triangles in 2D and tetrahedral in 3D, but cells can be of any other forms if needed. Structured grids usually imply shorter resolution time, however the unstructured meshes may better represent the geometry and have been gaining popularity in recent years. A recent example of how to develop efficient computational analysis using unstructured grid can be found in Yasushi (2012). On the other hand, Luo & Spiegel (2010) propose a method to generate a hybrid mesh (coupling strutucred and unstructured grid). The basics concepts of grid generation can be found in Anderson (1995) and a detailed discussion about the influence of grid in CFD applications can be found in Thompson et al. (2010).

FLACS simulation software applies a structured Cartesian grid, in which the cells are hexahedral. It is a robust method that usually implies reduced resolution time. The mesh is composed of cubic or cuboid-shape cells which edges are horizontal and vertical lines, the set of cells form a single block. The mesh resolution can be adjusted in any Cartesian direction; however, it is not possible to build the mesh with inclined or curved lines (GexCon AS, 2013). The grid refinement in one region can lead to unnecessary refinement in other regions due to the single block approach applied in the software; however, this approach usually provides shorter simulation runtime. Figure 4 shows an example of grid representation in FLACS; the simulation volume consists of a single block composed by the macro grid (the prevailing cells), the micro grid (smaller cells in the central region of the volume), the smooth grid (transition area where the cells of the micro grid gradually increase until the macro grid) and the stretched grid (when is necessary save runtime simulation the grid may be stretched, the cells grow toward the limits).

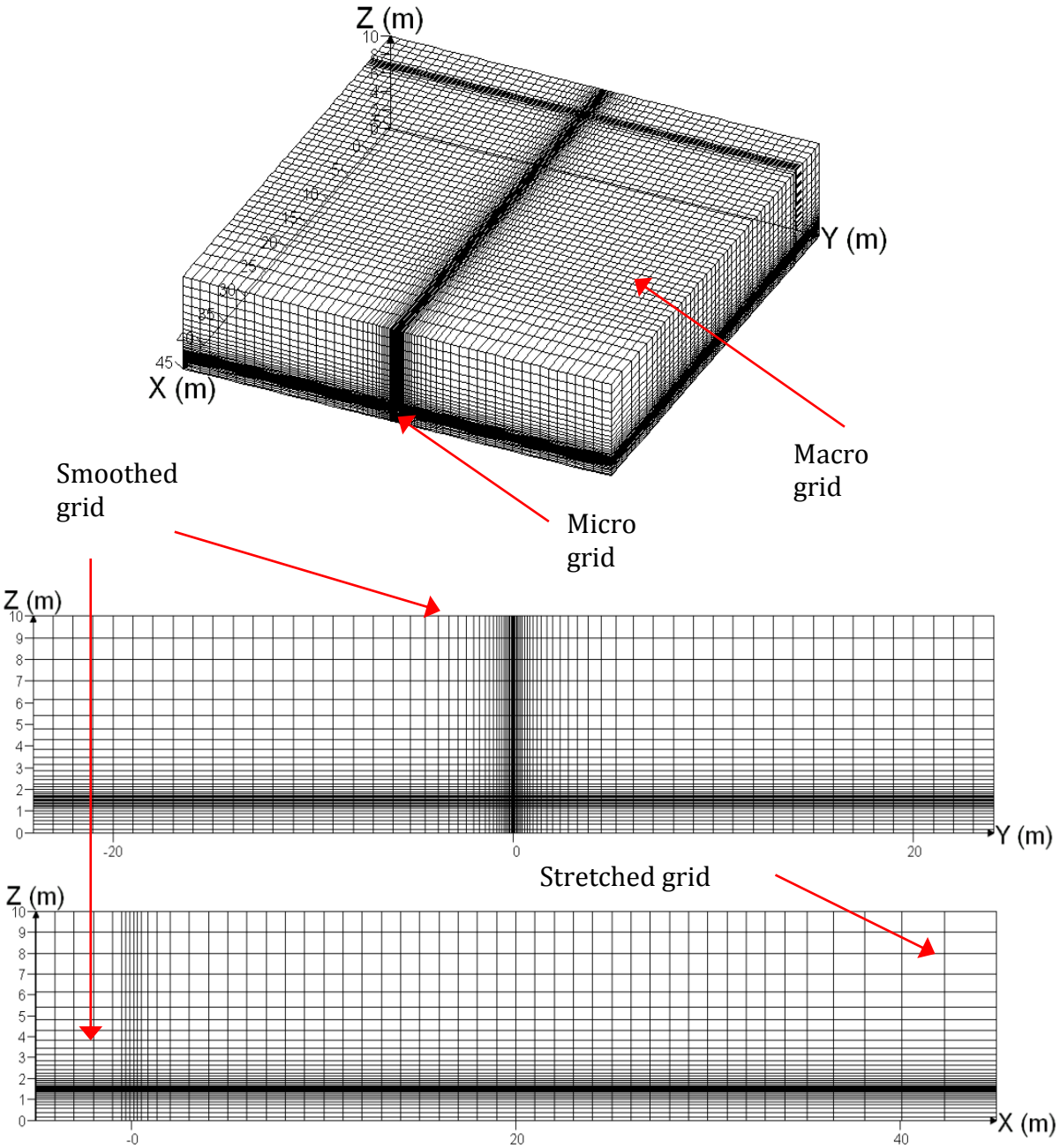

Figure 4 - Grid representation

It is important that all objects are well geometrically represented in the grid when evaluating the effects of the obstacles; even small objects, smaller than the grid, should be included since they all can affect significantly the results. Obstacles such as pipes are represented in FLACS defining a surface porosity on the control volume faces and a volume porosity referred to the interior of the control volume; the porosity is the fraction of the area or the volume that is accessible for a fluid to flow. There are three surface porosities to be

defined at each control volume, one for each inlet surface of the control volume (Arntzen, 1998). The porosity is represented by a value between 0 and 1, where 0 means that the control volume is completely blocked and 1 means that the control volume is completely unblocked (GexCon AS, 2013).

The porosity of a cell face has to be also established by taking into account the objects that the cell has inside. The final value of a surface porosity will be obtained by considering the smallest porosity of all the planes located between the centres of two adjacent cells. Figure 5 adapted from Arntzen (1998) shows an example of two adjacent cells containing blocks and cylinders smaller than the grid cell; the porosity in face *e* is actually 100%, however to take into account the effects of those small objects, the porosity in this face will be set as 50% (line *s*), since this is the value of the smallest porosity in any plane located between *P* and *W* (the centre lines of the grid cells).

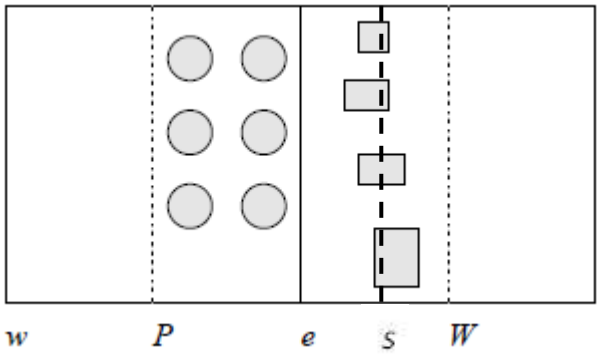

Figure 5 - Two cells containing sub-grid geometry
Source: Arntzen (1998)

The grid guidelines of FLACS recommends that the large objects (objects larger than 1.5 control volume) should be aligned with the grid lines, since the program that evaluates the porosities adjusts automatically the large objects to match with the mesh; and this can cause some undesired situations, like leak corners (i.e. if a wall is moved to match the closest grid line). For sloping cases a "staircase" representation is used. The objects will be adjusted to match the grid lines; however, in many cases, it is not possible to represent suitably the smaller objects in the grid, and thus these objects must be treated by subgrid models.

Subgrid objects (objects that are smaller than a grid cell) contribute to turbulence generation. With the presence of such tiny elements, the flow kinetic energy lost due to drag

forces is compensated as a source term for turbulent energy. In FLACS, the end surface contributions (the contribution of the additional source term) are calculated for objects smaller than two control volumes, thus the turbulence contribution due to subgrid obstructions is given by;

$$G_0 = C_0 \beta_v \rho |\vec{u}| u_i^2 f_i \tag{3}$$

Where u is velocity component, C_0 is a constant, f_i is a parameter of friction forces depending on subgrid objects, both calculated as presented by Hjertager (1992) and β_v is the volume porosity present in the next section.

Finally, the grid guidelines of FLACS recommend a four step procedure for dispersion analysis: to cover the computational domain with a uniform grid, to refine the grid in the region of the release, to smooth the grid between the micro and macro grid and to stretch the grid outside the main region towards the boundaries. Additionally, the guidelines suggest that a starting point of cell grids dimensions equal to 1-1.5 m can be used for structures higher than 8.5 m and equal to 0.5 m for lower structures. Moreover, for terrains with slope, the grid must be refined (in a range between 0.1 and 0.5 m) in vertical direction.

3.1.2 Governing equations

FLACS uses conservation equations for mass, energy, and momentum. It solves RANS equations based on the standard $k - \varepsilon$ model of Launder & Spalding (1974) presented in the next section.

As reported by Hjertager (1992), the presence of geometrical details affects the governing equations in two aspects: only a part of the total control volume is available for the flow and the solid objects cause additional resistance and turbulence to flow.

Considering the control volume in Figure 6, the volume fraction available for flow (volume porosity) can be defined as:

$$\beta_v = \frac{V_f}{V_f + V_s} = \frac{V_f}{\Delta x \Delta y \Delta z} \tag{4}$$

Where V_f is the fluid volume and V_s is the volume occupied by the obstacles.

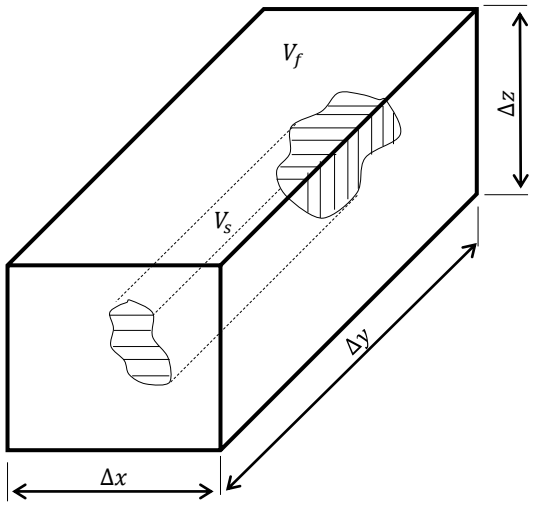

Figure 6 - Control volume partially occupied by solid.

The fraction of the surface available for the flow (surface porosity) in x direction can be defined by Eq. (5) and similarly to the others directions.

$$\beta_x = \frac{\int fluid\ surface\ dydz}{\Delta y \Delta z} \tag{5}$$

Then, the governing equations of the fundamental physical principles of fluid flow are implemented by applying this concept of porosity. As reported by Hjertager (1992), applying the principle of conservation of mass in the control volume of Figure 6 taking into account the geometry details, the mass conservation equation becomes:

$$\frac{\partial}{\partial t}(\beta_v \rho) + \frac{\partial}{\partial x_j}\left(\beta_j \rho u_j\right) = 0 \tag{6}$$

Where ρ is the density and u_j is the velocity component in y direction. This equation represents that the net mass flow out of the element must be equal to the time rate of decrease of mass inside the control volume (Anderson, 1995).

Taking into account the geometry details, the momentum conservation equation implemented in FLACS is based in the model reported by Hjertager (1992) and described as:

$$\frac{\partial}{\partial t}(\beta_v \rho u_i) + \frac{\partial}{\partial x_j}(\beta_j \rho u_i u_j) = -\beta_v \frac{\partial p}{\partial x_i} + \frac{\partial}{\partial x_j}(\beta_j \sigma_{ij}) + F_{0,i} + \beta_v F_{w,i} + \beta_v(\rho - \rho_0) g_{i,} \quad (7)$$

Where σ_{ij} is the stress tensor (turbulent flux of momentum at the control volume surface that is more detailed in section 3.1.3), $g_{i,}$ is the gravitational acceleration in the x_i direction, p is the pressure, $F_{0,i}$ is the resistance due to sub-grid obstructions (an additional resistance caused by obstacles inside the control volume) and $F_{w,i}$ is the resistance due to walls (the wall friction force) (GexCon AS, 2013).

And finally the energy conservation principle, that is based on the first law of thermodynamics, states that the rate of energy exchange (expressed in terms of enthalpy in Eq. (8)) is equal to the net rate of heat addition, plus the heat rate of work done, plus the rate of heat added or removed by a heat source. Thus, the energy conservation equation implemented in FLACS, with the effects of the detailed geometry, is given by:

$$\frac{\partial}{\partial t}(\beta_v \rho h) + \frac{\partial}{\partial x_j}(\beta_j \rho u_i h) = \frac{\partial}{\partial x_j}\left(\beta_j \frac{\mu_{eff}}{\sigma_h} \frac{\partial h}{\partial x_j}\right) + \beta_v \frac{Dp}{Dt} + \frac{\dot{Q}}{V} \quad (8)$$

Where h is the enthalpy, μ_{eff} is the effective viscosity, σ_h is the Prandtl-Schmidt number of enthalpy, $\dot{Q}$ is the heat rate added or removed and V is the volume.

In addition to the conservation equations of mass, momentum and energy, FLACS solves conservation equations of mass fraction (the fraction of fuel in the mixture of fuel, air and combustion products) and mixture fraction (that describe the degree of scalar mixing between fuel and oxidant) as described in Eqs. (9) and (10).

$$\frac{\partial}{\partial t}(\beta_v \rho \Upsilon_{fuel}) + \frac{\partial}{\partial x_j}(\beta_j \rho u_i \Upsilon_{fuel}) = \frac{\partial}{\partial x_j}\left(\beta_j \frac{\mu_{eff}}{\sigma_{fuel}} \frac{\partial \Upsilon_{fuel}}{\partial x_j}\right) + R_{fuel} \quad (9)$$

$$\frac{\partial}{\partial t}(\beta_v \rho \xi) + \frac{\partial}{\partial x_j}(\beta_j \rho u_i \xi) = \frac{\partial}{\partial x_j}\left(\beta_j \frac{\mu_{eff}}{\sigma_\xi} \frac{\xi}{\partial x_j}\right) \quad (10)$$

Where Υ_{fuel} is a mass fraction of chemical specie, σ_{fuel} is the Prandtl-Schmidt number for the fuel and R_{fuel} is the fuel reaction rate (the production rate by chemical reaction of the species inside the control volume). ξ is the fraction of the mixture and σ_{ξ} is the Prandtl-Schmidt number for the fraction of the mixture.

The Prandtl-Schmidt numbers are dimensionless numbers originally defined as the ratio of momentum diffusivity (viscosity) and mass and thermal diffusivity; they represent the diffusion of the corresponding variable compared to the dynamic viscosity. Table 4 gathers the Prandtl-Schmidt numbers considered in FLACS.

Table 4 – Prandtl - Schmidt numbers

σ_k	σ_ε	σ_h	σ_{fuel}	σ_ξ	σ_b
1.0	1.3	0.7	0.7	0.7	0.9

3.1.3 Turbulence model

In many practical scenarios, like the dispersion over complex terrain, there is turbulence present in the flow. This turbulence is due to shear stresses within the flow caused by fluctuations in velocity. Visualizations of turbulent flows show the presence of turbulent eddies (rotational flow structures) of many different length and velocity scales. The length and velocity of largest eddies are of the same order of magnitude of the length and velocity of the mean flow, which indicates that these eddies are dominated by inertia effects; these eddies tends to breed new instabilities within the flow and thus to create small eddies. Energy is transferred from the largest to smallest eddies until they become very small and hence dominated by viscous effects.

In atmospheric flows, turbulence is the dominant mechanism in the mixing and dilution of the material released and can lead to fluctuations in important flow properties such as density, temperature, and concentration (Sklavounos and Rigas, 2004).

In order to evaluate accurately a turbulent flow using only the governing equations presented in the previous section, it would be necessary a very dense grid, with cell sizes of the smallest eddies formed. This would require a huge and often impractical number of cells.

Therefore, turbulence models are implemented, which consist of a set of differential and algebraic equations that coupled with the governing equations simulate the turbulent flows.

As presented by Salas (1999), Warnatz et al. (2001) and more recently by Yeoh and Yuen (2009), there are three different approaches to deal with turbulence: the conventional models (Reynolds-Averaged Navier-Stokes - RANS and Favre-Averaged Navier-Stokes - FANS), Direct Numerical Simulation (DNS) and Large Eddy Simulation (LES). The DNS approach solves directly the governing equations without taking any averaging or approximation except those needed to apply the discretization method; therefore DNS provides a comprehensive description of the flow. However, this approach requires a grid with cells small enough to capture each significant effect of the turbulence, which implies huge computational resources often unavailable.

As an alternative to minimize the computational cost, the LES approach views the turbulence motions in two scales: large and small. LES treats the large scale motions exactly as in the DNS approach and use approximations to treat the small scale motions (the details about the motion scales are presented by Pope (2000) and a complete description of the DNS and LES approaches can be found in Yeoh and Yuen (2009)). Although the LES approach requires less computational recourses than DNS, it still requires significant resources. The conventional approach by RANS and FANS equations that resolves only the mean flow and evaluates the turbulence by sub models (saving computational resources) is the most used nowadays.

In the conventional approach the properties of the flow (such as density and velocity) are calculated for the mean values of the flow properties, in other words, the governing equations described in previous sections are averaged and solved for the mean values; thereby RANS equations are obtained, and with some simplifications for compressible flows, the FANS equations are also expressed.

Both RANS and FANS equations present unknown variables (associated with energy flux and viscous forces) in momentum and energy equations. These variables can be estimated using particular turbulence sub-models; there are many sub models available in the literature, such as the models proposed by Shih et al., (1995), Chien, (1982) and Wilcox, (1998). The most applied approach in the current CFD tools consists of the RANS equations coupled with standard $k - \varepsilon$ sub-model (or some variation of it) proposed by Launder and Spalding (1974).

The standard $k-\varepsilon$ model of Launder and Spalding (1974) evaluates the turbulence by the magnitudes of two turbulence quantities: the turbulent kinetic energy k and its dissipation rate ε; they are calculated from transport equations solved simultaneously with those governing the mean flow behavior. According Launder and Spalding (1974) the conservation equations that determine the distribution of k and ε are:

$$\frac{\partial(\rho k)}{\partial t}+\frac{\partial}{\partial x_j}\left(\rho u_j k\right)=\frac{\partial}{\partial x_j}\left(\frac{\mu_{eff}}{\sigma_k}\frac{\partial k}{\partial x_j}\right)+G-\rho\varepsilon \tag{11}$$

$$\frac{\partial(\rho \varepsilon)}{\partial t}+\frac{\partial}{\partial x_j}\left(\rho u_j \varepsilon\right)=\frac{\partial}{\partial x_j}\left(\frac{\mu_{eff}}{\sigma_\varepsilon}\frac{\partial \varepsilon}{\partial x_j}\right)+C_1\frac{\varepsilon}{k}G-C_2\rho\frac{\varepsilon^2}{k} \tag{12}$$

Where σ_k and σ_ε are the Schmidt numbers, C_1 and C_2 are also constants equals to 1.44 and 1.79 respectively (all constants obtained from examination of turbulent flows, presented by Launder and Spalding (1974)), G is the rate of turbulence and μ_{eff} is the effective viscosity given by the sum of the laminar and turbulent viscosity:

$$\mu_{eff}=\mu+\mu_t \tag{13}$$

The laminar viscosity depends on the substance and the turbulent viscosity μ_t is obtained by:

$$\mu_t=C_d\rho\frac{k^2}{\varepsilon} \tag{14}$$

Where C_d is constant equal to 0.09, as specified in Launder and Spalding (1974).

The equations of the turbulence model (in case of the $k-\varepsilon$ model: Eq (11) and (12)) coupled with the RANS equations and with the boundary conditions provide the fluid flow description.

As presented by Middha et al. (2009), FLACS solve the RANS equations based on the standard $k-\varepsilon$ model of Launder and Spalding (1974); however, there are some modifications in the model implemented on FLACS (Hjertager (1992) and Arntzen (1998)): the modified model allows the consideration of the turbulence generated by subgrid objects, allows the inclusion of a wall function and finally permits the inclusion of source terms to represent the

turbulence generated by Rayleigh-Taylor instabilities (instabilities created on the boundary between two fluids of different densities).

The conservation equations that determine the distribution of k and ε (Eq. (11) and Eq.(12)), after the modifications implemented in FLACS, are given by:

$$\frac{\partial(\beta_v \rho k)}{\partial t} + \frac{\partial}{\partial x_j}\left(\beta_j \rho u_j k\right) = \frac{\partial}{\partial x_j}\left(\beta_j \frac{\mu_{eff}}{\sigma_k}\frac{\partial k}{\partial x_j}\right) + \beta_v P_k - \beta_v \rho \varepsilon \tag{15}$$

$$\frac{\partial(\beta_v \rho \varepsilon)}{\partial t} + \frac{\partial}{\partial x_j}\left(\beta_j \rho u_j \varepsilon\right) = \frac{\partial}{\partial x_j}\left(\beta_j \frac{\mu_{eff}}{\sigma_\varepsilon}\frac{\partial \varepsilon}{\partial x_j}\right) + \beta_v P_\varepsilon - C_2 \beta_v \rho \frac{\varepsilon^2}{k} \tag{16}$$

Where β_v and β_j are the volume and surface porosity, C_2 is constant and equal to 1.92 (GexCon AS, 2013), P_k is the turbulent kinetic energy and P_ε is the production of dissipation.

Considering the flow shear stresses G_s, the wall shear stresses G_w, the buoyancy force G_b and turbulence due to subgrid objects G_o (Eq. (3)), P_k is given by:

$$P_k = G_s + G_w + G_b + G_o \tag{17}$$

And P_ε by:

$$P_\varepsilon = C_1 \frac{\varepsilon}{k} P_k (1 + C_3 R_f) \tag{18}$$

Where C_1 and C_3 are constants equal to 1.44 and 1.33 respectively (GexCon AS, 2013) and R_f is the buoyancy term given by:

$$R_f = \frac{G_b}{P_k}\frac{|\vec{u} \times \vec{g}|}{|\vec{u}||\vec{g}|} \tag{19}$$

Additionally, the turbulence model allows to estimate the stress tensor σ_{ij} present in Eq. (7):

$$\sigma_{ij} = \mu_{eff}\left(\frac{\partial u_i}{\partial x_j} + \frac{\partial u_j}{\partial x_i}\right) - \frac{2}{3}\delta_{ij}\left(\rho k + \mu_{eff}\frac{\partial u_k}{\partial x_k}\right) \tag{20}$$

Where:

$$\delta_{ij} = \begin{cases} 1 & if\ i = j \\ 0 & if\ i \neq j \end{cases} \tag{21}$$

The turbulent kinetic energy and it dissipation rate present large variation in the region near the walls and obstructions surfaces, then the numerical solution for this region requires large computational resources. In order to simulate this region, the wall functions are used to model the turbulent parameters in the wall point (the point closest to the wall where the transport equations are solved). Thus, as reported in GexCon AS (2013) the turbulent kinetic energy G_w is given by:

$$G_w = \begin{cases} 0 & if\ y^+ < 11 \\ \dfrac{2\tau_w^2 ln\left(\dfrac{y^+}{11}\right)}{y_{cv}\rho\kappa C_\mu^{1/4} k^{1/2}} & if\ y^+ \geq 11 \end{cases} \tag{22}$$

Where τ_w is the wall shear stress, y_{cv} is the distance from the wall point to the wall, C_μ is constant equals 0.09 and y^+ is a dimensionless wall distance defined by:

$$y^+ = \frac{\rho C_\mu^{1/4} k^{1/2} y}{\mu} \tag{23}$$

And finally, the term G_b which represents the third modification included on FLACS, of the inclusion of source terms to represent the turbulence generated by Rayleigh-Taylor instabilities:

$$G_b = -\frac{1}{\rho}\frac{\mu_{eff}}{\sigma_b} g_i \frac{\partial \rho}{\partial x_i} \tag{24}$$

3.1.4 Boundary conditions

The boundary and initial conditions of the flow dictate the particular solution obtained from the governing equations; in FLACS the user must specify the boundary conditions for

the outer boundaries of the simulation domain. The FLACS manual recommends four boundary conditions alternatives: Euler, nozzle, plane wave and wind.

The first tree options (Euler, nozzle and plane wave) are used for explosions scenarios that are out of the scope of this work; the wind boundary condition is recommended for dispersion analysis.

The wind boundary condition models an external wind field; the velocity and turbulence profiles at the boundaries have to be defined, these profiles are calculated by FLACS from the speed and direction of the wind at a specific height and from the turbulence parameters. As presented in item 3.1.3, the turbulence parameters are the turbulent kinetic energy k and its dissipation rate ε; these parameters are calculated in FLACS by the relative turbulence intensity I_T and turbulence length scale l_{LT} or by the Pasquill class (Dharmavaram et al. 2005). The relative turbulence intensity I_T and turbulence length scale l_{LT} can be set manually by user and then, in order to estimate the turbulence parameters, equations (25) and (26) are used (GexCon AS, 2013).

$$I_T = \left(\frac{3}{2k}\right)^{1/2} \frac{1}{U_0} \tag{25}$$

Where U_0 is the mean flow velocity.

$$\varepsilon = \frac{C_\mu k^{3/2}}{l_{LT}} \tag{26}$$

If the Pasquill class is known instead of the relative turbulence intensity and turbulence length scale, first the Monin-Obukhov length is estimated by Eq. (2) and Table 2, then the wind velocity profile is defined as:

$$U(z) = \begin{cases} \dfrac{u^*}{\kappa} \ln\left(\dfrac{(z - z_d) - z_0}{z_0}\right) - \psi_u(z) & if\ z_0 > 0 \\ U_0 & if\ z_0 = 0 \end{cases} \tag{27}$$

Where z_d is the canopy height (the height above the ground where the boundary layer actually starts, for example due to the presence of trees in the field that influences the wind profile); z_0 is the roughness length and u^* is the friction velocity, given by:

$$u^* = \frac{U_0 \kappa}{\ln\left(\frac{\left(z_{ref} - z_d\right) + z_0}{z_0}\right) - \psi_u(z_{ref})} \tag{28}$$

Where z_{ref} is the reference height for wind velocity (the height relative to the ground where the velocity of the wind profile is equal to the wind speed known) and $\psi_u$is given by:

$$\psi_u(z) = \begin{cases} 0 & if\ L = 0 \\ 2\ln\left(\frac{1+\vartheta}{2}\right) + \ln\left(\frac{1+\vartheta^2}{2}\right) - \arctan(\vartheta) + \frac{\pi}{2} & if\ L < 0 \\ -17\left(1 - exp\left(-0{,}29\frac{z}{L}\right)\right) & if\ L > 0 \end{cases} \tag{29}$$

Where:

$$\vartheta = (1 - 16z/L)^{1/4} \tag{30}$$

At this stage, the set of equations proposed by Han et al. (2000) are used to define the turbulent kinetic energy k and its dissipation rate ε; these equations were proposed based on previous studies of different authors and experimental data (Monin & Obukhov, 1954; Deardorff, 1972). For unstable stability classes, the parameter that most contributes to the instability is the mean surface heat flux, thus, considering the heat velocity w^*, the turbulence parameters are given by:

$$k(z) = \begin{cases} 0.36w^{*2} + 0.85u^{*2}\left(1 - 3\frac{z}{L}\right)^{2/3} & if\ z \le 0.1h \\ \left(0.36 + 0.9\left(\frac{z}{h}\right)^{2/3}\left(1 - 0.8\frac{z}{h}\right)^2\right)w^{*2} & if\ z > 0.1h \end{cases} \tag{31}$$

And:

$$\varepsilon(z) = \begin{cases} \frac{u^{*3}}{\kappa z}\left(1 + 0.5\left|\frac{z}{L}\right|^{2/3}\right)^{3/2} & if\ z \le 0.1h \\ \frac{w^{*3}}{h}\left(0.8 - 0.3\frac{z}{h}\right) & if\ z > 0.1h \end{cases} \tag{32}$$

For stable and neutral conditions the main influence on turbulence comes from the friction velocity and the Monin-Obukhov length, thus the turbulence parameters are obtained by:

$$k(z) = \begin{cases} 6u^{*2} & if\ z \leq 0.1h \\ 6u^{*2}\left(1 - \left(\frac{z}{h}\right)^{7/4}\right) & if\ z > 0.1h \end{cases} \quad (33)$$

And:

$$\varepsilon(z) = \begin{cases} \frac{u^{*3}}{\kappa z}\left(1.24 + 4.3\frac{z}{L}\right) & if\ z \leq 0.1h \\ \frac{u^{*3}}{\kappa z}\left(1.24 + 4.3\frac{z}{L}\right)\left(1 - 0.85\frac{z}{h}\right)^{3/2} & if\ z > 0.1h \end{cases} \quad (34)$$

Concluding, the turbulence profiles at the boundaries are calculated from the turbulence parameters, which are defined directly by the relative turbulence intensity and turbulence length scale using Eq. (25) and (26) or from de Pasquill class; using Eq. (31) and (32) to unstable classes and Eq. (33) and (34) to stable an neutral classes.

3.1.5 Numerical schemes

FLACS uses a finite volume method (described on Appendix A) to solve the conservation equations and defines the time stepping for the simulations by two dimensionless parameters: the Courant-Friedrich-Levy number based on sound velocity (CFLC) and the Courant-Friedrich-Levy number based on fluid flow velocity (CFLV). These parameters were proposed in order to define the time step of the simulation ensuring that the numerical solution remained stable (Anderson, 1995). They link the simulation time step with the size of the control volume.

The CFLC correlates the velocity of the sound with the dimension of the control volume to specify the time step; each time step is chosen such that the sound waves may propagate only until a specific distance, which is the averaged control volume length multiplied by the CFLC. Whereas the CFLV correlates the velocity of the flow with the dimension of the control volume; each time step is chosen such that the fluid may propagate also a limited distance, which is the averaged control volume length multiplied by the CFLV (GexCon AS, 2013).

Usually in dispersion simulations, the time step imposed by the CFLC is dominant since the flow velocities are low; on the other hand, the time step imposed by the CFLV is dominant in simulations involving explosions, in which, after the explosion, the flow velocities are high.

The FLACS manual recommends a CFLC of 20 and a CFLV of 2 and alerts that any change in these parameters may compromise the solution. FLACS guidelines also state that a sensitivity analysis could be necessary. Additionally, GexCon AS (2013) reports that the CFLC can be increased by the factor of grid refinement near the leak, i.e. if the region near the leak is refined by a factor of 3, the CFLC could be 60.

3.1.6 Input variables

The inputs in the CFD dispersion simulations are the geometry, the grid, the scenario and the simulation parameters. In FLACS, the geometry can be defined directly or may be imported from a CAD (Computer Aided Design) system; the grid is Cartesian; the scenario parameters cover both initial conditions and boundary conditions of the domain and finally there are the simulation parameters, which characterize the modelling. The simulation parameters are used to define aspects of the computational treatment of the model; they will define items such as time step used in the simulations, time period simulated, output variables of interest, initial constants used in the turbulence model and features of the graphs generated with the output variables. Table 5 presents the parameters related to the scenario (initial conditions and boundary conditions) and a brief description of each one.

Table 5 - Scenario conditions

Parameter	***Unit***	***Description***
Ambient temperature	ºC	Ambient temperature in the domain
Ambient pressure	bar	Ambient pressure in the domain
Ground roughness	m	Ground roughness in the domain
Wind speed at reference height	$m.s^{-1}$	Wind velocity at a specific elevation
Reference height	m	Height relative to the ground where the velocity of the wind field is equal to the wind speed
Wind direction	º	Prevailing direction of the wind
Pasquill Class	-	Atmospheric stability class
Relative humidity	%	Relativity humidity of the air
Spill duration	s	Discharge duration
Estimated expanded leak area	m^2	Estimated expanded leak area in case of jet release; This is

Parameter	*Unit*	*Description*
		the jet area expected after the expansion at ambient pressure, assuming ideal gas. It is estimated by the Jet utility program of FLACS
Mass flow	$kg.s^{-1}$	Flow rate of the leak
Release temperature	ºC	Flow temperature at moment of the release
Release pressure	bar	Flow pressure at moment of the release
Start time	s	Instant at which the leak starts
Discharge direction	-	Jet direction
Discharge height	m	Height of the release point
Volume fractions	-	Volume fractions of species that constitute the mixture released
Equivalent ratios	-	A measure of the concentration of fuel compared to the stoichiometric concentration.

Table 6 presents the simulation parameters and a brief description of each one. These parameters can influence directly the results of simulation (i.e. the estimation of the flow field properties) or affect only the amount of data stored after the simulation and also the form in which the output variables are represented (e.g. graphs with smaller or bigger time intervals).

Table 6 - Simulation conditions

Parameter	*Unit*	*Description*
Monitor points	-	User-defined locations in the simulation domain where one or more variables are monitored during the simulation.
Single field 3D output	-	In the list of possible outputs available in FLACS, this option is used to choose the output variables of interest and thus define the variables that have their values as a function of time and space stored during simulation.
Maximum time of simulation	s	The simulation will last this maximum time interval.
CFLC	-	Courant-Friedrich-Levy number based on sound velocity, used to define the time step of dispersion simulation.
CFLV	-	Courant-Friedrich-Levy number based on fluid flow velocity, used to define the time step of explosion simulation.
Wind buildup time	s	Time stipulated for the boundaries velocities to rise from zero to wind speed. A value larger than zero gives a smooth start of the simulation.
Characteristic velocity	$m.s^{-1}$	Initial value of velocity used in eq. (25) to find values for initial turbulence fields.
MODD	$units.s^{-1}$	Frequency of data storage. It determines how often data for scalar-time plots are stored at the results file during a simulation.
DTPLOT	s	Time interval for field output, i.e. the time between the output plots.

3.1.7 Output variables

There is a large range of outputs available on FLACS; however, the program will not register all the possible outputs during the simulation, since it would make the simulation time too large. Thus, it is necessary to define the variables of interest before starting the simulation. The output data from the simulation is mostly presented in the postprocessor as 2D graphs and 3D animations, although there are also output text files with the results of the simulation according to the variables of interest chosen. Table 7 presents the main outputs for dispersion analysis, the complete set of outputs can be consulted in GexCon AS (2013).

Table 7 - Output variables

Variable	*Unit*	*Description*
FUEL	-	Gas mass fraction inside the volume defined as the monitoring region.
FMOLE	$m^3.m^{-3}$	Fraction of gas in the gas/air mixture.
T	K	Vapour temperature.
VVEC	$m.s^{-1}$	Velocity vector of the gas.
ER	-	Equivalence ratio, which is a measure of the concentration of fuel compared to the stoichiometric concentration.

3.2 Literature survey on historical data and first FLACS validation attempts

The validation process intends to verify by a structured comparison of simulated values with experimental data how closely the mathematical model agrees with the reality. With the increase of the use of complex models, the concern about the quality of validations also increases. Duijm et al. (1996) performed an evaluation of validation procedures for dense gases simulations and proposed a set of statistic performance measures, which should indicate if the model over or under predicts the values and also the level of scatter of the results. Based on these guidelines, many studies have been made in order to improve the validation procedure; for example, the Heavy Gas Dispersion Expert Group set up by Europe Commission incorporates the use of these statistic performance measures in their protocol to assess heavy gas dispersion models (Duijm et al., 1997).

More recently, Ivings et al. (2007, 2013) and Coldrick et al. (2009) have treated specifically the assessment of LNG vapour dispersion models. They have come up with the

Model Evaluation Protocol (MEP) to guide the validation process of LNG dispersion models and additionally they have created a LNG Model Validation Database which contains experimental data to be used during the evaluation of the MEP.

In the present section, a review of avaialble experimental data suited for validation of dispersion studies is presented and following, a review of studies of FLACS validation available on the literature is discussed.

3.2.1 Survey of experimental data to perform CFD models validation

Most of the field tests reported in the literature involve LNG dispersions, since an extensive experimental effort was conducted during the decades of 70 and 80 regarding to the behaviour of LNG when accidentally released. Recently, with the renewed interest, analytical studies addressing the possible consequences associated with a spill of LNG on water have been also performed (Hanlin, 2006). A smaller proportion of field tests involving other substances such hydrogen or tracer gases, have been also undertaken in this period in order to study the dispersion phenomenon. Table 8 shows the most important field tests found in the literature.

Table 8 - Field tests involving gas dispersion

Field test name	Year	Substance	Obstructed (O) /unobstructed (U)	Reference
Prairie Grass	1958	Sulphur dioxide	U	(Barad, 1958)
Thorney Island	1971 1981	Freon 12 and nitrogen	U	(McQuaid and Roebuck, 1985)
Esso	1973	LNG	U	(Hanlin, 2006)
Shell	1974	LNG	U	(Hanlin, 2006)
Maplin Sands	1980	LNG and propane	O	(Blackmore, Eyre and Summers 1982)
Burro	1980	LNG	U	(Koopman et al., 1982)
NASA-White Sands	1980	Hydrogen	U	(Witcofski and Chirivella, 1981)
Coyote	1983	LNG	U	(Goldwire et al., 1983)

Field test name	Year	Substance	Obstructed (O) /unobstructed (U)	Reference
Falcon	1987	LNG	O	(Brown et al., 1990)
Kit Fox	1995	Carbon dioxide	O	(Hanna and Chang, 2001)
CEC - Riso National Laboratory	1996	Ammonia	U	(Nielsen et al., 1997)
Gaz de France	2001	LNG e GLP	O	(Butler and Royle, 2001)
MUST	2001	Tracer gas	O	(Biltoft, 2001)
MID05	2005	Tracer gas	O	(Allwine and Flaherty, 2007)
MKOPSC	2007	LNG	O	(Cormier et al., 2009)
Jack Rabbit	2010	Ammonia	U	(Hanna et al., 2012)

Among the experimental tests performed during the decades of 70 and 80, the two most frequently used to validate dispersion models are the Falcon and the Burro series (reported by Koopman et al. 1982 and Brown et al. 1990 respectively. Both tests consisted of LNG spills; the Burro tests were undertaken on an open area without obstacles whereas the Falcon tests were performed in a terrain with obstacles. These tests have been extensively used for models validation (Gavelli et al., 2008; Hansen et al., 2010); however, it is important to note that the tests were made decades ago, when the range of measurement and data logging equipment was not as comprehensive as nowadays and therefore data available from these tests is scarce for an overall CFD validation exercise.

From the table above, one can also notice that there has been an increased interest in field tests from 2000, but the available data of these experiments is also limited. Tests conducted by the company Gaz de France and Associates (Butler and Royle, 2001) consisted of dense gas dispersion in an environment with obstacles. However, the study of the cloud dispersion was not their main focus, since it was actually the study of flash fires. Thus, despite providing interesting data, there is not much about dispersion, since in most trials the cloud was ignited just a few seconds after the gas release. Tests MUST, MID05 and MKOPSC were carried out by a consortia involving private companies. Therefore, only a small portion of the collected data is publicly available through published reports, which hampers its use to perform

validation studies. Finally, the Jack Rabbit test conducted in 2010 (Hanna et al., 2012) shows the behavior of the dispersion of an ammonia cloud generated by an instantaneous release; and although it is rated as a test with obstruction, its scenario is very restricted, since the obstruction is just the result of the terrain depression.

A literature review of the field test shows that the data related to the dispersion in an environment with obstacles are scarce; large part of the tests were performed long time ago and therefore the range of data generated is limited, on the other hand, mostly of the data obtained with the recent tests are not available for the open public. Therefore, new experiments particularly designed for intensive CFD validation purposes are needed, being those one of the main objectives of the present work.

3.2.2 Review of existing FLACS validation studies

The CFD tool FLACS was created initially to model explosions; therefore, there are many validation studies involving explosion scenarios (Hjertager et al., 1988 and Skjold et al., 2006). However, the software ability to perform dispersion analysis is more recent, and hence less validations in this sense are found in the literature.

Hanna et al. (2004) present a validation study for air quality models in which simulated values by FLACS are compared with experimental data of the field tests Kit Fox, MUST and Prairie Grass and with data coming from a wind tunnel experiment. The object of study was the maximum concentration present on the monitored region around buildings and other large roughness obstacles. Brief descriptions are presented about the experiments and about the source term modelling; however, there are no details about the grid domain or the size of the cells. It is also unclear whether the regions around some of the obstacles present are refined in the grid or whether the subgrid models are used to solve these areas. In order to determine if the performance of the model is acceptable, they define that the simulated values should have at least 50% of the predictions within a factor of two of the observations. Furthermore, they consider that a relative mean bias should be within a range of ±30% and that the relative scatter should be of a factor of three; according to these criteria, they end up saying that FLACS performance is acceptable.

Later, Hanna et al. (2006) present a model validation of five CFD tools (including FLACS) involving urban dispersion field tests undertaken in Manhattan in 2005 (Allwine and Flaherty

2007). In this test a tracer gas was released and air velocity and gas concentration were measured within an urban area with many buildings. Qualitative results and plots of velocity are presented; however, none quantitative data is given. Details about the simulation parameters, grid and domain are also not presented.

Hansen et al. (2007) present the results of a validation exercise in which trials of the field experiments Burro, Coyote and Maplin Sands were used. The details about the simulation set-up are not avaialble, there is no information about the the grid genaration and the results are presented in a general way: they afirm that "in general, good simulation results are seen". In a much more comprehensive study, Hansen et al. (2010) present the results of a validation exercise performed with the set of experiments (Burro, Coyote, Thorney Island, Falcon and Maplin Sands) recommended by the Model Evaluation Protocol for LNG vapour dispersion models (MEP) proposed by Ivings et al. (2007) and rewied by Coldrick et al. (2009). Hansen et al. (2010) provide much more information about the simulation process and the scenarios applied; however, the simulated parameters such as those presented in section 3.1.6 are not described, and hence the reproduction of the results is not possible. Statistical parameters such as mean relative bias, geometric variance and mean relative square error are used to verify the ability model to provide realistic predictions. According to the results, the model is considered adequate forLNG dispersions.

Middha et al. (2009, 2011) present validation studies for hydrogen dispersion; the former reports results of a validation exercise carried out by the International Association for Hydrogen Safety (HySafe) from the European Union and the International Energy Agency (IEA). The results are presented in a qualitative way and, in general, the model presents good agreement with the experimental measures. However, there is no information about the model set-up. In the second study, some experiments carried out by NASA involving liquefied hydrogen releases are simulated and good agreement between measured and simulated values is achieved. Additionally, a sensitive analysis of atmospheric stability classes is performed, in which these parameters are found to be sensitive, i.e. to have a significant influence on the results.

In summary, the validations studies reported for FLACS present essentially only qualitative results and do not provide enough information for a comprehensive quantitative

performance assessment. Moreover, most of the studies do not provide sufficient information about the grid generation and the simulation parameters.

3.3 Investigation of FLACS performance using historical data

Although the literature survey has shown some experimental data available for validation studies, none of the works already analysed include comprehensive exercises giving new insights of how to perform accurate CFD simulations nor giving precise rates of FLACS performance. In order to overcome these issues, in this section, FLACS predictive capacity is initially explored using different sets of historical data. Next, the reproducibility of FLACS results and the grid dependence is investigated and finally a sensitivity analysis is performed in order to detect the most critical input variables whose uncertainty may have a larger impact on the simulation results.

3.3.1 Preliminary FLACS performance tests using historical data

This section compares experimental data of the Burro and Falcon series, reported by Koopman et al. (1982) and Brown et al. (1990) respectively, with simulations obtained using FLACS. These two experimental series were chosen due to the availability of the data and, because both series present the dispersion of the same substance; the Burro series present a LNG release over flat terrain and the Falcon series over a terrain with barriers. The results presented here are also partially reported by Schleder and Martins (2013).

The HSE in the MEP recommends four trials of the Burro series for model validation purposes, trials 3, 7, 8 and 9 (Ivings, 2007). The trials simulated here are the same recommended by MEP, except for trial 8 which was discarded since the weather conditions were not totally defined. Concerning to the Falcon series, the MEP recommends three trials for validation purposes, trials 1, 3 and 4; thus the trials simulated are the same recommended by MEP.

Burro series simulation

The Burro series experiments were conducted in the Naval Weapons Center, China Lake, California. The data about Burro series is presented by Koopman et al. (1982). The experiments consisted of a LNG spill onto a 58 m diameter water pound whose surface was at 1.5 m above the ground level and the water depth was approximately 1 m (a 58 m diameter

bund). The LNG was spilled by a splash plate on the water surface to get a LNG flow horizontally across the water. To measure the concentration cloud, gas sensors were placed radially at 57 m, 140 m, 400 m and 800 m from the release point. Parameters used in this study are presented in Table 9. In trial 3, Pasquill stability class was modified from B (experimental) to D (simulated) because the current version of FLACS may become unstable with such atmosphere condition (this problem was reported previously by Hansen, 2010).

Table 9 - Initial conditions of Burro series

Parameter	Trial 3	Trial 7	Trial 9
Volume [m^3]	34.6	39.4	25.3
Duration of spill [s]	167	174	79
Wind speed [$m.s^{-1}$]	5.4	8.4	5.7
Atmospheric pressure [kPa]	94.8	94.0	94.0
Air temperature [ºC]	33.8	33.7	35.4
Relative humidity	0.052	0.074	0.144
Pasquil Stability	B	C/D	D
Roughness length [m]	0.0002	0.0002	0.0002
Bund diameter [m]	58	58	58

Grid was specified using an orthogonal base defined by the axes X, Y and Z; the Y direction is the horizontal and parallel to wind, the X direction is the perpendicular to wind and horizontal and Z direction is the vertical direction. The computational domain extended 160 m in the X direction (symmetric crosswind plan), 500 m in the Y direction (from 40 m upwind to 460 m downwind) and 10 m in the Z direction. This domain was discretized using a regular Cartesian grid of cubic cells of 1 m side.

However, the grid was refined in the area near the leakage: in the Y direction, the length of the cells was reduced to 0.5 m in the region between 30 m in the upwind direction and 30 m in the downwind direction of the leakage point. Additionally, the grid was stretched away from the leakage point (the length of cell growing continuously at a rate of 1.15 times the previous cell size with increasing distance from the source): in X direction, the cells were stretched after 40 m from the leakage point; in the Y direction, they were stretched after 400 m in the upwind direction; and in Z direction, after 6 m above the surface. These adjustments

were made such that the dimensions of the cells were of the same order of magnitude recommended in a similar analysis by FLACS manual (FLACS 2013).

Concerning the results obtained, the values estimated by the CFD-model fit well within the factor of 2 range (recommended for validation threshold by MEP (Coldrick et al., 2009)). Figure 7 shows the correlation between the maximum concentrations measured at the height of 1 m (in different distances from the release point) and the maximum concentration values obtained by simulation; the area between the dashed lines is the range of factor 2. To reduce the computational time, only the values related to the arcs at 57 m, 140 m and 400 m from the release point were used in this analysis; the values for the arc at 800 m were not analysed.

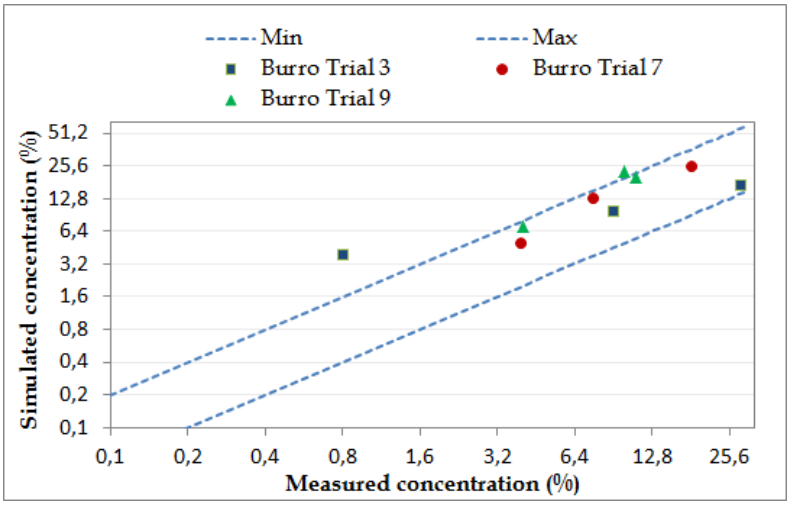

Figure 7 - Burros series results

Falcon Series Simulation

The Falcon series consisted of LNG spills up to 66 m^3 onto a 40 x 60 m water pound limited by a fence. The set-up was equipped with a water circulating system to maximize the LNG evaporation; tests were conducted at Frenchman Flat, on the Nevada Test Site (Brown 1990).

The LNG was released by four pipes fitted with splash plates. The fence around the pound was 44 x 88 m and was raised to a height of 8.7 m. There was also a 17.1 m wide barrier placed inside the fence, raised to a height of 13.3 m, upwind of the pound to generate turbulence typical of a storage tank (Figure 8). To measure the concentration cloud, 57 gas sensors were placed radially at 50 m, 150 m, and 250 m from the release point. The detailed

description of the Falcon series is presented by Brown et al. (1990) and the parameters used to perform the simulations are presented in Table 10.

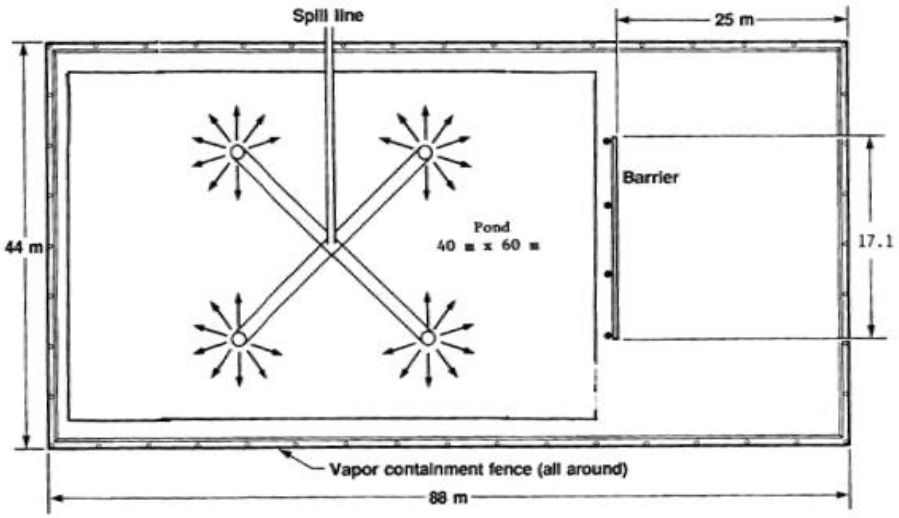

Figure 8 - Representation of discharge area of Falcon series
Source: Brown et al. (1990)

Table 10 - Initial conditions of Falcon series

Parameter	Trial 1	Trial 3	Trial 4
Volume [m^3]	66.4	50.7	44.9
Duration of spill [s]	131	154	301
Wind speed [$m.s^{-1}$]	2.2	4.53	5.93
Atmospheric pressure [kPa]	90.89	90.08	90.63
Air temperature [ºC]	33.4	34.8	31.4
Relative humidity	no data	0.04	0.12
Pasquil Stability	F	D	D/E
Roughness length [m]	0.008	0.009	0.010
Bund area [m^2]	2400	2400	2400
Bund height[m]	0.76	0.76	0.76
Release pressure [bar]	4.48	2.76	8.62

The orthogonal base defined by the axes X, Y and Z was used to specify the grid. As for the Burro series simulation, the Y direction was set horizontal and parallel to wind, the X direction was set perpendicular to wind and horizontal and Z was set to be the vertical direction. The computational domain extended 80 m in the X direction (symmetric crosswind plan), 500 m in the Y direction (from 100 m upwind to 400 m downwind) and 15 m in the Z direction. This domain was discretized using a regular Cartesian grid of 1 m side cubic cells.

The grid was also refined in the area near the leakage: in the Y direction, the length of the cells was reduced to 0.5 m in the region between 40 m in the upwind direction and 40 m in the downwind direction of the leakage point. As in the later case, the grid was stretched away from the leakage point (the length of cell growing continuously at a rate of 1.19 times the previous cell size with increasing distance from the source): in X direction, the cells were stretched after 30 m from the leak point; in the Y direction, they were stretched after 64 m in the upwind direction and 100 m in the downwind direction; and in Z direction, after10 m above the surface.

FLACS software was able to model the fence effect around the release point. The values simulated fit well to the factor of 2 range as in the Burro series simulation (Figure 9).

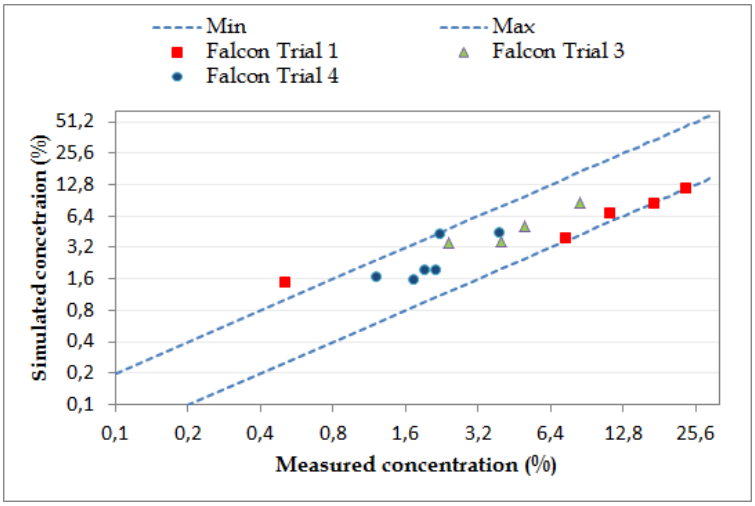

Figure 9 – Results of Falcon series

To summarize, from this preliminary performance study it can be said that FLACS presents good performance concerning maximum concentrations; however, the available experimental data does not allow time dependent analysis.

3.3.2 Reproducibility, grid dependence and sensitivity analysis

As mentioned in previous sections, in CFD modelling, the analyst has to choose a large number of parameters and these can affect significantly the results. As presented earlier, these parameters may be related to the grid definition, to the physical inputs regarding the source term and the environmental conditions or to the inputs needed by the numerical resolution algorithms. Many authors assert the importance of performing sensitivity analyses in order to control these effects (Plasmans et al., 2012; Sklavounos & Rigas, 2004; Dharmavaram et al., 2005; Blocken & Gualtieri, 2012). However, there are very few published sensitivity analyses concerning dispersion studies (Pandya et al., 2012; Gant et al., 2013).

Cormier et al. (2009) presented a sensitivity analysis focused on the influence of atmospheric conditions on the source term (a pool of liquefied natural gas) and did not assess the influence of the simulation parameters. Later on, Pandya et al (2012) used a statiscal tool to asses the influence of variations in the release conditions on the dispersion of three toxic substances; the analysis was performed using the software Simlab (package developed by the European Commission's Joint Research Centre) that explores the multidimensional space of the inputs using a search curve that scans the entire input space providing sensitivity indices. More recently, Gant et al. (2013) assessed the influence of release and atmopheric parameters on carbon dioxide dispersion; they also used a software to find sensitive indices from statiscal analyses. Middha et al. (2010) reported a sensitivity analysis concerning merely the atmopheric stability class and Middha (2010) performed a sensitivity analysis regarding the CFLC number and the turbulence parameters.

As reported by Pandya et al. (2012), there are three varieties of sensitivity analysis methods: local, global and screening methods. The local methods evaluate the effects on the outputs considering variations of one input variable at a time around a baseline point; the global methods are more sophisticated and aim to evaluate quantitatively the influence of the entire range of input values on the outputs uncertainty. Finally, the screening methods are based on computing for each input a number of incremental ratios, which are then averaged to assess the importance of the input (Pandya et al., 2012). Furthermore, some additional guidelines to perform an adequate sensitivity analysis can be found in Saltelli et al. (2004).

The global and screening methods are comprehensive methods that assess the sensitivity of the models in more detail; however, these approaches deal with the variables as density

functions, therefore they are more time consuming and require more complex tools for their development such as the software used by Pandya et al. (2012) and Gant et al. (2013) mentioned above.

The literature review shows that there is not a widely applied sensitivity analysis methodology nor a complete sensitivity analysis performed in CFD outputs when modelling dispersion. Therefore, in the present work, a comprehensive inspection of all the possible sources of uncertainty that may have an effect on the ouput variables when simulating dispersion is performed. The first investigation concerns the reproducibility capacity: as the numerical methods used to solve the set of equations implemented in CFD models are initialized by randomly set values, a study of the effect that the uncertainty associated to the initialization values may have on the simulation outputs is prescribed. Following, the grid dependence is analysed, since the size of the cells determine the volumes in which the conservation equations and turbulence equations are solved, and hence may have a significant effect on the outputs. Last, a sensitivity analysis following a local approach (which is less time consuming and does not neet a specific software) is undertaken considering physical and simulation parameters that need to be set when simulating with FLACS. The outcomes of this section may allow mapping the critical points when setting complex dispersion scenarios to be simulated with FLACS software or other tools alike.

Baseline Scenario

In order to inspect all the above mentioned sources of uncertainty, it is necessary to choose a baseline scenario from which the alterations if inputs can be made to observe potential changes in simulation results. Two trials of the field tests performed by Health and Safety Laboratory (HSL) at the HSL laboratories in Buxton, England (Butler and Royle, 2001) were chosen as baseline scenarios.

In the HSL trials, liquefied propane was released at rates of up to 4.9 kg/s at 1.5 m high from the ground. The resulting vapour cloud was characterized in terms of temperature and concentration of propane vapour at different locations. The trials set-up comprised a liquefied propane storage facility, a release system and a discharge area. The layout of the trials site is shown in Figure 10.

The discharge area was located within an area of approximately 100 m wide by 200 m long. The area was aligned with the prevailing wind, having its long dimension running south-west to northeast. Open fields were adjacent to the north and west of the area. Sensors were placed over a 600 m^2 area (100 m in downwind direction and 6 m in crosswind direction), located within the gas dispersion site; they were located at heights of 0.20, 0.85 and 1.50 m above the ground on the first 40 m of the centreline and at a height of 0.20 m in all the other points, as indicated in Figure 10.

Some of the trials undertaken were designed to investigate the influence of an obstruction placed in the path of the vapour flow. From observations of the flow of gas in preliminary tests, a 1 m high fence was chosen to be a suitable obstruction. Using this height, the top of the fence was approximately in the middle of the gas cloud height, allowing a significant volume of gas to flow unobstructed, whilst at the same time providing an obstruction for the lower part of the cloud. The fence was constructed using 2 m by 1 m steel sheets; ten sheets were used, producing a 20 m long fence, which was positioned 15 m apart from the release nozzle, perpendicular to the centerline of the trials site. The fence was centred so that there was 10 m of fence at either sides of the centerline of the site. A photo of the trial site is presented in Figure 11.

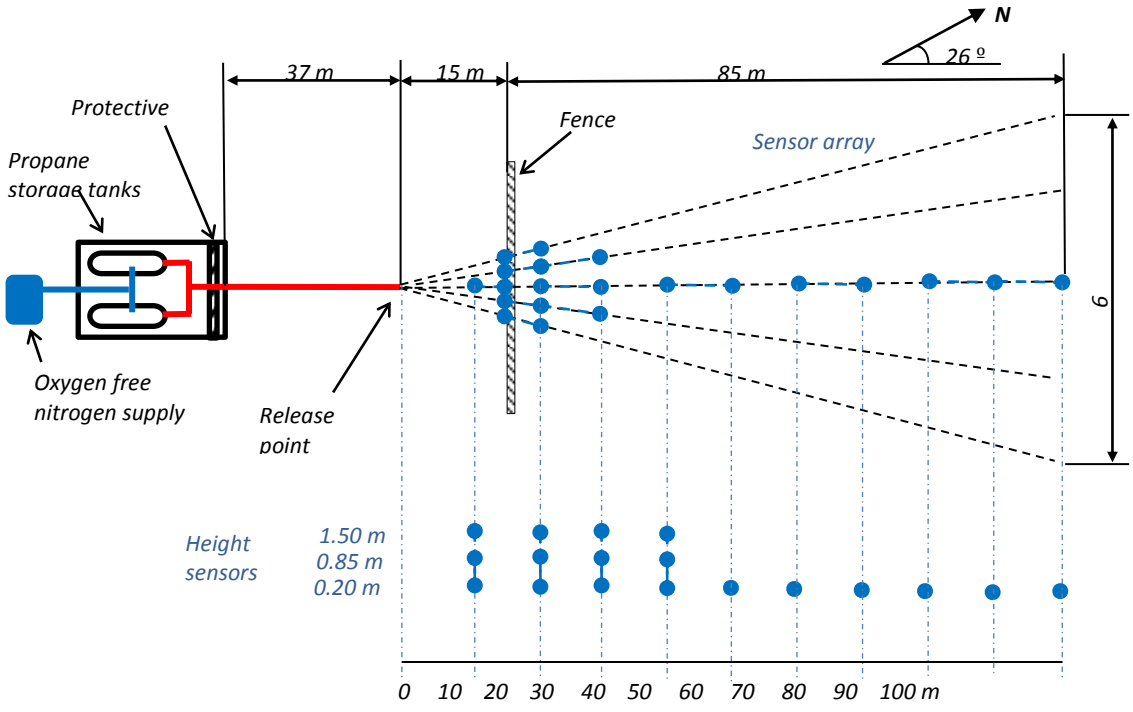

Figure 10 – Layout of the test site
Adapted from Butler & Royle (2001)

Figure 11 - Trial set with a fence
Source: Butler & Royle (2001)

The report of these tests (Butler and Royle, 2001) presents only the results of 8 trials; trials 4, 6, 7, 8 and 9 that are unobstructed releases and trials 11, 15 and 16 that are releases with the fence present. Trials 8 and 11 were selected as baseline scenarios (B1 unobstructed representing trial 8 and B2 obstructed representing trial 11). The input parameters used to perform the simulations are presented in Table 11 and Table 12.

Table 11 - Scenario conditions of baseline scenarios

Variable	Unit	Trial 8 – B1	Trial 11 – B2
Ambient Temperature	ºC	14.5	17.5
Atmospheric pressure	hPa	1000	1000
Ground roughness	m	0.03	0.03
Wind speed	$m.s^{-1}$	3.0	5.0
Reference height	m	10	10
Wind direction	º	195-225	110-225
Pasquill Class	-	D	D
Relativity humidity at height of 1.5 m	%	63	63
Spill duration	s	131	141
Estimated expanded leak area	m^2	0.012	0.014

Variable	Unit	Trial 8 – B1	Trial 11 – B2
Mass flow	$kg.s^{-1}$	2.5 ± 0.3	3.4 ± 0.3
Release temperature	ºC	11.96	11.26
Release pressure	hPa	7870	7580
Start time of release	s	10	10
Discharge direction	-	horizontal	horizontal
Discharge height	m	1.5	1.5
Volume fractions	-	100 propane	100 propane
Equivalence ratios	-	1.00E+30; 0	1.00E+30 ; 0

Table 12 - Simulation parameters for the baseline scenarios

Variable	Unit	Trial 8 – B1	Trial 11 – B2
Monitor points	-	In the same positions of gas sensors	In the same positions of gas sensors
Single field 3D output	-	FMOLE and TEMP	FMOLE and TEMP
Maximum time of simulation	s	180	180
CFLC	-	20	20
CFLV	-	2	2
Wind buildup time	s	5	5
Characteristic velocity	$m.s^{-1}$	0.1	0.1
MODD	-	500	500
DTPLOT	-	2	2

The domain was divided in three areas: the first one around the release point (micro grid), formed by the cells where the leak takes place and the adjacent cells (the regions near the height of 1.5 m and near the point (0,0) in X and Y directions); the second, the prevailing grid formed by the area where the dispersion is expected (macro grid); and the third, the stretched area in the far field where no relevant concentrations are expected. The transitions among these areas are made gradually in order to obtain stable simulations.

The domain was discretized using a single block Cartesian grid; the domain and the grid of the baseline scenarios were built following the guidelines of the user manual GexCon AS (2013). An orthogonal base X, Y and Z was used, being; the X direction horizontal and parallel to wind, the Y direction perpendicular to wind and horizontal and Z direction vertical.

The computational domain extended 170 m in the X direction (from 20 m upwind to 150 m downwind), 30 m in the Y direction (symmetric crosswind plan) and 10 m in the Z direction; being the point (0,0,1.5) the location of the orifice; the cells were initially represented by 1 m edge cubes (forming the macro grid).

Concerning the micro grid dimensioning, the guidelines (GexCon AS, 2013) specify that the area of the expanded jet must be solved in only one cell and that the area across the jet of this cell should be larger than the area of the expanded jet but not larger than twice. Figure 12 represents the control volume in which is the expanded jet area: A_{jet} is the jet area expected after the expansion at ambient pressure and A_{cv} is the area of the cell across the jet, the area dimensions are given by: $A_{jet} < A_{cv} < 2\ A_{jet}$. The jet area expected after the expansion at ambient pressure was estimated and the dimensions of the face cell across the jet defined so that the area fell between these limits. Furthermore, it is recommended that the aspect ratio (the ratio between the smallest and largest side of the cell) of the refined leak cells is not larger than five to avoid numerical instabilities. Once the dimensions of the cells around the leak were defined, cells nearby were smoothly increased to macro grid resolution.

Thus, in B1 scenario, the width and height of the micro grid cells were fixed at 0.15 m (as a function of the jet area expected after the expansion at ambient pressure) and, in order to maintain the aspect ratio smaller than 5, the length of the cells was fixed at 0.5 m. In B2 scenario, the width and height of the micro grid cells were fixed at 0.17 m and the length of the cells was fixed at 0.86 m.

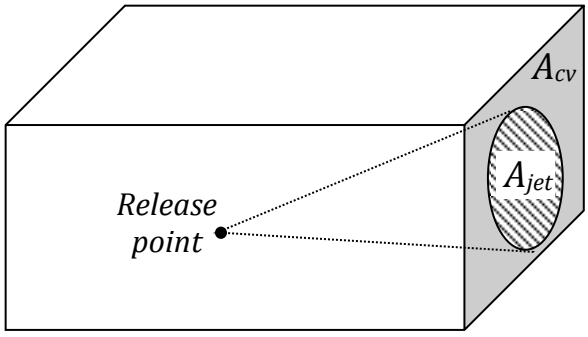

Figure 12 - Representation of the control volume in which is the expanded jet area.
A_{jet} is the jet area expected after the expansion at ambient pressure and A_{cv} is the area of the cell across the jet.
The area dimensions are given by: $A_{jet} < A_{cv} < 2\ A_{jet}$

Lastly, in both scenarios, the grid was stretched in X direction away from the leakage point (the length of cell grows continuously at a rate of 1.15 to provide a smooth growth with increasing distance from the source): the cells were stretched after 100 m from the leakage point because after this distance significant concentrations of gas are not expected. Thus, the micro grid was defined in function of the jet as previously mentioned, the stretched grid was defined in the far field (after 100 m from the leakage point) by cells larger than the macro grid cells and the macro grid was defined by the initial grid of 1 m edge cubes.

Taking into account that the focus of this study is the dispersion of a cloud, the main variable of interest was defined as the concentration as function of time and space. Monitoring points were inserted in the simulation specifications at the same locations where the gas sensors were placed in the field tests, which allowed the measured values of concentration to be compared with the simulated values.

Reproducibility and grid dependence

As mentioned on section 3.1, CFD tools transform the governing equations in discretized algebraic forms, which are solved to find the flow field properties at specific discrete points. The numerical process used to solve the equations is initialized by randomly selected values; consequently, there is an educated guess that this variability can be transferred to the converged values of the variables of interest. Furthermore, it should be kept in mind that these equations are solved for each control volume of the domain (i.e. cell) and then the results can be also affected by the grid definition.

In order to determine the reproducibility capacity of the model and the grid dependence, a set of simulations of the baseline scenarios were performed using randomly eight cores Intel Xeon Quad-Core 5520 de 2.26 GHz (Table 13). The main variable of interest was the concentration of the cloud.

The grid dependence analysis was performed in three phases: first, the influence of variations of up to ±20% in the dimensions of the macro grid was studied: next, it followed the analysis of the variations of up to ±20% in the dimensions of the micro grid; and finally, the effects of variations by more than 20% in the macro grid were also examined.

In order to verify the grid dependence, each dimension of the macro grid cells was changed independently of the others, increased and decreased by 10% and 20%; for example, when the width was increased by 10%, the other dimensions remained the same as those defined in the baseline scenario. The same approach was used for both baselines scenarios. The micro grid around the release point was not modified when doing this analysis. It should be noted that the baseline scenario was simulated 6 times to study reproducibility.

Table 13 - Simulations to verify grid dependence and reproducibility

Scenario	Dimensions of the control volume			Simulations
	Length [m]	Width [m]	Height [m]	
B	1	1	1	6
L1	1.2	1	1	1
L2	1.1	1	1	1
L3	0.9	1	1	1
L4	0.8	1	1	1
W1	1	1.2	1	1
W2	1	1.1	1	1
W3	1	0.9	1	1
W4	1	0.8	1	1
H1	1	1	1.2	1
H2	1	1	1.1	1
H3	1	1	0.9	1
H4	1	1	0.8	1

Concerning the reproducibility capacity of the software, the statistical analysis of the results of both scenarios showed that the greater standard deviation was equal to 0.01% what demonstrates that the software has a very high reproducibility capacity. The detailed results are presented in Appendix B.

Regarding to the grid dependence analysis, Figure 13 shows the converged values after the variation on each grid dimension of baseline scenario B1; the blue line “Exp” represents the experimental data, the line B1 represents the predicted values obtained using the initial grid for baseline scenario B1, the lines L1//H1/W1 and L2/ H2/W2 represent the predicted values obtained using the cell Length/Height/Width increased 20% and 10 % respectively; and the lines L3/H3/W3 and L4/H4/W4 represent the decrease by 10% and 20% respectively

(according to the Table 13). Figure 14 presents the results after similar variations in baseline scenario B2. The complete list of the estimated values for each monitor point, according to the variation of the control volume dimension of both scenarios is presented in Appendix B.

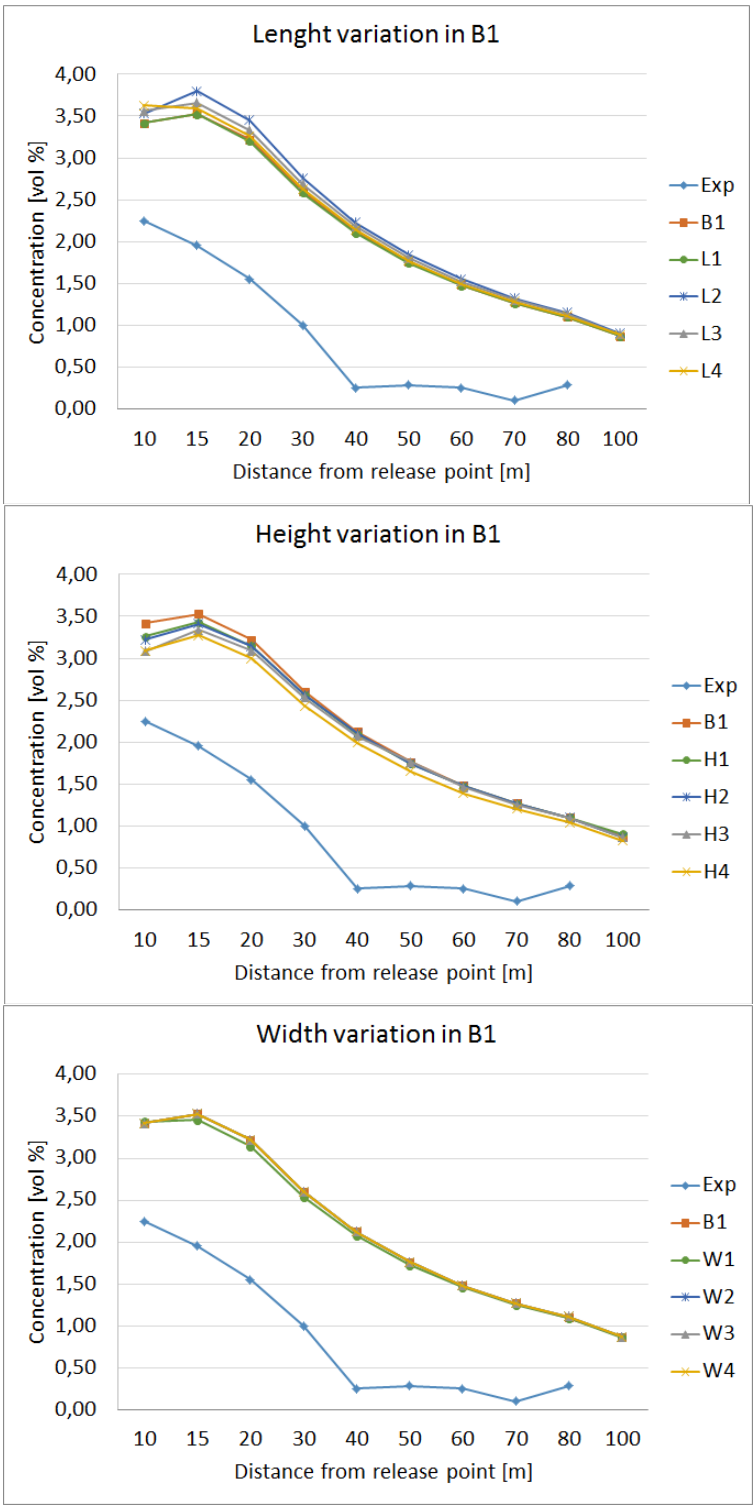

Figure 13 - Effects of grid variation on scenario B1

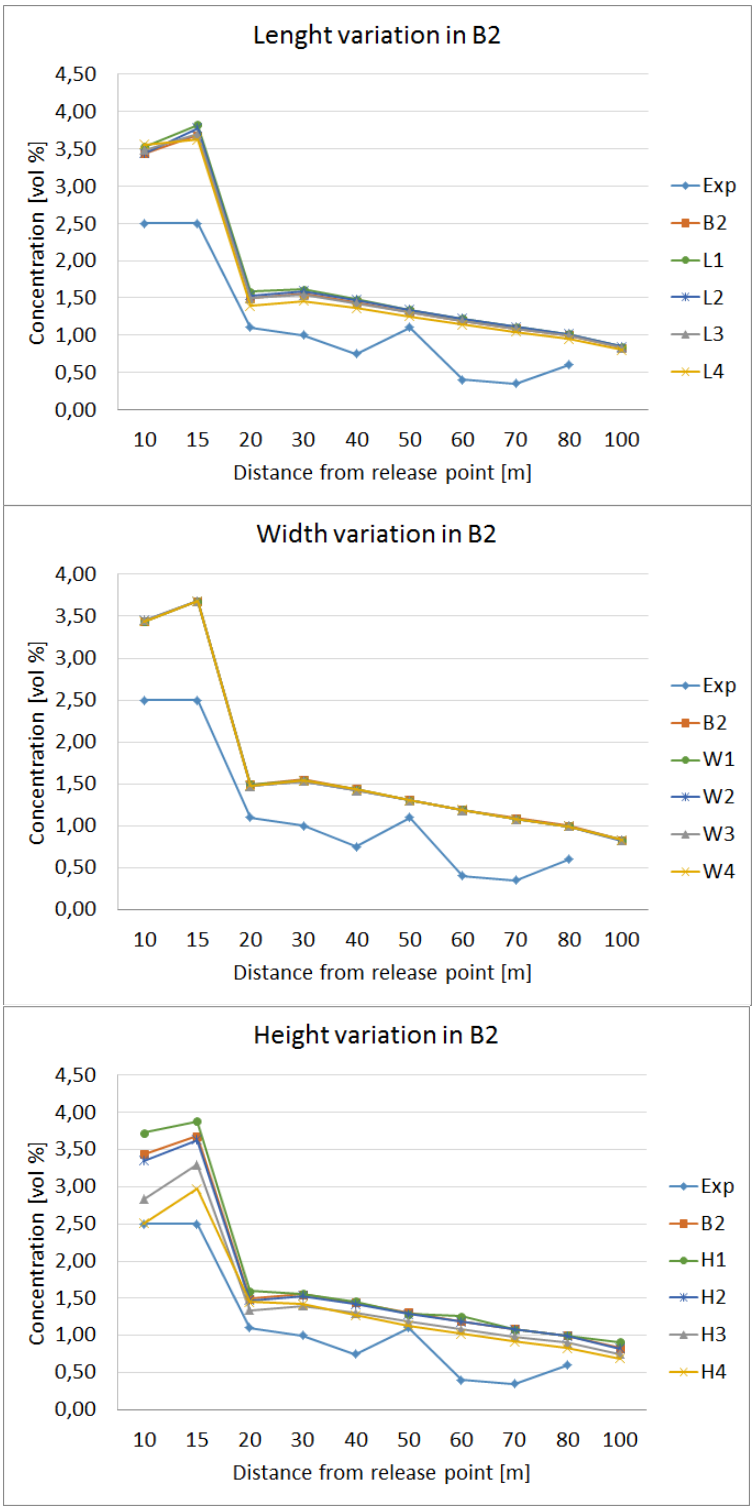

Figure 14 - Effects of grid variation on scenario B2

In the figures, it is not possible to see clearly all the lines presented in the legend because some of them are overlapped due to very small differences between the results, especially in the graphs where width variation is plotted. In both baseline scenarios (B1 and B2), the change that caused the minor influence was the alteration of the control volume width (Y direction), in which the major relative variation with respect to the baseline scenario B1 was about 2%. This is the control volume side across the wind and leak directions. Therefore, this minor influence is expected since the flow is less affected in this direction by the turbulence forces of the source term and by the wind.

Concerning the simulation runtime, the grid refinement by a rate of 20% resulted in an increase of approximately 2 hours: for scenario B1 increased from 8.4 to 10.3 hours and from scenario B2 from 9.5 to 11.6 hours.

Comparing the results among the variations in the three dimensions of the control volume, it can be seen that the closest results to the experimental data are obtained by altering the cell height (see how lines H4, are more separated from the baseline scenario line than the others), reaching the relative difference from the baseline a maximum value 27% (scenario B2).

Figure 15 and Figure 16 show the comparison among the best results obtained with variation in each dimension of scenarios B1 and B2 respectively. It is possible to see that the best results were achieved by the alteration of height in both scenarios. This occurs because the substance is a dense gas. The parcel related to weight in the momentum governing equation might have a significant impact in the results and therefore the refinement in the control volume height allows a better representation of this parcel. Moreover, the better representation of this parcel allows a better representation of the fence effects on scenario B2 (Figure 16); with a more refined grid the cloud simulated is more similar to the experimental cloud which is suffering the influence of the turbulence generated by the fence.

Finally, in both scenarios, it is possible to see significant effects concentrated in the region near the release point and minor effects in the far field. This occurs due to the turbulence effects of the source term on the flow, since in the initial phase of the dispersion the properties of the source term define the flow (as shown in section 1.2).

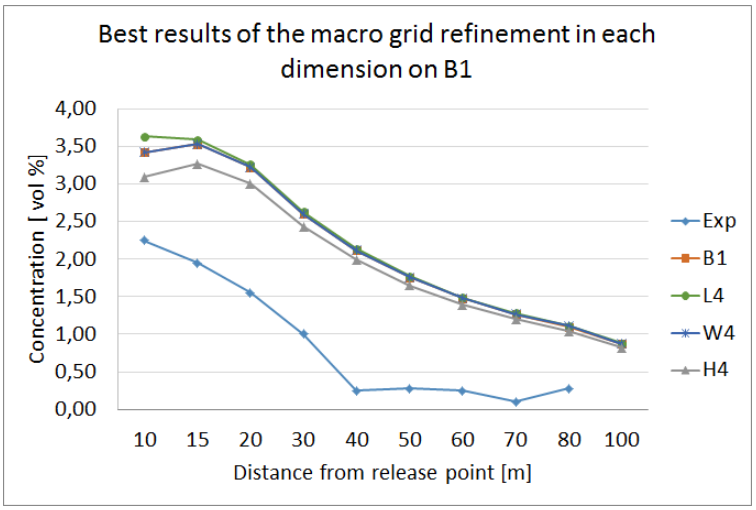

Figure 15 - Comparison among grid refinement of each dimension on B1

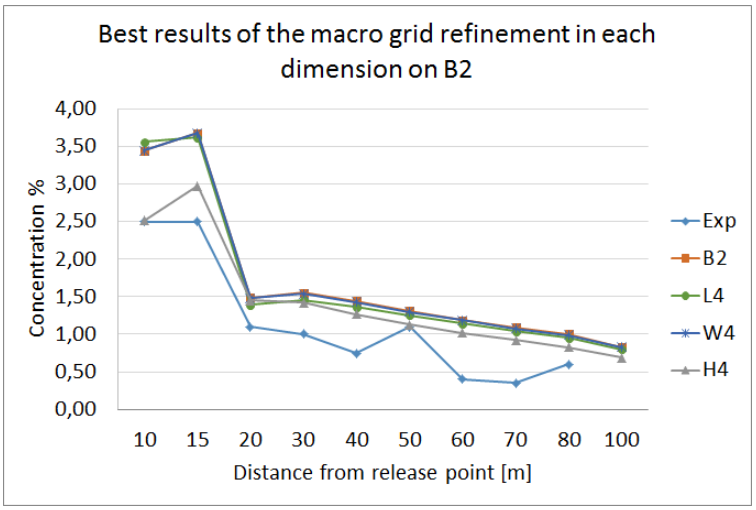

Figure 16 - Comparison among grid refinement of each dimension on B2

Next, a dependence grid analysis in the micro grid around the release point was performed in order to obtain more information about the influence of the grid in the first region of the flow. To perform the analysis, each dimension of the control volumes in the micro grid was changed independently of the other; each one was increased and decreased by 20%. The same approach was used to both baselines scenarios. The macro grid around the release point was not modified in this analysis. Table 14 shows the simulations executed for each baseline scenario and the dimensions of the micro grid cells.

Table 14 - Simulations to verify micro grid dependence

Scenario	Dimensions of the control volume in the area of the expanded jet			Simulations
	Length [m]	With [m]	Height [m]	
B1	**0.5**	**0.15**	**0.15**	**1**
L5	0.6	0.15	0.15	1
L6	0.4	0.15	0.15	1
W5	0.5	0.18	0.15	1
W6	0.5	0.12	0.15	1
H5	0.5	0.15	0.18	1
H6	0.5	0.15	0.12	1
B2	**0.86**	**0.17**	**0.17**	**1**
L5	1.03	0.17	0.17	1
L6	0.69	0.17	0.17	1
W5	0.86	0.20	0.17	1
W6	0.86	0.14	0.17	1
H5	0.86	0.17	0.20	1
H6	0.86	0.17	0.14	1

As observed in the macro grid analysis, the change that caused minor influences was the alteration of the control volume width. The major effects were again concentrated in the region near the release point and decreased in the far field.

Additionally, comparing the results among the variations in the three dimensions of the control volume, it could be seen that the closest results to the experimental data were obtained again by altering the height. Figure 17 and Figure 18 present the comparisons among results for B1 and B2 baseline scenarios, and it can be clearly observed how the best results are relative to lines H6. The major relative variation with respect to the baseline scenario (B2) was about 28%. As in the previous analysis, the parcel of the weight in the momentum governing equation has a significant impact in the results. Concerning the simulation runtime, like in the macro grid, the micro grid refinement by a rate of 20% resulted in an increase of approximately 2 hours.

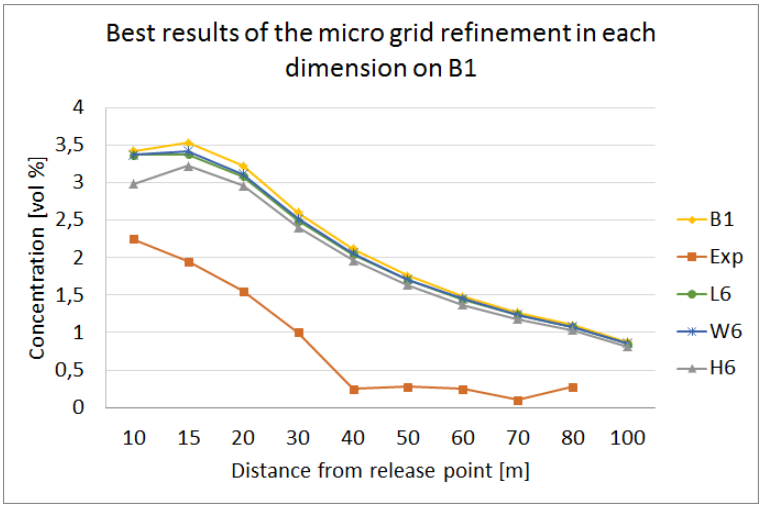

Figure 17 – Better results after micro grid refinement in each dimension on B1

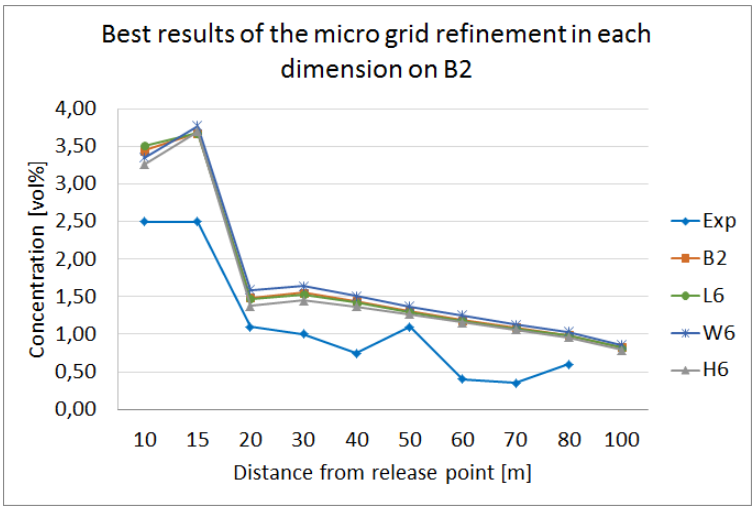

Figure 18 - Better results after micro grid refinement in each dimension on B2

Comparing the results of the micro and macro grid refinement, it can be noted that the micro grid refinement produces roughly the same improvement on simulating scenario B1 of those achieved by the macro grid refinement. Concerning scenario B2, the refinement of the macro grid contributes more to the accuracy of the results since the effects of the turbulence generated by the fence are better represented, while the refinement in micro grid only improve the representation of the source term. Figure 19 presents a comparison between the results (on scenario B1) of the height refinement in the macro grid (line H4) and in the micro grid (line H6) and Figure 19 presents the results of baseline scenario B2.

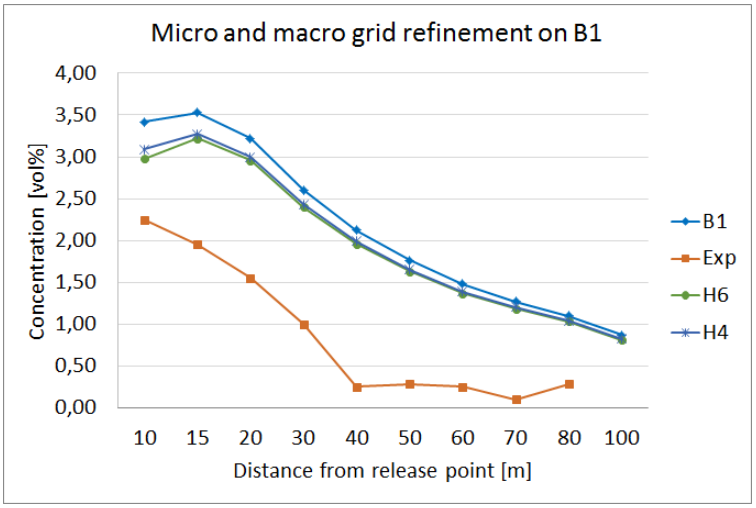

Figure 19 - Comparison between micro and macro grid refinement on B1

Line H4 belongs to the macro grid refinement analysis, and line H6 belongs to the micro grid refinement analysis.

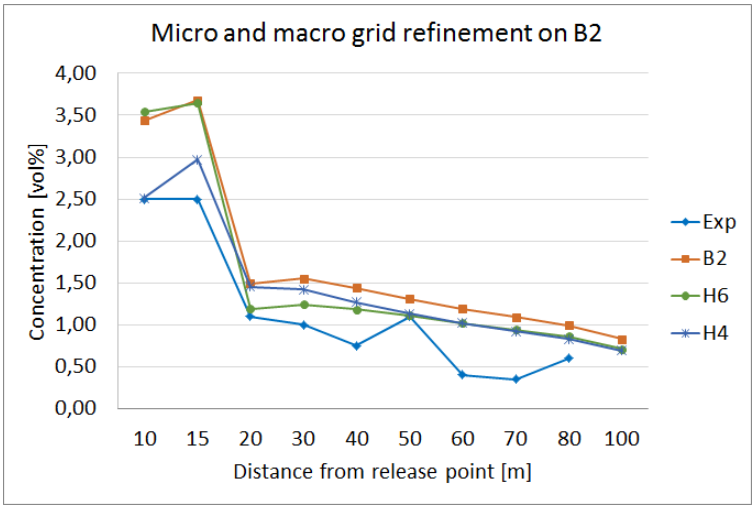

Figure 20 - Comparison between micro and macro grid refinement on B2

Line H4 belongs to the macro grid refinement analysis, and line H6 belongs to the micro grid refinement analysis.

After observing that the height refinement of the macro grid produced better simulations results, especially in the scenario with a barrier that is the focus of this thesis, narrower grids were tested; the height of the cells of the baseline scenarios were decreased also by 30%, 40%, 50% and 60%.

The subsequent results are presented in figures Figure 21 and Figure 22 for scenarios B1 and B2 respectively. There is an improvement on the results with the grid refinement until the rate of 50% (lines H3-10%, H4-20%, H7-30%, H8-40% and H9-50% respectively). Comparing the results of the original grid with the grid refined in 50% (line H9 of the Figure 22) an improvement of 12% was achieved. However, doing the decrease of 60% in the height of the cells (line H10), the distance between the numerical results and the experimental data increases. This occurs because while keeping the other dimensions untouched the aspect ratio between the cells dimensions increase. For ratios larger than 2, the results become as inaccurate as with the original grid (non refined grid). This last refinement of the macro grid by rates between 20% and 60% did not result in a significant change in runtime simulation.

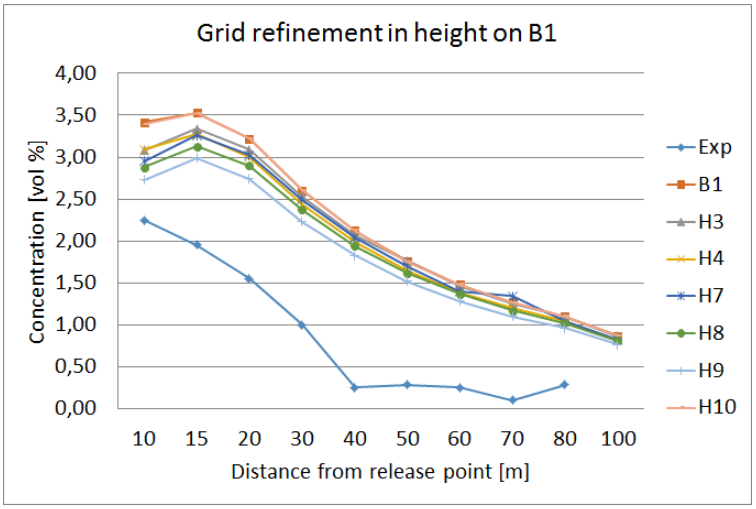

Figure 21 - Comparison among grid refinement in height on B1

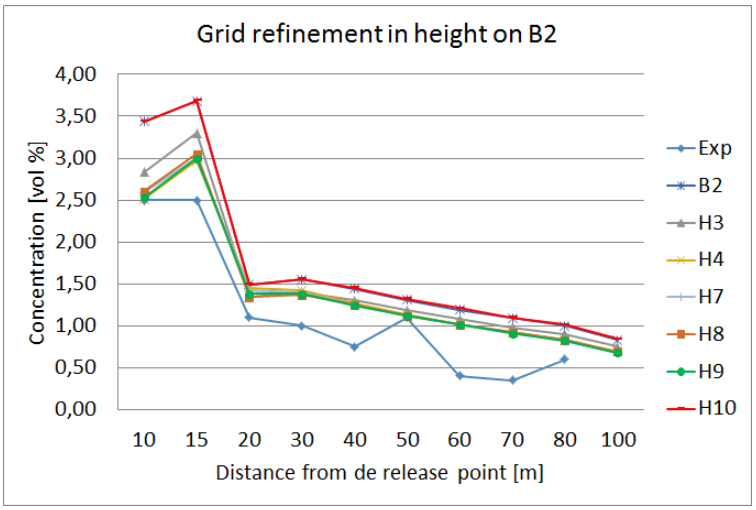

Figure 22 - Comparison among grid refinement in height on B2

Concluding, the variations in the length and width of the cells produces minor effects; then the recommendation which arises from this study is to maintain these dimensions reasonably coarse in order to save simulation runtime. However, height variation of the macro grid cells produces significant effects since the refinement in this dimension allows a better representation of the parcel of the weight in the momentum governing equation, which in the case of a dense gas, has a great influence on dispersion.

The analysis of the micro grid refinement has shown that variation until ±20% in the micro grid dimensions does not produce significant changes in the results, thus the grid near the source can be fixed at the most at a value 20% greater than the recommended by the guidelines in order to minimize computational cost.

Finally, effects of variations by more than 20% in the macro grid cell height dimensions have been examined. This later grid refinement has improved significantly the results. However, the aspect ratio among the cells dimensions has to be kept lower than two. If a finer grid is needed, one should consider refining the grid in other directions also. For scenarios similar to those discussed here, it is recommended cell heights no greater than 0.5 m in the region between the release point and the ground.

Sensitivity analysis

The objective of the sensitivity analysis is to increase understanding of the relationships between input and output variables so that to detect how the presence of uncertainty in the inputs can affect the results of the simulation.

As seen on section 1.2.2 the atmospheric conditions affect directly the dispersion; however, in most cases the exact values of the parameters that characterize the atmospheric conditions are not known and approximate values have to be used. Thus, variables such as wind speed, ground roughness, ambient temperature and ambient pressure are potential inputs to consider in a sensitivity analysis.

Reminding the influence of the source term in the cloud formation and dispersion (seen on section 1.2.1), the effects of the uncertainty related to the duration of spill, the mass flow and the location of release point may have also an effect on the simulation outputs. Furthermore,

other non-physical simulation parameters intrinsic to the software used (CFLC, for instance) may be also investigated in terms of how sensible are the outputs to their uncertainty.

A sensitivity analysis was performed starting from the two different baseline scenarios B1 and B2 described in Table 11 and Table 12 in order to study the effect of the uncertainty related to the above mentioned variables (Table 15). The grids used in both scenarios were the best found in the last section (microgrid dimensions refined by 50% and macrogrid dimensions increased by 20%). Input variables were increased and decreased by 10% excepting the CFLC number that was varied in ±50%. Each variable was changed independently of the others

17 simulations were performed for B1 and B2 scenarios, respectively: the first of each set using the original values presented on Table 11 and Table 12 and the others considering one variation at each time from those gathered in Table 15, in which the first two columns describes the variable of interest and its unit, the third is the variation applied over the original value of this variable and the last two the final value of each variable for scenarios B1 and B2 respectively.

Table 15 – Variations in each scenario

Input variable	Unit	Variation in the input variable	Scenario B1	Scenario B1
Ambient temperature	ºC	-10%	13.05	15.75
		+10%	15.95	19.25
Atmospheric pressure	hPa	-10%	900	900
		+10%	1100	1100
Ground roughness	m	-10%	0.027	0.027
		+10%	0.033	0.033
Wind speed	$m.s^{-1}$	-10%	2.7	4.5
		+10%	3.3	5.5
Spill duration	s	-10%	117.9	126.9
		+10%	114.1	155.1
Mass flow	$Kg.s^{-1}$	-10%	2.25	3.06
		+10%	2.75	3.74
Discharge height	m	-10%	1.35	1.35
		+10%	1.65	1.65
CFLC	-	-50%	10	10
		+50%	30	30

Monitor points verifying concentration in time every 10 m following X direction were inserted in the simulations at three heights: 0.2, 0.8 and 1.5 m and thus the comparative analysis between the simulated concentrations of the original baseline scenarios and the simulations after the variation of each parameter was made for each distance and height (Tables of the estimated values for each monitor point according to the variation of each variable of interest for both scenarios B1 and B2 are presented in Appendix B).

The sensitivity was then graded by means of Bartelink's (1998) relative sensitivity parameter. This parameter gives an estimation of the partial derivative of the output variable (concentration in this case study) with respect to the perturbation of the input variable (Cruz et al., 2003):

$$RS = \frac{|C_{+10\%} - C_{-10\%}|}{0.2\ C}$$

Where RS is the relative sensitivity, $C_{+10\%}$ and $C_{-10\%}$ are the output values of concentration obtained when the value of the input under analysis is changed by ±10% and C is the resulting output value of concentration under default conditions (i.e. simulating the baseline scenarios). A RS score scale can be defined as follows: RS scores less than 0.5 indicates insensitivity, RS scores between 0.5-1 indicates slightly sensitivity. Variables showing RS between 1-2 are considered moderately sensitive and those showing RS greater than 2 are highly sensitive (Cruz et al., 2003).

The sensitivity maps for scenarios B1 and B2 are shown in Table 16 and

Table 17. RS has been computed for each key variable at each monitoring point, but only RS of monitoring points at 0.2 m and 0.8 m height are shown (no sensitive points are found in points located at 1.5 m height. RS values indicating moderate/high sensitivity are coloured in red, and RS values indicating slight sensitivity are coloured in orange.

With these results it can be affirmed that the variables that made concentration values more sensitive to inputs uncertainty were discharge height, wind speed, atmospheric pressure and mass flow. Discharge height uncertainty had a major effect on concentration, with RS indicating high and moderate sensitivity in different locations of the cloud. Concentration sensitivity was observed to be higher close to the source term at both monitoring heights in

both scenarios, B1 and B2. Discharge height was the only significant input variable in the sensitivity analysis in scenario B1, whereas concentration values in the scenario B2 (the one with the presence of an obstruction) were sensitive to the rest of already mentioned inputs. This was notable particularly at distances far from the source, where less mass was forming the cloud due to the blockage effect of the barrier, and hence the dispersion was more dominated by turbulence and atmospheric variables.

Table 16- Sensitivity map for scenario B1

		Relative sensitivity														
	Distance	10	15	20	30	40	50	60	70	80	100	10	15	20	30	40
	Height	0.2	0.2	0.2	0.2	0.2	0.2	0.2	0.2	0.2	0.2	0.8	0.8	0.8	0.8	0.8
Input Variable	Temperature	0.05	0.03	0.04	0.04	0.03	0.03	0.00	0.00	0.00	0.00	0.03	0.03	0.04	0.03	0.00
	Wind	0.44	0.23	0.16	0.09	0.03	0.03	0.08	0.09	0.05	0.07	0.13	0.10	0.08	0.05	0.06
	Roughness	0.00	0.02	0.02	0.00	0.03	0.03	0.00	0.00	0.05	0.07	0.00	0.00	0.00	0.00	0.00
	Pressure	0.22	0.08	0.05	0.09	0.08	0.16	0.16	0.18	0.26	0.33	0.03	0.05	0.08	0.13	0.19
	Spill duration	0.00	0.00	0.00	0.00	0.00	0.00	0.00	0.00	0.00	0.07	0.00	0.00	0.00	0.00	0.00
	Mass flow	0.24	0.08	0.07	0.09	0.11	0.16	0.20	0.23	0.26	0.33	0.03	0.03	0.08	0.13	0.19
	Discharge height	2.16	0.99	0.69	0.43	0.30	0.23	0.23	0.18	0.16	0.20	0.93	0.46	0.32	0.23	0.19
	CFLC	0.00	0.02	0.00	0.00	0.03	0.00	0.00	0.05	0.00	0.00	0.00	0.00	0.00	0.03	0.00

Table 17 - Sensitivity maps for scenario B2

		Relative sensitivity														
	Distance	10	15	20	30	40	50	60	70	80	100	10	15	20	30	40
	Height	0.2	0.2	0.2	0.2	0.2	0.2	0.2	0.2	0.2	0.2	0.8	0.8	0.8	0.8	0.8
Input Variable	Temperature	0.06	0.05	0.07	0.07	0.04	0.04	0.05	0.00	0.06	0.07	0.04	0.05	0.03	0.07	0.04
	Wind	0.61	0.33	0.04	0.18	0.28	0.36	0.45	0.49	0.55	0.66	0.16	0.22	0.03	0.18	0.29
	Roughness	0.00	0.00	0.00	0.00	0.04	0.00	0.05	0.00	0.06	0.07	0.01	0.00	0.00	0.00	0.00
	Pressure	0.45	0.25	0.11	0.07	0.20	0.31	0.45	0.55	0.67	0.81	0.10	0.17	0.03	0.11	0.25
	Spill duration	0.00	0.00	0.00	0.00	0.00	0.00	0.00	0.00	0.00	0.00	0.00	0.00	0.00	0.00	0.00
	Mass flow	0.45	0.25	0.14	0.07	0.20	0.31	0.40	0.49	0.61	0.81	0.11	0.17	0.10	0.11	0.25
	Discharge height	1.56	0.72	0.29	0.25	0.28	0.22	0.20	0.22	0.24	0.29	0.72	0.50	0.27	0.25	0.21

Changes in temperature caused minor effects in the results of the modelled scenarios, since this variation was not enough to represent a change in the atmospheric stability. However, it is important to note that in different scenarios in which the evaporation process may take longer

(such in a case of pool formation), the influence of variations in the ambient temperature may increase, since it will directly affect the vaporization rate.

Furthermore, the roughness variation was found to be not large enough to modify the turbulence profile hence showing no significant effect on the results. The variation of the spill time was not substantial in this case either, since the spill had a short duration and a low flow rate and therefore the cloud diluted almost instantly after the release stop; however, in cases with greater flow rates, in which the cloud takes longer to dilute after the release, changes in this parameters may have a significant effect on the results.

The results were also poorly sensitive to changes in CFLC; however, this parameter directly affects the simulation runtime: decreasing the CFLC value by 50% in scenario B1 the simulation runtime increased from 12 to 19 hours and increasing the CFLC by 50% the runtime decreased from 12 to 8 hours. In scenario B2, by decreasing the CFLC the simulation runtime increased from 7.6 to 13 hours; however, when was used the CFLC increased by 50% (CFLC equals to 40) the simulation crashed because it did not find a converged solution. The greatest value for this scenario that provided stable simulations was 25, which decreased the simulation runtime from 7.6 to 6 hours. Scenario B2 was more sensitive to changes in CFLC because de flow rate is higher; thus, increasing the CFLC the time step increases and the simulation not converge because there is more mass in each control volume to treat using a longer time step.

The key input variables found in the sensitivity analysis were deeper inspected. Figure 23 shows the simulated concentrations in each monitor point at 0.2 m height for the baseline scenario B2, varying wind speed. The yellow bars represent the simulated values for the baseline scenario B2, the green bars represent the simulated values obtained using the wind speed value decreased by 10% and the blue bars represent the results obtained using the wind speed value increased by 10%. In scenario B2 the variations of wind speed affected the results near the source term where there is more turbulence due to the jet and therefore there are more eddies generated by this turbulence. The wind contributes to the formation of eddies and consequently to the cloud dilution. Furthermore, in the far field the results were also significantly affected. In this case, the wind contributed to the cloud dilution in the region near the source, after few meters the turbulence decreased; however, the fence at 15 m

blocked partially the cloud and caused turbulence, being the latter again sensitive to wind variations.

Concerning to variations in the pressure atmospheric values, Figure 24 shows the simulated concentrations in each monitor point at height 0.2 m for scenarios B2 respectively: the yellow bars represent the simulated values for the baseline scenario, the green bars represent the predicted values obtained using the atmospheric pressure value decreased by 10% and the blue bars represent the results obtained using the atmospheric pressure value increased by 10%.

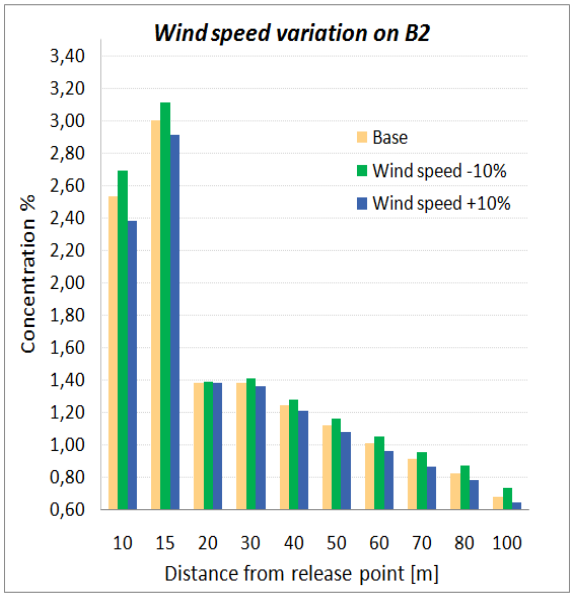

Figure 23 - Simulated concentrations varying wind speed on scenario B2

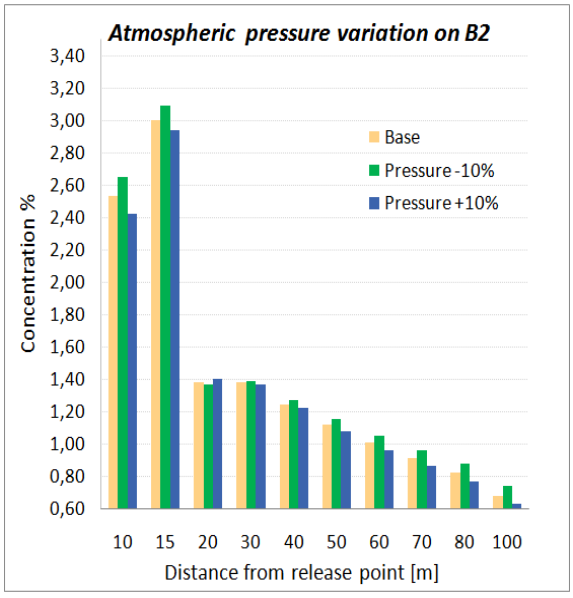

Figure 24 - Simulated concentrations varying atmospheric pressure on scenario B2

When the atmospheric pressure increased by 10% the simulated concentration for the gas phase decreased, and when the atmospheric pressure decreased by 10% the simulated concentration increased (anti-symmetric effect). This probably occurred because with a higher pressure the liquid fraction into the cloud took longer to evaporate. From the results of the monitor points at different heights, it is possible to note that the influence of the pressure variations was not noticeable at 0.8 m height nor at 1.5 m (the highest part of the cloud), where the liquid fraction was smaller.

Concerning to variations in the mass flow values, Figure 25 shows the simulated concentrations of the sensitivity analysis performed for scenario B2, for monitor points are 0.2 m. When the mass flow value was increased by 10% the simulated values for concentration for the gas phase increased and when the value was decreased by 10% the simulated values for concentration also decreased. This effect clearly is symmetric, since the more mass involved in the leakage, the more concentration found in the cloud.

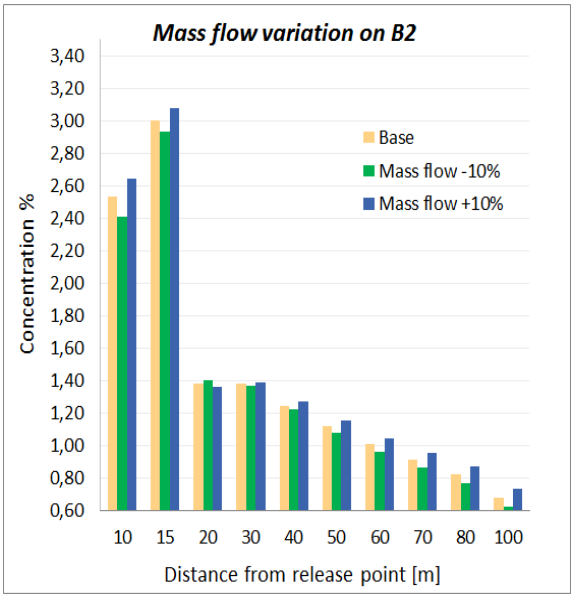

Figure 25 - Simulated concentrations varying mass flow on scenario B2

Finally, concerning to variations in the discharge height, on scenario B1 (Figure 26) the greatest effects were found in the near field and at height of 0.2 m (although the closest monitor from the source at 0.8 also showed some sensitivity and is not represented in Figure

26). An antisymmetric effect was observed when analysing the effect of this variable point; the released gas is a dense gas and, as reported on section 1.2.2, in dense gas dispersion the cloud experiences descending movements until reaches the ground. Consequently, decreasing the discharge height, makes the cloud touching the ground earlier being the concentrations higher near the ground. Figure 27 shows three simulated clouds of scenario B1, 90 seconds after the release start, originated for the baseline scenario B1 (upper cloud), the scenario with a 10% discharge height decrease (cloud in the middle) and the scenario with an increase of 10% of the discharge height (lower cloud). It is possible to observe that with the discharge height equal to 1.5 m the cloud touches the ground nine meters after the release point. With a decrease in the discharge height, this distance is reduced roughly to eight meters and with a discharge height increase this distance goes up to roughly eleven meters.

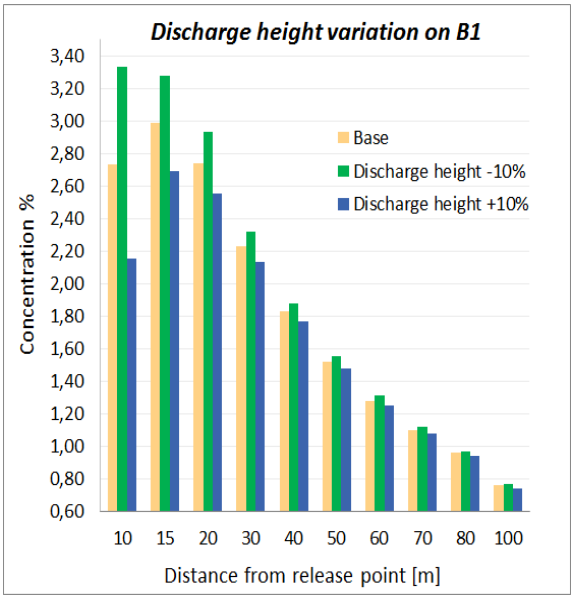

Figure 26 - Simulated concentrations varying discharge height on scenario B1

Finally, concerning scenario B2 it is worth noting that the effects on results due to variations in the discharge height differ from those found in scenario B1 (Figure 28). Concentration was found to be insensitive to the decrease of the discharge height, the cloud stays partially trapped before the fence and the decrease of the discharge height did not affect the results. On the other hand, the increase in height produced major effect on results. Before the fence, the simulated values of concentration decreased because a smaller portion of the

cloud was trapped by the fence. Locating the source at a higher position allowed more mass passing over the fence, being the concentrations monitored after the fence also higher.

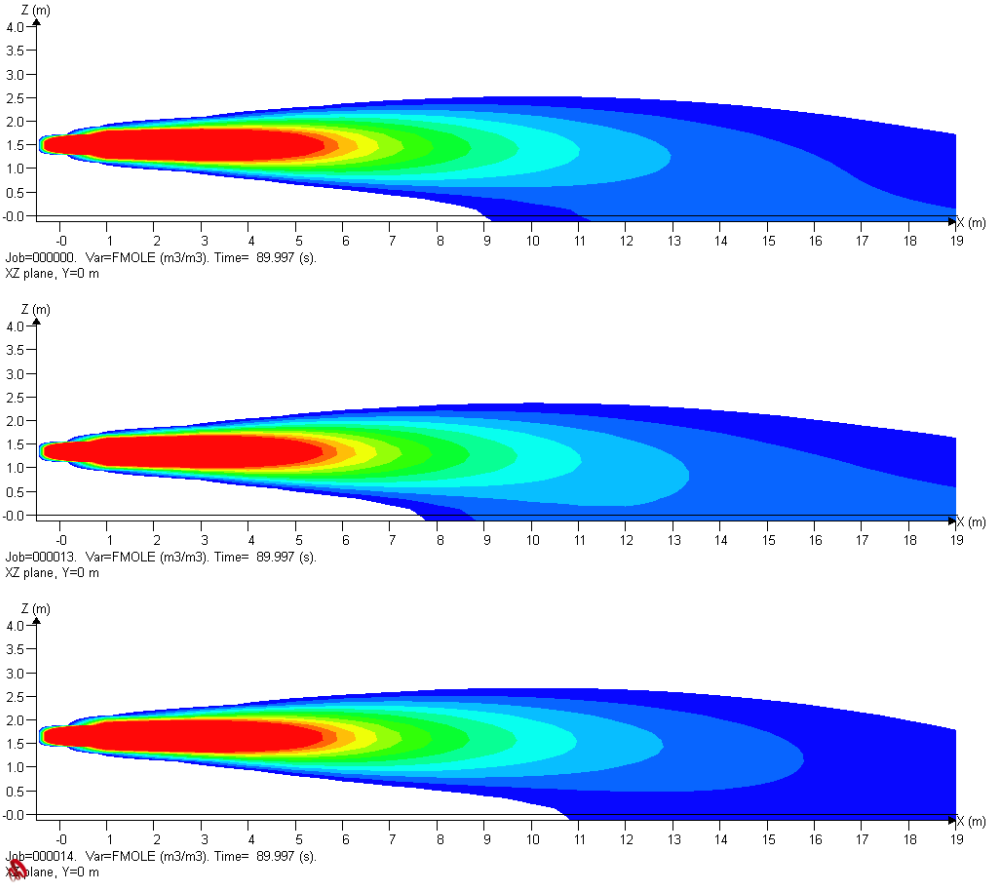

Figure 27 - 2D Cut plane comparing different discharge heights

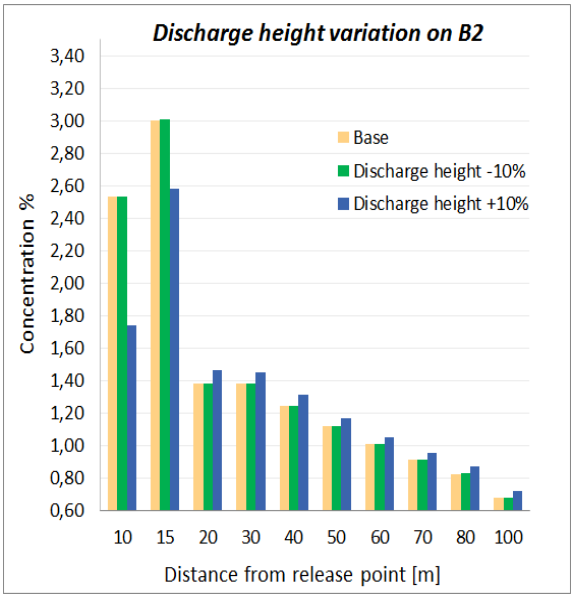

Figure 28 - Simulated concentrations varying discharge height on scenario B2

3.4 Preliminary guiding principles for CFD dispersion simulation

The main outcomes of the previous investigation in terms of models implemented, numerical schemes, and validation studies (those found in the literature and those performed within the framework of the present work), allow mapping critical points in quantitative dispersion analysis of leakage of flammable and/or toxic substances on realistic environments with barriers (using a CFD tool). They can be shaped as practical guiding principles to be used when performing dispersion analysis using FLACS software or tools alike.

The outlines proposed here have been designed with focus on the users of CFD tools to perform a dispersion analysis to risk assessment purposes; it is not intend guiding models development. In other words, the outlines presented here are directed to those responsible for evaluate or assess safety analysis.

It is important to note that the guiding principles suggested here are applicable to scenarios similar to those presented in this study: dispersion of dense gas releases with the presence of obstacles. A critical review of these principles may be necessary when intended to be used for others scenarios. Blocken and Gualtieri's (2012) work can be alternatively followed for more general guiding of CFD in complex environmental fluid mechanics processes.

The suggested guiding principles are presented according to the logic sequence of actions needed to perform accurate dispersion simulations using CFD tools: objectives and scope definition, scenario definition, tool selection, geometry and grid construction, parameters set up and estimation of uncertainty.

1. Objectives and scope definition

In this phase the primary purpose of the analysis to be performed should be well established. The framework and aims of a cloud dispersion analysis can be diverse: basic research for fundamental studies, predictive analysis for emergency planning or for process safety studies (e.g. inherent safe design, control, and mitigation), etc. This frame of reference will condition the scope of the analysis in terms of the spatial and temporal range, the outputs of interest and the degree of accuracy desired.

2. Scenario parameters definition

The scenario to simulate has to be defined in terms of *i)* the initial conditions concerning the source term and atmospheric variables and *ii)* the boundary conditions of the domain. This step is crucial since these inputs have a direct effect on the results. Thus, it is basic to know the uncertainties associated with these parameters and, if necessary, to perform a sensitive analysis within the range that the key variables are expected to cover.

Special attention is recommended to discharge height, wind speed, atmospheric pressure and mass flow rate, since these variables have been the ones showing higher sensitivity towards the cloud concentration profile (section 3.3.2).

3. Tool selection

As presented on section 2.5, the type of tools suitable to perform dispersion analysis with the presence of obstructions have to be CFD-based. There are a large number of CFD tools available to perform dispersion analysis; thus, in this step the most adequate tool to tackle the problem defined in step 1 should be chosen. As previously discussed, there is a lack of experimental data and comprehensive validation studies devoted to dispersion analysis in scenarios with obstacles; thus, it is important to verify, reviewing the appropriate literature, if the models (implemented in the tool to be used have been constructed in solid scientific basis, and evaluated for the purpose of the study following standard methodologies and protocols (e.g. Duijm & Carissimo, 2002). At present, FLACS is so far the most appropiate tool to perform cloud dispersion simulations with the presence of barriers, since it has specific models implemented for consequence analysis that allow the representation of complex geometries.

4. Geometry and grid construction

In order to perform the simulations it is necessary to define the geometry and the grid for the specified scenario. This is a rather complex process, which should be faced considering the following recommendations:

- All objects should be well geometrically represented; even the small objects should be included, since they can affect significantly the results.

- The computational domain should be defined by means of a uniform rather coarse grid (macro grid) which should be refined in the region of the release and the obstacles that the scenario may present by means of a thinner grid (micro grid). The transition between both

grids should be gradual by a factor smaller than 50%. Finally, a grid stretching towards the domain boundaries is also recommended. This grid configuration represents a compromise between accuracy and computational cost.

- Objects present in the domain are recommended to be adjusted to match the grid lines (if the tool used to perform the analysis incorporates the porosity concept presented on section 3.1.1). As such, sloping terrains are recommended to be established using a "staircase" representation, with each step aligned with the lines. For this type of geometry, the vertical dimension of the grid is recommended to be established between 0.1-0.5 m.

- The particular dimensions of the macro and micro grid cells should be defined taking into account several aspects: *i)* the area of the expanded jet must be solved in only one cell and the area across the jet of this cell should be larger than the area of the expanded jet but not larger than twice. Therefore, the jet area expected after the expansion at ambient pressure must be estimated before performing the simulations in order to establish the right measures of the micro grid cells (the jet area can be estimated by one-dimensional model for the release of an ideal gas from a pressurized reservoir through a nozzle into an open atmosphere). Moreover, the aspect ratio (the ratio between the smallest and largest side of the cell) of micro grid cells should be kept lower than two, implying that if a finer grid is needed in one direction, one should consider refining the grid in other directions also *ii)* Height variation of the macro grid cells can produce significant effects; for scenarios similar to those discussed in this study, cell heights no greater than 0.5 and cell width and length no greater than 1.0 m are recommended.

5. Simulation parameters setting

The simulation parameters are needed to define aspects of the computational process of the model; they define features such as the time step used in the simulations, the period of time simulated, the output variables of interest, etc.; thus, when setting these parameters, the objectives and scope of the simulations defined in step 1 should be recalled. However, two main issues have to be considered in order to control the simulation runtime; the former concerning the outputs that the simulations shall provide: using as few variables as possible to achieve the goals of the simulation is strongly recommended, since it will minimize the computational cost and the amount of data to be processed afterwards. The later deals with the time step parameter CFLC: FLACS guidelines (GexCon AS, 2013) recommend a CFLC of 20 for dispersion analysis, however this parameter can be increased to save simulation runtime.

The factor of increase can be inversely proportional to the relation between the macro grid and the micro grid size (i.e. if the region near the leak has been refined by a factor of 3, the CFLC can be 60). Nevertheless, if this increase causes stability problems, CFLC has to be reduced until getting a stable simulation.

6. Verification of uncertainty

As seen on Chapters 2 and 3, CFD modelling is sensible to a wide range of variables (both related to the mathematical model and to the numerical algorithms) that may have a significant effect on the results. Thus, it is essential to know the uncertainty associated to the main outcomes that the CFD tool can provide.

In this context, this study suggests that even if the tool's performance has been already studied in previous works for scenarios similar to those of interest, a grid dependence analysis is still recommended as well as the identification of the inputs causing more output sensitivity, with simple methodologies like those used in section 3.3.2.

If there is not any study assessing the performance of the CFD tool in scenarios similar to those wanted to be studied, then a complete validation including an estimation of the uncertainties should be performed. Oberkampf & Trucano (2002) give valuable recommendations of how to tackle this problem. The authors present a comprehensive study about verification and validation of CFD models discussing key issues of methodologies of validation, creation of validation cases, validation metrics and others relevant subjects. In summary, their approach is based on the following steps: first, characterization of the sources of uncertainty (i.e. mapping the parameters that affect the results and assigning probability distributions to them); second, implementation of a set of simulations using the values found in the first step; third, quantification of the uncertainty using statistical inference to estimate the probability distribution of the results.

4 FIELD TESTS

The literature review included in section 3.2.1 showed that, although there are experimental tests of gas dispersion reported, their data are not suitable for a comprehensive CFD validation exercise. The vast majority of experiments found in the literature were carried out many years ago, when there was no availability of suitable equipment for taking intensive measurements. On the other hand, recent experiments are also rare and in most cases the data generated are restricted to the private sector and not available for the scientific community. Experiments involving scenarios with barriers or any degree of confinement are even scarcer. Therefore, new experiments designed for comprehensive validation studies are needed, being those one of the main aims of the work at hand. In this chapter, the field campaign undertaken within the framework of this thesis is reported.

The field tests were performed by a joint venture between University of São Paulo and Universitat Politècnica de Catalunya; the experimental campaign was undertaken at Can Padró Security and Safety training site during 22nd-25th July of 2014 (sponsored by São Paulo Research Foundation – FAPESP, project grant 2013/18218-2). The field tests consisted of LPG clouds formation and dispersion tracking. The vapour clouds were intensively monitored to determine concentration evolution with time and space.

4.1 Experimental arrangement

4.1.1 Supply system

The site layout consisted of a LPG storage tank, a release and distribution system and a discharge area in which the clouds were produced and monitored. The LPG composition consisted of 97% propane (volume), 1.5% butane and 1.5% of other gases such as hydrogen and nitrogen. It was stored in a 4 m^3 pressurized vessel (saturation pressure at ambient temperature) located roughly 45 m apart from the cloud dispersion path on an upper site, at a relative elevation from the ground of 15 m. The fuel flowed through a 38 mm diameter pipe with a total length of 50 m up to the release point, which was located at 1.5 m high as shown in Figure 29; Figure 30 and Figure 31 present details of the storage tank and the release point. It can be observed how the system has two main controlling valves, one close to the tank and

the other to the outlet orifice, by which the LPG vaporization process within the system can be optimized in order to avoid a two phase flow release (Palacios, 2011).

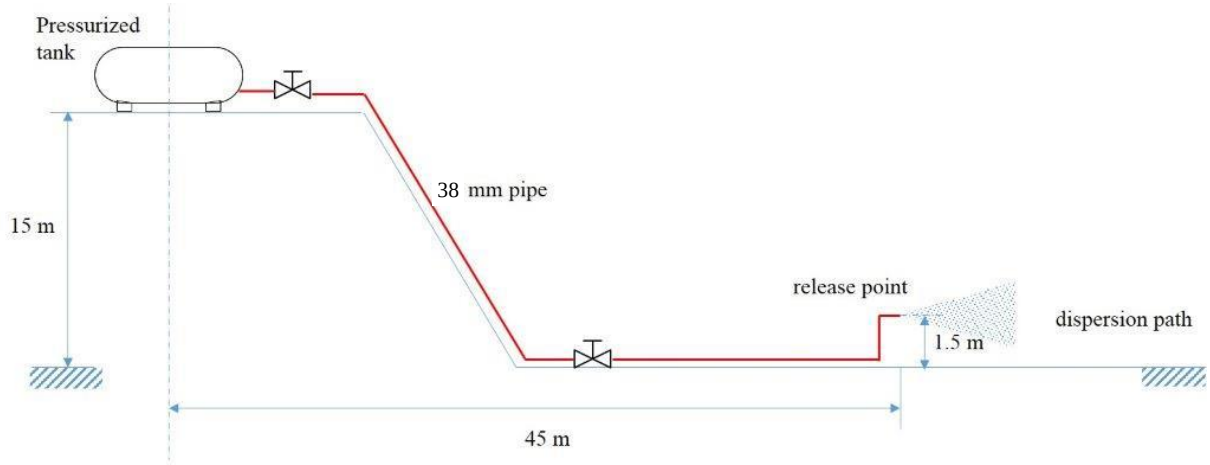

Figure 29 - Supply system layout

Figure 30 - LPG tank

Figure 31 - Release point

4.1.2 Instrumentation

Sensors were placed over a 700 m^2 flat discharge area (35 m in release direction and 20 m in cross direction) to measure cloud features, environmental variables and source characteristics. Some of the experiments were designed to investigate the influence of an obstruction placed in the dispersion path; thus, in some trials a 1.3 m-height 1 m-width fence

was placed perpendicular to the jet direction at the centreline of the discharge area 10 m apart from the release point.

Release point measurements

Pressure and temperature were monitored at the release point by an electronic pressure transmitter (Barksdale, type UPA5) and two K-type thermocouples located 0.05 m upstream of the outlet orifice at a frequency of 4 Hz; thus, the mass flow rate at the outlet orifice was calculated assuming isentropic expansion between the stagnation point and the orifice jet exit by applying the appropriate thermodynamic relationships.

Meteorological measures

The meteorological parameters were monitored by one meteorological station (Vantage Vue Wireless of Davis Instruments), which registered the ambient pressure, the relative humidity, the ambient temperature and the wind speed and direction at a frequency of 0.5 Hz. Additionally, 5 ultrasonic wind sensors (WindSonic OP1 of Gill Instruments) were used to monitor the wind speed and direction (1 Hz frequency); the former placed at 1 m height aligned with the release point, other 2 placed at 1 and 2 m height 7 m apart from the release point and the remaining 2 also at 1 and 2 m height 14 m apart from the release point, all on the side of the discharge area. Figure 32 shows a scheme of the discharge area in which the position of all the sensors can be found. The numbered orange dots represent the location of the wind sensors. As explained there were 3 positions (W1-W3). The letter code used to designate the height at which the sensor was placed is as follows: anemometers located at 1 m height were designated by an “A”, and anemometers located at 2 m height were designated by a “B”.

Concentration measurements

The concentration of LPG was indirectly obtained measuring oxygen concentration at the cloud path, assuming that any decrease in the concentration of oxygen is caused by the displacement of oxygen by the LPG vapour; the oxygen concentrations within the cloud were measured using 47 self-powered electrochemical oxygen sensors (2FO flue gas sensor of CiTicel) capable of measuring oxygen concentrations in the range 0-25 volume percentage. Oxygen sensors were made of a galvanic cell, being the current flow between the cell

electrodes proportional to the oxygen concentration to be measured. The sensors contained a bridge resistor to provide a voltage power (mV) output. A small amount of oxygen was consumed in the cell reaction in order to produce the current flow and the subsequent voltage power output.

As reported in the manual of the sensors (City Technology, 2010), the concentration of oxygen is estimated by:

$$S = k \log_e \frac{1}{1 - C} \tag{35}$$

where:

S is the sensor signal

C is the oxygen concentration

k is a sensor constant

Assuming that the air is formed by oxygen and nitrogen, and that any decrease in the concentration of oxygen is caused by displacement of oxygen by LPG vapour, the LPG concentration is given by:

$$C_{LPG} = \left(1 - C_{O_2} - C_{N_2}\right) \cdot 100 \tag{36}$$

where:

C_{LPG} is the LPG concentration

$C_{O_2}$is the concentration of oxygen

$C_{N_2}$is the nitrogen concentration

Thus, considering the composition of air equal to 20.9% of oxygen and 79.1% of nitrogen, the LPG concentration can be calculated as:

$$C_{LPG} = \left(1 - C_{O_2} - \frac{79.1}{20.9} C_{O_2}\right). 100 \tag{37}$$

The oxygen sensors were placed at 18 different locations within the discharge area at three different heights: 0.1, 0.6 and 1.3 m. Figure 32 shows a scheme of the discharge area in which the position of the oxygen sensors can be found. The numbered blue points represent the

location of the mast by which the sensors were sustained. The code used to number the sensors is as follows: sensors located at 0.1 m were designed by an “A”, sensors at 0.6 m by a “B” and sensors at 1.3 m by a “C”. As an example, mast 3 supported 3 sensors (designed in the figure as 3ABC, whereas mast 17 only supported sensors at 0.1 m and 0.6 m (designed 17AB in the figure).

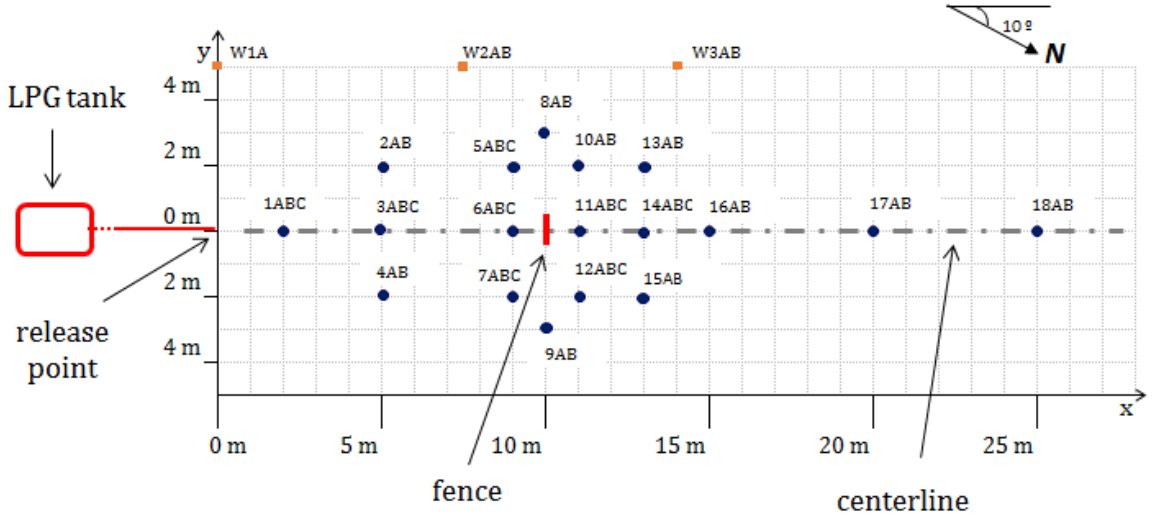

Figure 32 – Sensor array.
Oxygen sensor array (blue points); the numbers are identifiers of the masts where the sensors were attached and the letters A, B and C represent the sensors height, at 0.1 m, 0.6 m and 1.3 m respectively. The orange points named W1-W3, represent the location of the anemometers at 1 m height (A) and 2 m height (B).

Visual records

Experiments were also recorded by a visible camera. Figure 33 shows an image of one of the tests performed, where it can be observed the release point, several masts used to sustain the oxygen sensors (positions 1, 2, 3, 4, 5, 8 and 10) and the 3 higher masts (positions W1, W2 and W3) used to support the anemometers and the vapour cloud formed.

Data gathering

During the field tests, in order to register data, one datalogger (DataTaker DT85) with 2 expansion modules CEM20, and one Field Point data acquisition system (National Instruments) were used; data were recorded at a rate of 4 Hz.

The data collected by the meteorological stations and the dataloggers were stored by two portable work stations with the following characteristics: 3rd Generation Intel Core i5-3340M (2.7GHz to 3.4GHz with Intel® Turbo Boost 2.0, 4 Threads, 3MB Cache).

Figure 33 - Image of trial P25_2, showing the release point and masts; at 40 s from the beginning of the release and release rate of 0.17 $kg.s^{-1}$.

4.1.3 Safety measures

Safety measures were planned and taken into account before and during the tests. It has to be highlighted that the experiments did not represent any risk to population due to the fact that Can Padró training centre is located in an isolated spot. Safety measures considered can be summarized as follows:

- All persons who participated in the tests (7 persons of UPC and USP) had knowledge about measures of safety and had training in technological and labour risks.

- The Can Padró training centre staff provided logistical support and the personnel in charge of operating the controlling valves; this personnel was equipped with full protective equipment.

- A safety zone was previously established for people to remain during the test duration (i.e. gas release and full cloud dilution).

- There was a firefighting truck near the experimental area ready to go, which could be triggered in case of a necessary intervention.

- Areas adjacent to the experimental area had their activities suspended and were isolated in order to maintain a safety perimeter.

4.1.4 Trials and procedures

In order to define the trials of the field tests, preliminary CFD-based simulation jobs were performed to obtain initial information on flows, concentrations and sizing of the LPG clouds expected. Previous simulations were made starting with some flux conditions that were specified elsewhere (Palacios, 2011) when using the same LPG installation to undertake other type of experiments, such as flash fires. The results of these preliminary simulations were analysed in terms of the distance at which the jet would touch the ground, the maximum distance reached by the cloud with concentrations greater than 1.0% (1/2 LFL) and the total time needed for cloud dilution, i.e. the duration of the release plus the time that the cloud would take to dilute at concentrations less than 1.0%. The main outcomes of these preliminary simulations were that the field tests should be performed with flow rates up to 1.0 $kg.s^{-1}$ to get maximum distances of around 50-60 m and dilution times around 60 s (more information in Appendix B).

During the first two days of the campaign, the experimental area was prepared and preliminary tests were performed to set-up the main experimental conditions (i.e. to identify the best position for the equipment, to adjust the instrumentation and to test the operation of the whole system). On the third day, four trials were taken during the period at which the meteorological conditions remained favourable (i.e. gentle wind aligned with the direction at which the sensors were deployed and no precipitation). The specifications of the trials are gathered in Table 18.

However, during the first and the fourth trials, pressure data at the release outlet were not recorded due to technical problems with the data acquisition system. Therefore, it was not possible to calculate the flow rate of these trials and hence they were discarded for further analysis. Thus, in the present study two trials are presented and intensively discussed: P25_2 and P25_3. As shown in Table 18, the former trial consisted of a release of 8 kg of propane with no obstacles present at the discharge area and the second consisted of a release of 6 kg of propane with the presence of a fence, both releases of 40 s of duration.

Table 18 - Trials of the field tests

Characteristics	Trials			
	P25_1	P25_2	P25_3	P25_4
Obstructed (O)/ Unobstructed (U)	U	U	O	O
Duration of spill [s]	30	40	40	60
Valve close to the tank [% opening]	25	25	25	25
Valve close to the outlet orifice [% opening]	100	100	100	50
Amount of mass released [kg]	-	8	6	-

The test procedure was established as follows:

- To place the oxygen sensors at the predetermined locations within the dispersion area;

- To install the pressure transducer and the thermocouple at the outlet orifice;

- To place the anemometers and the set their connection to the portable work station;

- To connect the oxygen sensors to dataloggers;

- To place the video camera at the required position and to set its field of view to capture the whole evolution of the cloud;

- To place the meteorological station and set its recording conditions;

- To synchronize all the instrumentation;

- To start the data-logging system;

- To double check that all the instruments were working properly;

- To personnel evacuate the test site to the safe area;

- To open the manual valves at the LPG supply line;

- To visually observe the release and the dispersion of the gas;

- To close the manual valves at the LPG supply line;

- To waiting the total LPG dilution;

- To check, download and store registered data.

4.2 Results of the field tests

The release rates were calculated from the pressure and temperature ranges at the outlet orifice registered during the trials (in both cases measured values averaged by 1 s were used). The jet velocity at the outlet orifice and the mass flow rate were calculated assuming isentropic expansion between the stagnation point and the orifice jet exit. The total amount of fuel released was obtained by the integral of the mass flow rate variation during the release. An amount of 8 kg was released during P25_2 and 6 kg were released during P25_3. Figure 34 shows the 1 second averaged mass flow rate for trials P25_2 and P25_3.

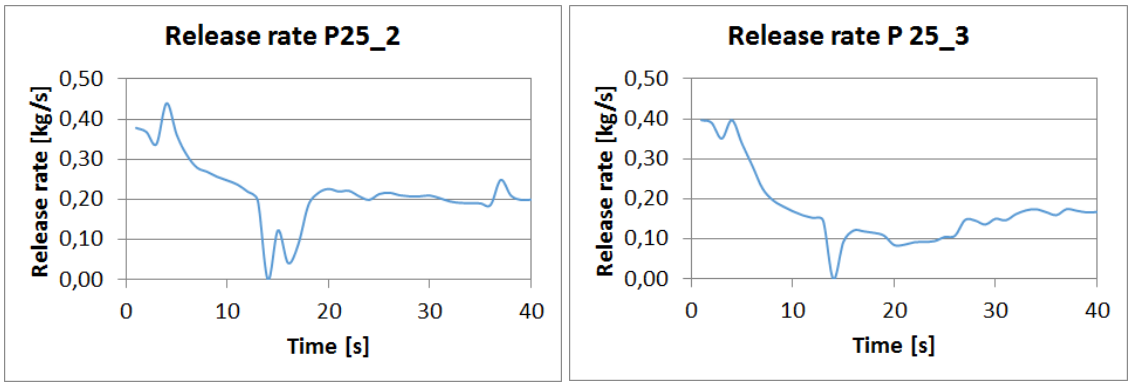

Figure 34 - Mass flow rate release averaged by 1 second of trials P25_2 (left) and P25_3 (right).

In both graphs, a sharp decay at around 15 s after opening the valves can be observed. These drops are related to the pressure drops registered at the outlet orifice. Figure 35 shows the pressure measured during the release at the outlet orifice (averaged by 1 s).

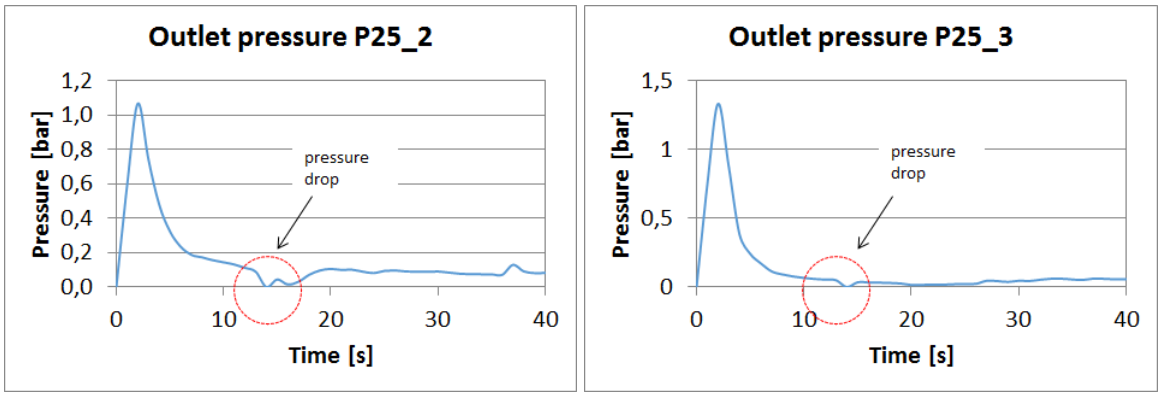

Figure 35 - Measured pressures at the outlet orifice averaged by 1second.

Mean meteorological conditions during the tests are shown in Table 19. 1 second-averaged values for general wind speed, temperature, relative humidity and atmospheric pressure can be found in Appendix D, as well as averaged values obtained from the anemometers.

Table 19 - Mean meteorological conditions during the tests

	Trial P25_2	Trial P25_3
Wind speed [km.h^{-1}]	2.5	3.4
Temperature [°C]	21.2	22.5
Relative humidity [%]	86.8	87.4
Pressure [hPa]	993	993

The 1 s averaged concentration measured by each available sensor is also included in Appendix D, as a function of time. It has to be said that it had been raining during 2 hours prior to the beginning of the tests and several sensors did not work well due to accumulated water over the sensor output. The experimental data of trial P25_2 fits within a range of 0.01%-7.43% of LPG and within a range of 0.03%-7.08% for trial P25_3. Maximum values were recorded at location (2.0; 0.0; 1.3) for both trials. As expected, the highest concentrations were measured in the first 5 m from the release point.

Data on concentration as a function of time are very scarce in the literature; usually the experimental data reported is plotted for specific instants or only peak concentrations as a function of the distance from the release point are provided. The experimental data provided here is comprehensive in time and space and, as such, it is optimum for validation studies and time-dependent analyses.

Figure 36 shows an example of a concentration profile obtained by one of the sensors located 15 m apart from the release point at 0.6 m height (sensor 16B, as the codification used in Figure 32) during the test P25_2 and P25_3. Comparing the trials, it is noted that the concentrations of this sensor in the trial with obstruction decrease faster, there was more

turbulence generated by the fence at this trial and the cloud diluted faster in P25_3 than in P25_2.

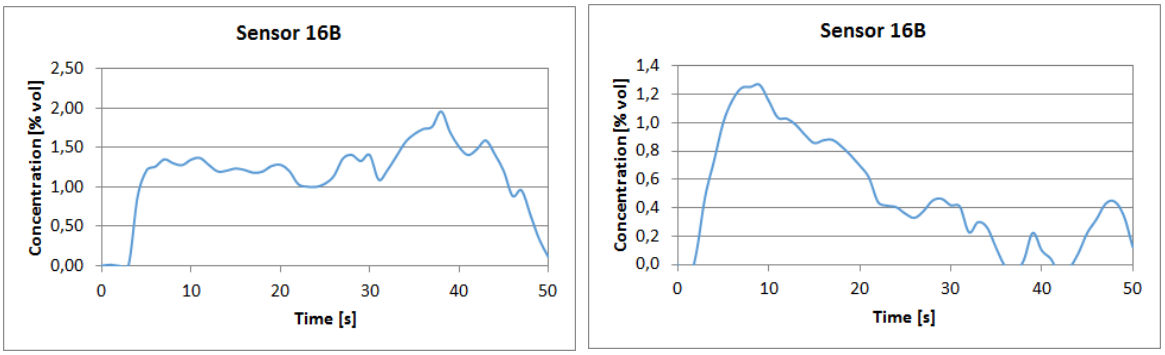

Figure 36 - Concentrations as function of time at sensor 16B of trials P25_2 (left) and P25_3 (right)

5 SIMULATION OF THE FIELD TESTS

CFD simulations of trials P25_2 and P25_3 were undertaken with FLACS software in order to study the software performance when challenged against the experimental data. The scenario conditions set to perform the simulations are presented in Table 20. The values of ambient temperature, ambient pressure, relativity humidity and wind direction and speed were considered as the median of the recorded values during the duration of each test. At the moment of the trials, there was a cloud cover of around 80% and it had been raining during 2 hours prior to the beginning of the tests. This condition reduced considerably the heat emitted from the ground leading to stable atmospheric condition; thus, the Pasquill class used was E – slightly stable. The ground roughness was assumed equal to 0.03 which is the typical value for concrete surface (GexCon AS, 2013).

The pressure and temperature ranges at the outlet orifice are detailed on Table 20 by the minimum and the maximum values registered during the duration of the trials. The simulations were performed by considering a 1 second-averaged variable mass flow rate presented previously in Figure 34.

Table 20 - Scenario conditions

Variable	Unit	P25_2	P25_3
Ambient Temperature	ºC	21.2	22.5
Ambient pressure	hPa	993	993
Relativity humidity	%	86.85	86.90
Wind direction	º	185	235
Wind speed at 1 m high	$m.s^{-1}$	0.49	0.70
Pasquill Class	-	E	E
Ground roughness	m	0.03	0.03
Discharge direction	-	horizontal	horizontal
Discharge height	m	1.5	1.5
Discharge orifice diameter	m	0.038	0.038
Release duration	s	40	40

Variable	Unit	P25_2	P25_3
Temperature release range	ºC	-28.10/4.71	-28.41/10.26
Pressure release range (min/max)	hPa	100/1200	100/1300
Amount of fuel released	kg	8.0	6.5
Discharge rate (min/max)	$Kg.s^{-1}$	0.04/0.38	0.08/0.39

The simulation domain was discretized using a single block Cartesian grid, defined following the guidelines presented in section 3.4. An orthogonal base X, Y and Z was used, being X horizontal and parallel to the jet direction, Y horizontal and perpendicular to the jet direction and Z vertical. The domain extended 50 m in the X direction (from 5 m before the release point to 45 m after the release point), 48 m in the Y direction (centred on the release point) and 10 m in the Z direction (from de ground level). As such, the release orifice was located at the point (0, 0, 1.5) in the domain. The domain was divided in two types of meshes: the former being a coarse (macro) grid, representing the zone where the dispersion is expected to occur; and the latter being a fine (micro) grid, representing two different swaths intersecting around the release point: one vertical, formed by a mesh of cells at the centreline of the dispersion path, and the other horizontal, formed by a mesh of cells centred at 1.5 m height (i.e. release height). In order to obtain stable simulations, FLACS considers a certain transition among the micro and the macro grid. The grid was not stretched toward the limits because the area analysed was not large and was not necessary save runtime simulation.

The cells were represented by 1 m edge cubes at the macro grid. In order to specify the micro grid were used the guidelines presented in section 3.4, which specify that the area of the expanded jet must be solved in only one cell and that the area of this cell across the jet should be larger than the area of the expanded jet but not larger than twice. Thus, the jet area expected after the expansion at ambient pressure was estimated using the FLACS jet utility (the jet utility is based on a one-dimensional model for the release of an ideal gas from a pressurized reservoir through a nozzle into an open atmosphere (GexCon AS, 2013)) and the dimensions of the cell across the jet defined so that the area fell between the specified limits. Thus, the width and height of the micro grid cells were fixed at 0.04 m (as a function of the jet area expected after the expansion at ambient pressure).

It is also recommended that the aspect ratio (the ratio between the smallest and largest side of the cell) of the micro grid should be no larger than five (due to stability of the numerical solution); thus, the length of the cells was fixed at 0.20 m. Next, the cells nearby the leak were smoothly increased to the macro grid resolution, maintaining the maximum change in grid resolution from one grid cell to the next less than 40%, the amount of cells smoothed were the minimum necessary to maintain this rate (as recommended in section 3.4). The simulation volume consisted of a single block composed by the macro grid, the micro grid and the smoothed area, as presented in section 3.1.1 - Figure 4.

Finally, monitoring points were inserted in the simulation specifications at the same locations where the sensors were placed in the field, which allowed the measured values of concentration to be compared with the simulated values.

5.1 Results and discussion

Trial P25_2

Figure 37 shows measured versus simulated values of peak LPG concentrations calculated from 12 active oxygen concentration sensors at the centreline during trial P25_2 (as previously mentioned, several sensors did not work well due to the rain before the tests). FLACS performance was assessed using the factor of two range (FAC2), which analyses whether the simulated values fall within a ±factor of two of the measured data. This factor is widely used for CFD validation purposes. It was one of the parameters recommended by Weil et al. (1992) and Hanna et al. (2004) to evaluate air quality models, later on, it was recommended by HSE in the Model Evaluation Protocol (Ivings et al. 2007) and more recently it was used by Coldrick et al. (2009) and Ivings et al. (2013). FAC2 confidence limits are included in the figure as dashed lines; 75% of the plotted points fit within this range.

The same FAC 2 analysis was performed considering all the sensors that worked well during the tests not just those located at the centreline. In this case, 70% of the simulated/experimental values fit well on the FAC 2 range (Figure 38).

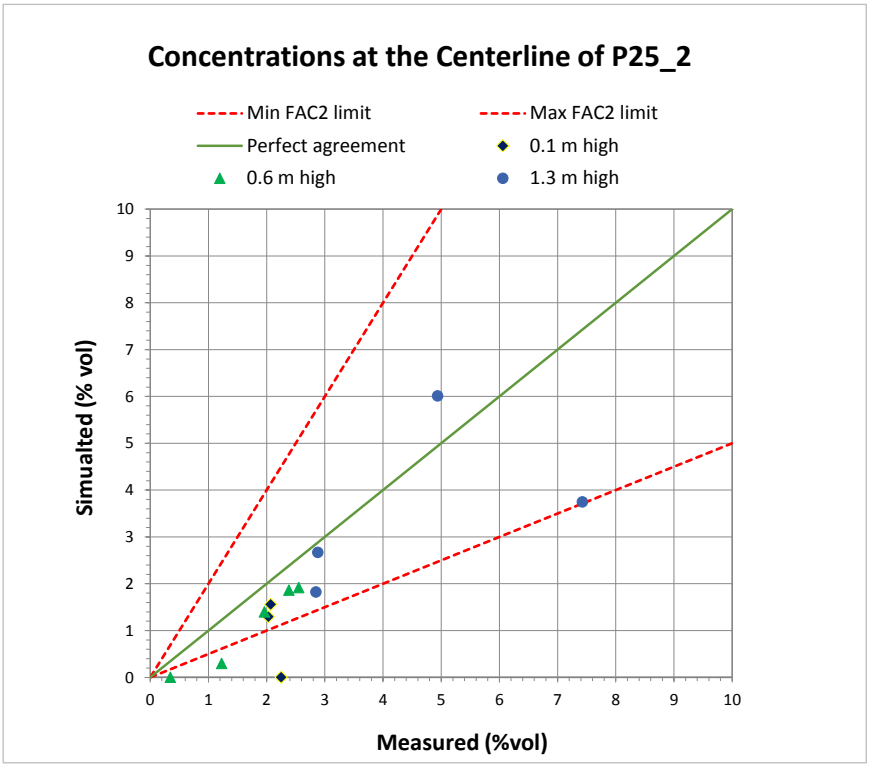

Figure 37- Comparison between simulated peak concentration and experimental data of centreline monitored points of trial P 25_2; the area between the dashed lines is the range of factor 2.

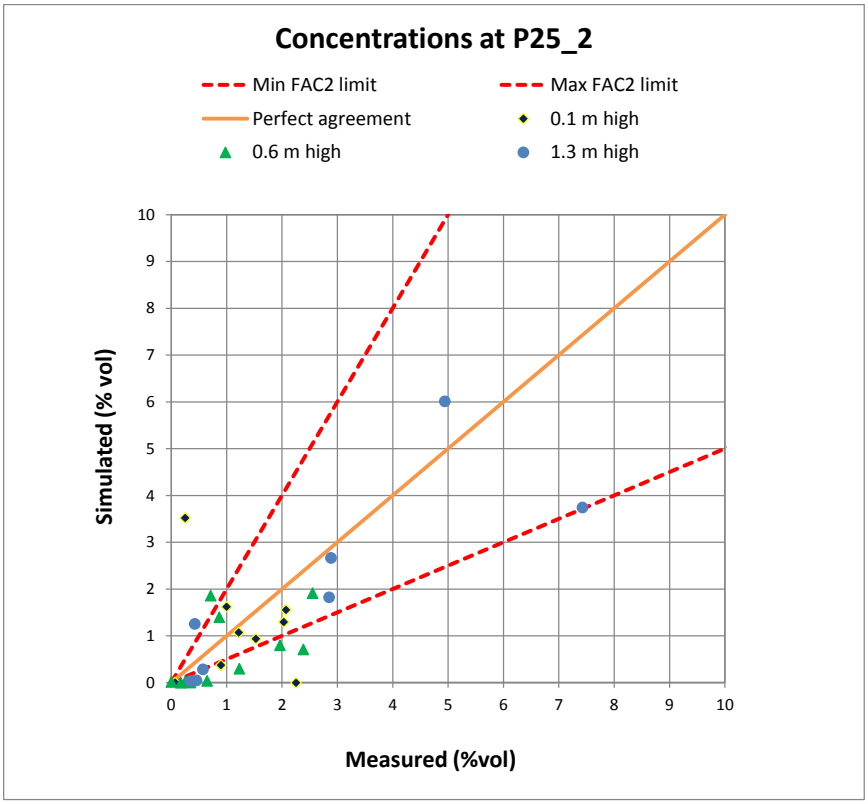

Figure 38 - Comparison between simulated peak concentration and experimental data of all monitored points of trial P 25_2; the area between the dashed lines is the range of factor 2

Only three points did not adjust to the FAC2 range in Figure 37. Two of them were representing the concentrations measured by two sensors placed 2 m apart from the release point at 0.1 and 0.6 m high, respectively. In those locations, the simulated values (both <0.1%) were significantly lower than the measured concentration real sensors (0.3 % and 2.2%), these two points can be observed in previous figures by the respective symbols fully stepping on the abscissa axis. The third sensor was placed 5 m from the release point at 0.6 high. The simulator also failed when trying to predict the maximum LPG concentration at a point (5, 0, 0.6), since the simulated value (0.3%) was significantly lower than the measured concentration (1.28%).

Concerning the evolution of the concentration with time, FLACS was able to peak the general trend for most of the sensors, excepting those placed near the source term (in the first 5 m of the discharge path) in which the simulator underestimated significantly the measured values, as previously noted.

Figure 39 and Figure 40 show two examples of the LPG comparison of the real/simulated concentration evolution with time plotted for two oxygen concentration sensors, the first located at the centreline 9 m apart from the release point (sensor 6A at a height of 0.1 m) and the other located 15 m apart from the release point, at the centreline too (sensor 16B, at a height of 0.6 m). Measured release rate (which acts also as input in the FLACS scenario) is also plotted for comparison purposes.

Regarding the sensor 6A, it can be observed how simulated concentration is more sensitive to release rate changes than the real concentration. As such, an initial peak (simulated, 1.3%) can be found around 5 s, which is the response of a maximum release rete occurring roughly one second before. The real concentration evolution is smoother, nevertheless showing also a peak (of around 1%) one second later than the simulated one. This tendency can still be observed when paying attention to the release rate drop occurring 14 s after the start of the test: simulated concentration reacts accordingly showing a drop 5 seconds after, whereas the real concentration takes longer to descend, showing a minimum 8 seconds after the release rate drop. Certainly, there is an increasing delay between the dynamics of the simulated cloud and the real one, and as such the simulated cloud dilutes faster than the real one. This is due to the fact that the simulated cloud is not able to pick the accumulation that the real one experienced. This becomes more evident 25 seconds after the start of the release, when real

concentration in sensor 6A increases, while the simulated one decreases according to the patter shown by the release rate evolution. Furthermore, it is also possible to note greater oscillations on the measured concentration values compared to the predicted values.

Sensor 16 B behaves in a similar way: although the first concentration maximum is accurately picked by the simulated cloud (both in terms of absolute value and instant of time), the simulated cloud disperses faster, not showing the accumulation registered by the real sensor. Also, simulated concentration curve is smoother compared to the real evolution.

One of the reasons that could explain these particular lacks of accuracy could be found in the simulated wind. A constant wind is considered in the simulations; however, during the execution of the test, there were oscillations on wind speed and direction, the wind speed ranged between 0.03 $m.s^{-1}$ and 1.02 $m.s^{-1}$ and the direction between 63º and 287º. With a simulated wind dynamics simpler than the real one, FLACS may represent less turbulent eddies than the real ones occurring in the experimental site. Therefore, the simulated cloud disperses smoothly than the experimental cloud. However, in order to verify this hypothesis more experimental data covering a wider range of wind conditions would be needed as well a better representation of wind profile in the simulations.

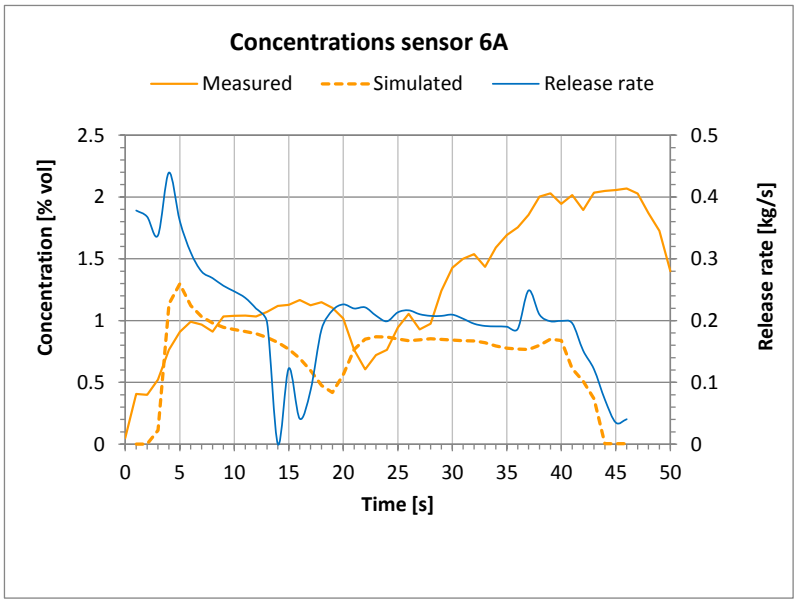

Figure 39 - Measured and simulated concentrations at sensor 6A position, in the centreline, 9m from the release point 0.1 m high.

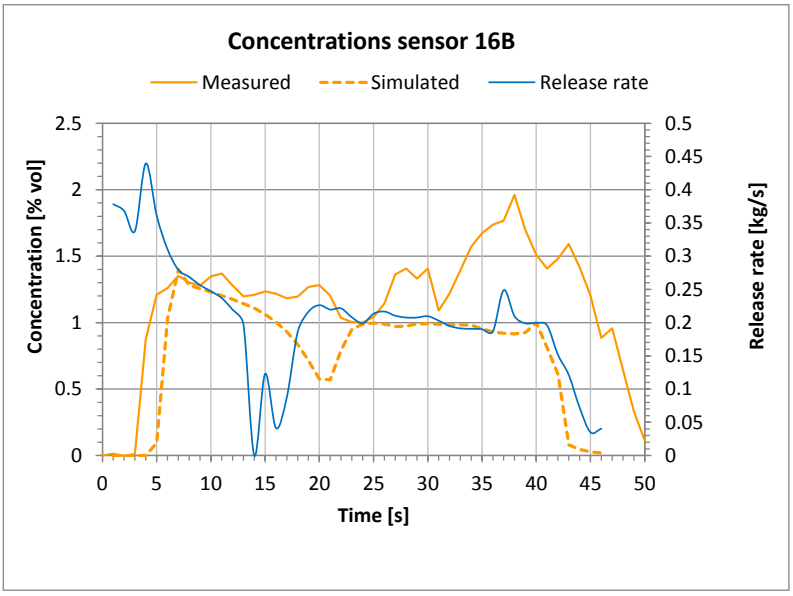

Figure 40 – Measured and simulated concentrations at sensor 16B position, in the centreline, 15 m from the release point 0.6 m high.

Trial P25_3

Figure 41 presents measured versus simulated values of peak LPG concentrations at the centreline calculated from 12 active oxygen concentration sensors during the trail P25_3. The trial P25_3 was undertaken some minutes after trial P25_2; thus, the values in Figure 41 correspond to the same sensors of the centreline that did work well during trial P25_2.

In this case, 83% of the predicted/measured points also fit well within the range of factor 2. In addition, performing the same FAC 2 analysis considering all the sensors (not just those located at the centreline) 72% of the points were found to fit well within the FAC 2 range (Figure 42). As in the previous trial, for the two sensors placed 2 m apart from the release point, at 0.1 and 0.6 m high, no significant concentrations were predicted.

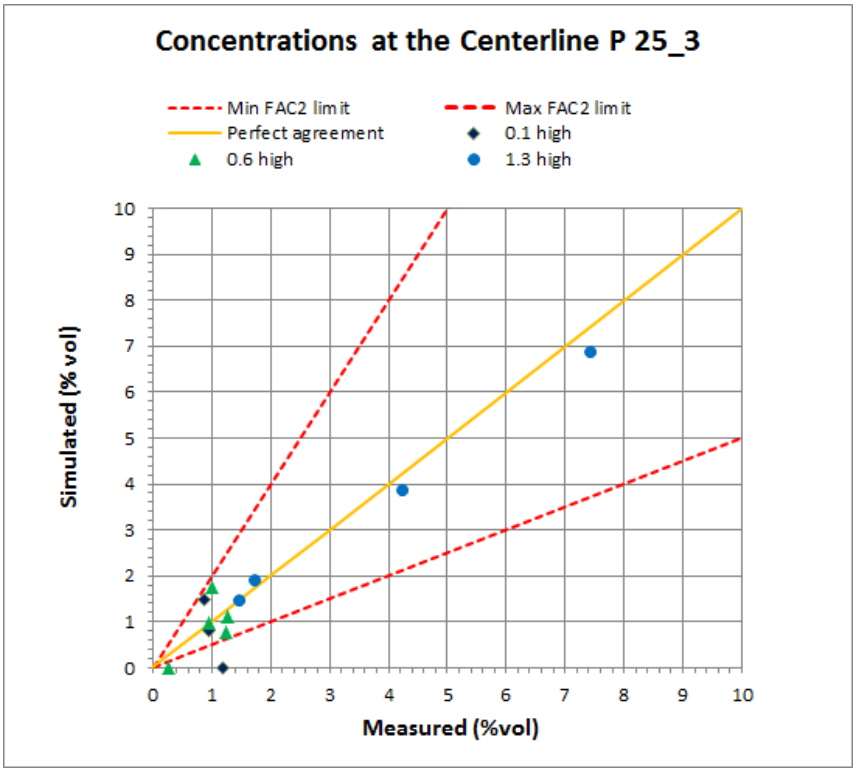

Figure 41 - Comparison between simulated values and experimental data of centreline points of trial P 25_3

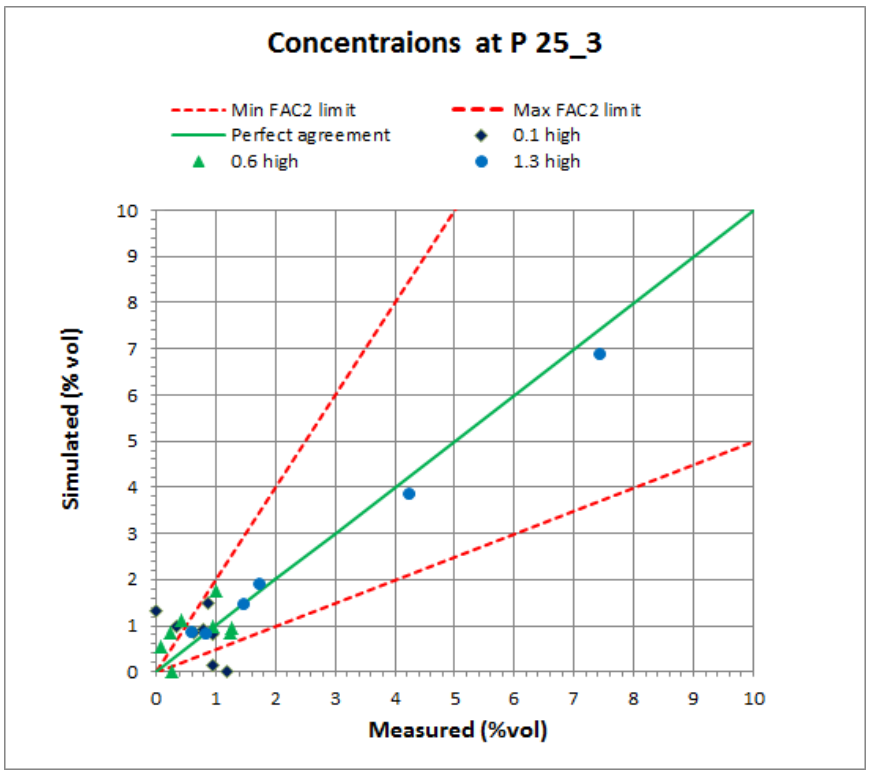

Figure 42 - Comparison between simulated peak concentration and experimental data of all monitored points of trial P 25_3; the area between the dashed lines is the range of factor 2

Figure 43 and Figure 44 show two examples of the LPG concentration evolution with time calculated from two oxygen concentration sensors, one located at the centreline, 1 m after the fence (0.6 m high) and the other, located at the same place, but at a height of 1.3 m; Concerning sensor 11B, it can be seen how both concentration curves, measured and simulated, present a very good agreement. It is worth noting that there is a time delay (of around 4 s) when comparing predicted vs. measured peak concentrations, but in this case the first maximum is the one corresponding to the measured concentration. Despite this initial delay, the simulated cloud again seems to dilute faster than the real one. The effect of the fence can be clearly observed in both real and simulated curves; although the release rate keeps around 0.15-0.2 $kg.s^{-1}$ during the last period of the experiment (between 28 s – 38 s), concentration values show a general decreasing trend. Again, it can be clearly seen how the simulated curve is smoother than the real one, for the above mentioned reasons.

Concentration evolution of sensor 11C is rather well simulated too. In this case, the simulated cloud shows a maximum peak in the 11C sensor location faster than the real one. However, the simulated cloud dilutes faster. Interestingly, the simulated cloud fails to represent the complex accumulation dynamics detected by the real sensor occurring from 30 seconds after the release. Rather, simulated concentration becomes negligible during this particular period.

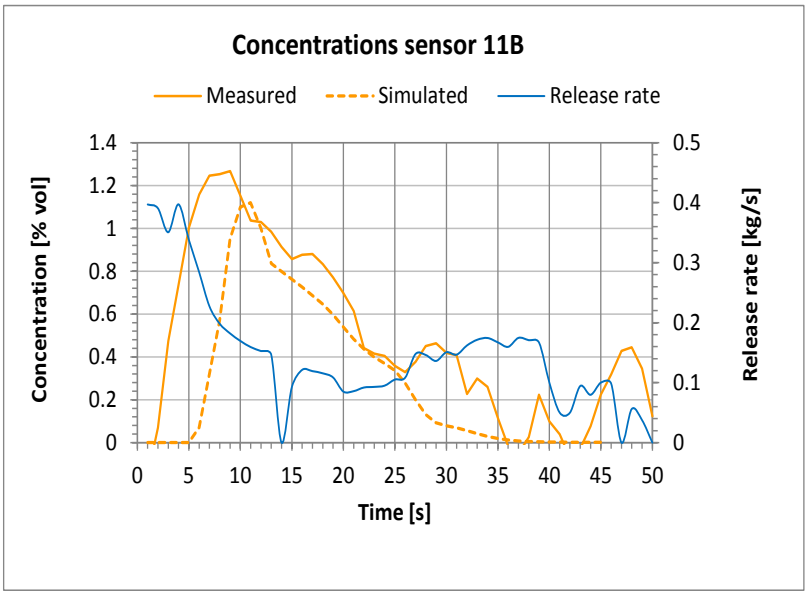

Figure 43 - Measured and simulated concentrations at sensor 11B position in trial P25_3 (1 m after the fence at 0.6 m high)

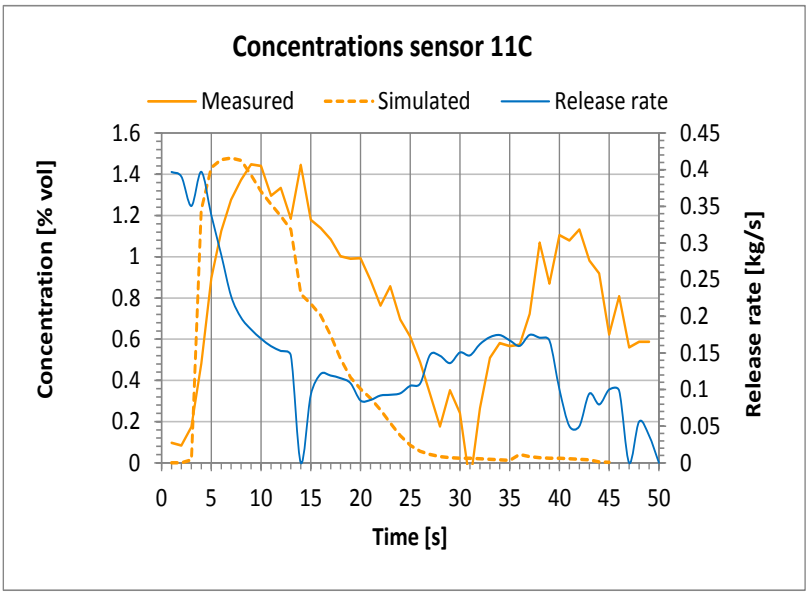

Figure 44 - Measured and simulated concentrations at sensor 11C position in trial P25_3 (1 m after the fence at 1.3 m high)

Figure 45 and Figure 46 show the cloud concentration profile at the central plane of the cloud path (Y=0) 10 s after the release start, for trials P25_2 and P25_3 respectively. Some monitor points with their related concentrations (experimental and simulated) are gathered in the box. In monitoring points of Figure 45, the mean error between measured and simulated values was 13%. It is worth noting that, at this instant, concentrations were low and although found maximum errors of around 39% were found (e.g. error in 11C), they do not represent large discrepancies, e.g. the maximum difference between the simulated and the measured volumetric concentration is only of 0.41% (sensor 11C).

Concerning to trial P25_3 (Figure 46), the mean error between simulated and experimental concentration was 18%, with a maximum error of 36% when simulating the concentration of the sensor 16B (errors roughly of the same order of magnitude than ones computed for the trial P25_2). Moreover, it is possible to verify the influence of the fence placed 10 m apart from the release point on the cloud dispersion, since part of the cloud is trapped before the barrier. In P25_3, the simulated propane concentration at locations 11B, 11C, 16A and 16B were significantly lower than the concentrations simulated at the same positions for trial P25_2, with decreases between 13% and 44%.

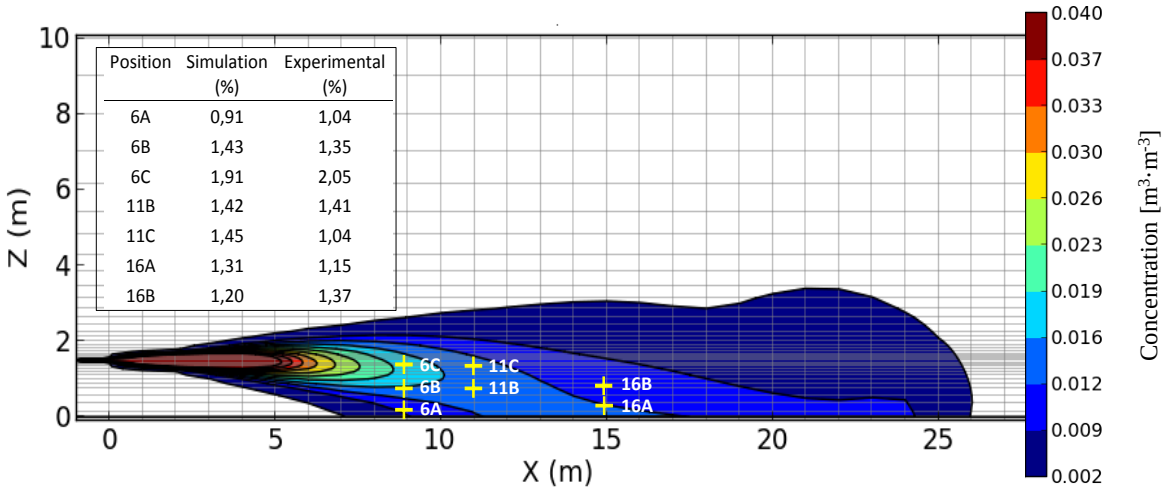

Figure 45 – Cloud profile concentration of Trial P25_2 at centreline, 10 s after the release start.

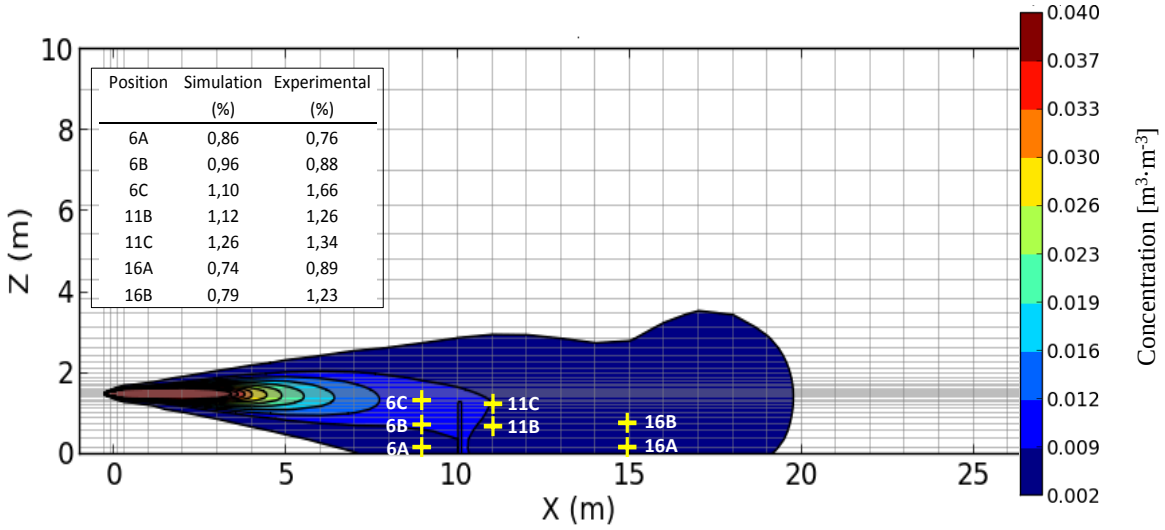

Figure 46 - Cloud profile concentration of Trial P25_3 at centreline, 10 s after the release start.

5.2 Conclusions

FLACS software was challenged against experimental data collected in Can Padró trials for a couple of tests, one unobstructed and another with the presence of an obstruction. In general terms, the CFD-based simulator has been shown good performance when simulating cloud concentration. It has to be highlighted that FLACS passes with good accuracy the FAC2 test, which is a well-established and standardized indicator for model validation purposes. FLACS shows mean errors of 13% for unobstructed scenarios, and of 18% for obstructed ones, which are acceptable given the general dynamics of the experimental tests

(i.e. unsteady release rate and wind fluctuations in speed and direction). Moreover, FLACS seems to successfully reproduce the presence of complex geometry and its effects on cloud dispersion, showing realistic concentration decreases due to cloud dispersion obstruction by the existence of a fence.

FLACS performance may be improved by setting the scenario considering more complex wind dynamics as the ones encountered during the field tests, at the expense, however, of the simulation runtime. In summary, the simulations set and calculated in this chapter show a good compromise between accuracy and computational cost, which proof the validity of the main guiding principles stated in previous section 3.4.

6 CONCLUSIONS

Dispersion of hazardous gas releases occurring in transportation or storage installations represent a major threat to health and environment. Therefore, forecasting the behaviour of a flammable or toxic cloud is a critical challenge in quantitative risk analysis. The main aim of this dissertation has been to provide new insights that can help technological risks analysts when dealing with complex dispersion modelling problems, particularly those problems involving dispersion scenarios with barriers or semi-confined. Literature survey, experimentation and CFD modelling have been the three fundamental cornerstones of the work at hand, which have allowed addressing the particular goals defined in the introduction. The main conclusions to be drawn from all the activities developed within the framework of this dissertation are the following:

- The empirical and integral models traditionally used in dispersion analysis, usually provide reliable and fast results for dispersions in scenarios over flat terrain; however, in scenarios with any degree of complexity, the predictions performed by these models tend to overestimate the impacts in the far field and underestimate the impacts in the near field.
- The physical models implemented on CFD tools need more computational resources to be solved than traditional models, but they are more suitable to analyse dispersions on environments with barriers. Among all the available tools, FLACS software is so far the most appropriate tool to be used. It has specific models for consequence analysis, which shall allow the representation of physical barriers present into the dispersion path. However, FLACS CFD software, as other codes alike, still needs to be fully validated. FLACS validations studies reported in the literature present essentially qualitative results and do not provide enough information for a comprehensive quantitative performance assessment.
- A literature review on dispersion field tests has shown that data related to the dispersion in an environment with obstacles are scarce; large part of the tests were performed long time ago and therefore the range of data generated is limited. On the other hand, most of the data obtained by recent tests are not available for the open public. Although the literature survey has shown some experimental data available for validation studies, none of the works include comprehensive exercises

giving new insights of how to perform accurate CFD simulations nor giving precise rates of FLACS performance. Therefore, new experiments designed for comprehensive validation studies are needed.

- This study also has pointed out that that when using a CFD tool, a certain estimation of the uncertainty related to the outputs provided by the simulator has to be performed. Quantification of uncertainty can be performed following diverse methodologies, but those have to include at least a grid dependence and a parametric sensitivity analysis. There has not been found any widely applied sensitivity analysis methodology nor a complete sensitivity analysis performed in CFD outputs when modelling dispersion. Therefore, a comprehensive inspection of all the possible sources of uncertainty that may have an effect on the ouput cloud concentration when simulating dispersion with FLACS software has been performed. Reproducibility capacity, grid dependence an a local approach sensitivity analysis for physical variables and simulation parameters have been inspected using historical data. FLACS has shown high reproducibility capacity, and some grid dependence, particularly concerning the height of the macrogrid and microgrid cells. Finally, the variables that have made concentration values more sensitive to inputs uncertainty have been found to be discharge height, wind speed, atmospheric pressure and mass flow.
- The main outcomes of preliminary FLACS investigations have been shaped as practical guiding principles to be used by risk analysts when performing dispersion analysis with the presence of barriers using FLACS software or tools alike. Those guidelines have been presented according to the logic sequence of actions needed to perform accurate dispersion simulations using CFD tools: objectives and scope definition, scenario definition, tool selection, geometry and grid construction, simulation parameters setting and estimation of uncertainty. Those guiding principles are meant to contribute to achieve more reliable and reproducible results in dispersion analysis.
- Propane cloud dispersion field tests (unobstructed and obstructed) have been undertaken in this study, by which intensive data on concentration has been acquired. Fine time and space dependent cloud concentration analysis can be performed with the available data. The field tests have contributed to the

reassessment of the critical points raised in the guiding principles and have provided experimental data to be used by the international community for dispersion studies and models validation exercises. The whole dataset of two trials has been included as an Appendix of the dissertation at hand.

- FLACS software has been challenged against the experimental data collected during the field tests. In general terms, the CFD-based simulator has shown good performance when simulating cloud concentration. However, simulated clouds have failed to represent the complex accumulation dynamics due to wind variation, since they have diluted faster than experimental clouds. FLACS seems to successfully reproduce the presence of complex geometry and its effects on cloud dispersion, showing realistic concentration decreases due to cloud dispersion obstruction by the existence of a fence. However, FLACS performance may be improved by setting the scenario considering more complex wind dynamics as the ones encountered during the field tests, at the expense, however, of the simulation runtime. To the best of author's knowledge, variable wind profiles in CFD simulations have never been considered for dispersion analysis and this is certainly a relevant point which shall have to be explored in future work. Further studies may also explore dependence grid analysis considering unstructured grids and hybrid meshes and may expand sensitivity analyses to source term features and other scenarios such as dispersion over water and pool formation.

BIBLIOGRAPHY

Allwine, K. J., & Flaherty, J. E. (2007). *Urban Dispersion Program Overview - PNNL-16696.* Pacific Northwest National Laboratory, Richland, US.

Amendola, A., Contini, S., & Ziomas, I. (1992). Uncertainties in chemical risk assessment: Results of a European benchmark exercise. *Journal of Hazardous Materials*(29), pp. 347-363.

Anderson, J. D. (1995). *Computational Fluid Dynamics - The basics with applications.* Maryland, USA: McGraw-Hill.

Ansys Inc. (2011). *ANSYS FLUENT Theory Guide.* Canonsburg.

Arntzen, B. J. (1998). *Modelling of turbulence and combustion for simulation of gas explosions in complex geometries.* Divison of appield mechanics, thermodynamics and fluid dynamics. Bergen: Thesis for the Doctor engineering degree - The Norwegian university of science and technology.

Barad, M. L. (1958). *Project Prairie Grass - A field program in diffusion.* Air Force Cambridge research Center. Bedford, Mass: Geophys. Res. Paper No. 59, Vols. I and II.

Bartelink, H. H. (1998). A model of dry matter partitioning in trees. *Tree Physiology, 18*, 91-101.

Biltoft, C. A. (2001). *Customer Report for Mock Urban Setting Test (MUST). DPG Doc. No. WDTC-FR-01-121.* West Desert Test Center, U.S. Army Dugway Proving Ground, Dugway, UT 84022-5000.

Blackmore, D. R., Eyre, J. A., & Summers, G. G. (1982, May 10). Dispersion and combustlon behauiour of gas clouds resulting from large spillages of LNG and LPG on to the sea. *The institute of marine engineers, 94*(29), pp. 1-18.

Blocken, B., & Gualtieri, C. (2012). Ten iterative steps for model development and evaluation applied to Computational Fluid Dynamics for Environmental Fluid Mechanics. *Environmental Modelling & Software*(33), 1-22.

Briggs, G. A. (1969). *Plume rise.* US Atomic energy commission Report TID - 25075.

Britter, R. E., & McQuaid, J. (1988). *Workshop on the dispersion of dense gases.* HSE Contract Research Report No 17.

Brown, T. C., Cerdewall, R. T., Chan, S. T., Ermak, D. L., Koopman, R. P., Lamson, K. C., et al. (1990). *Falcon series data report: 1987 LNG vapor barrier verification field.* Research Institute, Report nº GRI-89/0138.

Butler, C. J., & Royle, M. (2001). *Experimental data acquistion for validation of a new vapour cloud fire (VCF) modelling approach.* 1-102: Health and Safety Laboratory - HSE.

Casal, J. (2008). *Evaluation of the Effects and Consequences of Major Accidents in Industrial Plants* (Vol. Volumen 8 de Industrial Safety Series). (Elsevier, Ed.)

CCPS - Center for Chemical Process Safety. (1995). *Understanding Atmospheric Dispersion of Accidental Releases.* New York: Center for Chemical Process Safety.

CCPS - Center for Chemical Process Safety. (1998). *Estimating the flammable mass of a vapour cloud.* New York: Center for Chemical Process Safety.

CCPS - Center of Chemical Process Safety. (2000). *Guidelines for chemical process quantitative risk analysis* (Second ed.). New York: American Institute of Chemica Enginneers.

Chen, C. J., & Rodi, W. (1980). Vertical turbulent buoyant jets: A review of experimental data. *HMT - Science and Applications of Heat and Mass Transfer, 4*, p. 94.

Chien, K. Y. (1982). Predictions of channel and boundary-layer flows with a low-Reynolds-number two-equation model of turbulence. *AIAA Journal, 20*(1), pp. 33-38.

City Technology Limited. (2010, January 5). OP02 - Electrochemical Capillary Controlled Oxygen Sensors. Hampshire, UK.

Coldrick, S., Lea, C. J., & Ivings, M. J. (2009). *Validation database for evaluating vapor dispersion model for safety analysis of LNG facilities - Review.* The fire prtection research foundation.

Cormier, B. R., Ruifeng, Q., Yun, G., Zhang, Y., & Mannan, M. S. (2009). Application of computational fluid dynamics for LNG vapor dispersion modeling: A study of key parameters. *Journal of Loss Prevention in the Process Industries*, pp. 332-352.

Cruz, M. G., Alexander, M. E., & Wakimoto, R. H. (2003). Definition of a fire behaviour model evaluation protocol: a case study application to crown fire behaviour models. *USDA Forest Service Proceedings RMRS*, (p. 29).

Deardorff, J. W. (1972). Numerical Investigation of Neutral and Unstable Planetary Boundary layers. *Journal of Atmospheric Science, 29*, pp. 91-115.

Dharmavaram, S., Hanna, S. R., & Hansen, O. R. (2005). Consequence Analysis—Using a CFD model for industrial Sites. *Process Safety Progress, 24*, pp. 316-327.

Duijm, N. J., & Carissimo, B. (2002). Evaluation methodologies for dense gas dispersion models. In M. Fingas, *The Handbook of Hazardous Materials Spills Technology.* New York: McGraw-Hill.

Duijm, N. J., Carissimo, B., Mercer, A., Bartholome, C., & Giesbrecht, H. (1997). Development and test of an evaluation protocol for heavy gas dispersion models. *Journal of Hazardous Materials*(56), pp. 273-285.

Duijm, N. J., Ott, S., & Nielsen, M. (1996). An evaluation of validation procedures and test parameters for dense gas dispersion models. *Journal of Loss Prevention in the Process Industries, 9*(5), pp. 323-338.

Ermak, D. L. (1990). *User's manual for SLAB: an atmospheric dispersion model for denser-than-air.* California: Lawrence Livermore National Laboratory.

Gant, S. E., Kelsey, A., McNally, K., Witlox, H., & Biblio, M. (2013). Sensitivity Analysis of Dispersion Models for Jet Releases of Dense-Phase Carbon Dioxide. *Chemical Engineering Transactions, 31*, 1-6.

Gavelli, F., Bullister, E., & Kytoma, H. (2008). Application of CFD (Fluent) to LNG spills into geometrically complex environments. *Journal of Hazardous Materials 159*, pp. 158-168.

GexCon AS. (2013). FLACS v10.0 User´s Manual ., (pp. 1-374). Norway.

Gifford, F. A. (1961). Use of routine meteorological observations for estimating atmospheric dispersion. *Nuclear Safety, 2*(47), pp. 47-51.

Goldwire, H. C., Cederwall, R. T., Rodean, H. C., Kansa, E. J., Koopman, R. P., McClure, J., et al. (1983). *Coyote Series Data Report, LLNL/NWC - LNG Spill Tests Dispersion,*

Vapor burn and rapid-phase transition. Livermore, California: vols. 1 and 2, UCID-19953 Lawrence Livermore National Laboratory.

Han, J., Arya, S. P., Shen, S., & Lin, Y. L. (2000). *An estimation of turbulent kinetic energy and energy dissipation rate based on atmospheric boundary layer similarity theory. NASA/CR-*. North Carolina State University. Raleigh, North Carolina, USA: Langley Research Center.

Hanlin, A. L. (2006). A review of large-scale LNG spills: Experiments and modeling. *Journal of Hazardous Materials, A132*, pp. 119-140.

Hanna, S. R., & Chang, J. C. (2001). Use of the Kit Fox field data to analyze dense gas modeling issues. *Atmospheric Environment, 35*(13), pp. 2231-2242.

Hanna, S. R., Briggs, G. A., & Hosker, R. P. (1982). *Handbook on atmospheric diffusion.* Springfield, Virginia, USA: Technical information center - US Department of energy.

Hanna, S. R., Brown, M. J., Camelli, F. E., Chan, S. T., Coirier, W. J., Hansen, O. R., et al. (2006). *Detailed Simulations of Atmospheric Flow and Dispersion in Urban Downtown Areas by Computational Fluid Dynamics (CFD) Models - An Application of Five CFD Models to Manhattan.* Bulletin of the American Meteorological Society.

Hanna, S. R., Hansen, O. R., & Dharmavaram, S. (2004). FLACS CFD air quality model performance evaluation with Kit Fox, MUST, Prairie Grass, and EMU observations. *Atmospheric Environment, 38*(28), pp. 4675-4687.

Hanna, S., Britter, R., Argenta, E., & Chang, J. (2012). The Jack Rabbit chlorine release experiments: Implications of dense gas removal from a depression and downwind concentrations. *Journal of Hazardous Materials*(212), pp. 406-412.

Hansen, O. R., Gavelli, f., Ichard, M., & Davis, S. G. (2010). Validation of FLACS against experimental data sets from the model evaluation database for LNG vapor dispersion. *Journal of Loss Prevention in the Process Industries*, pp. 857-877.

Hansen, O. R., Melheim, J. A., & Storvik, I. E. (2007). CFD-Modeling of LNG Dispersion Experiments. *AIChE Spring Meeting-7thTopical Conference on Natural Gas Utilization*, (pp. 1-10). Houston, Texas.

Haper, M. (2009). *UDM Theory Document.* London, UK: DNV Softaware.

Havens, J., & Spicer, T. (1985). *Development of an atmospheric dispersion model for heavier than air gas mixtures.* Report CG-D-22-85, vol I , U.S. Coast Guard.

Hjertager, B. H. (1985). Computer simulation of turbulent reactive gas dynamics. *Modeling, identification and control Journal, 5*(4), pp. 211-236.

Hjertager, B. H. (1992). Computer modelling of turbulent gas explosions in complex 2D and 3D geometries. *Journal of Hazardous Materials, 34*(2), pp. 173-197.

Hjertager, B. H., Fuhre, K., & Bjorkhaug, M. (1988). Gas explosion experiments in 1:33 and 1:5 scale offshore separator and compressor modules using stoichiometric homogeneous fuel/air clouds. *Journal of Loss Prevention in the Process Industries, 1*(4), pp. 197-205.

Hoot, T. G., Meroney, R. N., & Peterka, J. A. (1973). *Wind tunnel tests of negatively buoyant plumes.* Washington: US Environmental Protection Agency NTIS Report PB-231-590.

HSE-Health and Safety Executive. (2013). *Fire and Explosion Strategy - Issue 1*. Hazardous Installations directorate - Offshore division.

Hsu, S. A. (1992). An overwater stability criterion for the offshore and coastal dispersion model. *Boundary-Layer Meteorology, 60*, pp. 397-402.

Ivings, M. J., Lea, C. j., Lea, C. J., & Webber, D. M. (2007). *Evaluating vapor dispersion models for safety analysis of LNG facilities.* The fire protection research foundation.

Ivings, M. J., Lea, C. J., Webber, D. M., Jagger, S. F., & Coldrick, S. (2013). A protocol for the evaluation of LNG vapour dispersion models. *Journal of Loss Prevention in the Process Industries*(26), pp. 153-163.

Koopman, R. P., Cerdewall, R. T., Ermak, D. L., Goldwire, H. C., Hogan, W. J., McClure, J. W., et al. (1982). Analysis of Burro series 40m3 LNG spills experiments. *Journal of Hazard Materials, 6*, pp. 43-88.

Langtangen, H. P., Marda, K. A., & Winther, R. (2002). Numerical methods for incompressible viscous flow. *Advances in Water Resources, 25*, 1125-1146.

Launder, B. E., & Spalding, D. B. (1974). The numerical computation of turbulent flows., *3*, pp. 269-289.

Lauridsen, K., Kozine, I., Markert, F., Amendola, A., Christou, M., & Fiori, M. (2002). *Assessment of Uncertainties in Risk Analysis of Chemical Establishments - The ASSURANCE project.* Roskilde, Denmark: Risø National Laboratory.

Luo, H., & Spiegel, S. (2010). Hybrid Grid Generation Method for Complex Geometries. *American Institute of Aeronautics and Astronautics Journal*, *48*(11), 1-9.

Mazzoldi, A., Hill, T., & Colls, J. J. (2008). CFD and Gaussian atmospheric dispersion models: A comparison for leak. *Atmospheric Environment 42*, pp. 8046-8054.

Mazzoldi, A., Hill, T., & Colls, J. J. (2011). Assessing the risk for CO2 transportation within CCS projects, CFD modelling. *International Journal of Greenhouse Gas Control*, pp. 816-825.

McQuaid, J., & Roebuck, B. (1985). *Large scale field trials on desnse vapour dispersion. Report No. EUR 10029 (EN).* Commission of the European Communities - nuclear science and technology, Safety Engineering Laboratory, UNITED KINGDOM.

Middha, P. (2010). *Developement, use and validation of CFD tool FLACS for hydrogen safety studies.* Institute of Physics and Technology - University of Bergen, Bergen.

Middha, P., & Hansen, O. R. (2009). Using computational fluid dynamics as a tool for hydrogen safety studies. *Journal of Loss Prevention in the Process Industries, 22*, pp. 295-302.

Middha, P., Hansen, O. R., & Storvik, I. E. (2009). Validation of CFD-model for hydrogen dispersion. *Journal of Loss Prevention in the Process Industries*, pp. 1034-1038.

Middha, P., Ichard, M., & Arntzen, B. J. (2010). Validation of CFD modelling of LH2 spread and evaporation against large-scale spill experiments. *International Journal of Hydrogen energy*(36), pp. 2620-2627.

Monin, A. S., & Obukhov, A. M. (1954). Basic laws of turbulent mixing in the surface layer. *Tr. Akad. Nauk SSSR Geoph. Inst, 24*(151), pp. 163-187.

Nielsen, M., Ott, S., Jorgensen, H. E., Bengtsson, R., Nyrén, K., Winter, S., et al. (1997). Field experiments with dispersion of pressure liquefied ammonia. *Journal of Hazardous Materials, 56*, pp. 59-105.

Oberkampf, W. L., & Trucano, T. G. (2002). Verification and validation in computational fluid dynamics. *Progress in Aerospace Sciences, 38*, pp. 209-272.

Palacios, A. (2011). Study of Jet Fires Geometry and Radiative Features. *A dissertation submitted in partial fulfilment of the requirements forthe degree of Doctor of Philosophy in Chemical Engineering. Universitat Politècnica de Catalunya*, 1-221. Barcelona.

Pandya, N., Gabas, N., & Marsden, E. (2012). Sensitivity analysis of Phast's atmospheric dispersion model for three toxic materials (nitric oxide, ammonia, chlorine). *Journal of Loss Prevention in the Process Industries*(25), pp. 20-32.

Pasman, H. J., Jung, S., Prem, K., Rogers, W. J., & Yang, X. (2009). Is risk analysis a useful tool for improving process safety? *Journal of Loss Prevention in the Process Industries*(22), 469-777.

Pasquill, F. (1961). The estimation of the dispersion of windborne material. *Meteorol. Mag., 90*(1063), pp. 33-49.

Pitblado, R., Baik, J., & Raghunathan, V. (2006). LNG decision making approaches compared. *Journal of Hazardous Materials, 130*, pp. 148-154.

Plasmans, J., Donnat, L., de Carvalho, E., & Debelle, T. (2012). Challenges with the use of CFD for major accident dispersion modeling. *Process Safety Progress, 32*(2).

Pope, S. B. (2000). *Turbulent Flows* (Illustrated, reprint ed.). Cambridge University Press.

Reynolds, M. R. (1992). *ALOHA (Areal Locations of Hazardous Atmospheres) 5.0 Thoretical description.* Washington: NOAA Technical Memorandum NOS ORCA-65.

Riddle, A., Carruthers, D., Sharpe, A., McHugh, C., & Stocker, J. (2004). Comparisons between FLUENT and ADMS for atmospheric dispersion modelling. *Atmospheric Environment, 38*, pp. 1029-1038.

Salas, M. D. (1999). *Modeling complex turbulent flows* (1 ed.). (M. D. Salas, J. N. Refner, & L. Sakell, Eds.) Spreinger.

Saltelli, A., Tarantola, S., Campolongo, F., & Ratto, M. (2004). *Sensitivity analysis in pratice - A guide to assessing scientific models.* John Wiley & Sons.

Schleder, A. M., & Martins, M. R. (2013). The use of Integrals and CFD tools to evaluate the cloud dispersion of flammable and toxic substances leakages. *Proceedings of ESREL 2013 - European Safety and Reliability Con-gress*, (pp. 1-8). Amsterdam.

Seveso II. (2003). *Directive 2003/105/EC of the European Parliament and of the Council of 16 December 2003 amending Council Directive 96/82/EC on the control of major accident hazards involving dangerous substances.* Avaiable on: http://eur-lex.europa.eu/legal-content/EN/TXT/?uri=CELEX:32003L0105: Official Journal of the European Communities.

Shih, T. H., Liou, W. W., Shabbir, A., Yang, Z., & Zhu, J. (1995, March). A new k-ϵ eddy viscosity model for high reynolds number turbulent flows. *Computers & Fluids*, *24*(3), pp. 227-238.

Shu, C. W. (2010). High-order Finite Difference and Finite Volume WENO Schemes and Discontinuous Galerkin Methods for CFD. *International Journal of Computational Fluid Dynamics, 17*(2), 107-118.

Skjold, T., Arntzen, B. J., Hansen, O. R., Storvik, I. E., & Eckhoff, R. K. (2006). Simulation of dust explosions in complex geometries with experimental input from standardized tests. *Journal of Loss Prevention in the Process Industries*(19), pp. 210-217.

Sklavounos, S., & Rigas, F. (2004). Validation of turbulence models in heavy gas dispersion over obstacles. *Journal of Hazardous Materials*(A108), 9-20.

Thompson, J. F., Soni, B. K., & Weatherill, N. P. (2010). *Handbook of Grid Generation* (Ilustraded ed.). CRC Press.

TNO. (2005). *The Netherlands Organization of Applied Scientific Research. Methods for the calculation of physical effects due to releases of hazardous materials (liquids and gases) - Yellow Book* (Third Edition ed.). Committee for the prevention of disasters.

Turner, D. B. (1970). *Workbook of atmospheric dispersion estimates* (4th ed.). Research Triangle Park, North Caroline: Enviromental Protection Agency.

Villafane, D., Darbra, R. M., & Casal, J. (2011). Flash Fire: Historical analysis and modeling. (S. Pierucci, Ed.) *Chemical enginnering transactions, 24*, pp. 1111-1116.

Warnatz, J., Maas, U., & Dibble, R. W. (2001). *Combustion.: Physical and Chemical Fundamentals, Modelling and Simulation, Experiments, Pollutant Formation* (3nd ed.). Springer.

Webber, D. M., & Jones, S. J. (1990). *A model of steady discharge into a vaporizing pool.* Safety and Reliability Drectorate. Warrington, UK: UKAEA SRD/HSE R493.

Weil, J. C., Sykes, R. I., & Venkatram, A. (1992). Evaluating Air-Quality Models: Review and Outlook. *Journal of Applied Meterorology, 31*, pp. 1121-1145.

Wilcox, D. C. (1998). *Turbulence Modeling for CFD* (2nd ed.). (D. Industries, Ed.)

Witcofski, R. D., & Chirivella, J. E. (1981). Experimental and analytical analyses of the mechanisms governing the dispersion of flammable clouds formed by liquid hydrogen spills. *International Journal of Hydrogen Energy, 9*(5), pp. 425-435.

Witlox, H. W., Holt, A., & Veritas, D. N. (1999). A unified model for a jet, heavy and passive dispersion including droplet rainout re-evaporation. *CCPS International Conference & Workshop on Modeling the Consequences of Accidental Releases of Hazardous Materials, 28*.

Yasushi, I. (2012). Challenges in unstructured mesh generation for practical and efficient computational fluid dynamics simulations. *Computer & Fluids*, 1-6.

Yeoh, G. H., & Yuen, K. K. (2009). *Computational Fluid Dynamics in Fire Enginnering.* Oxford: Elsevier Inc.

Zeman, O. (1982). The dynamics and modeling of havier than air, cold gas releases. *Atmospheric Enviroment, 16*(4), pp. 741-751.

APPENDIX A – BASIC CONCEPTS OF CFD

In this appendix basic concepts of computational fluid dynamics required for the proper understanding of the models implemented in FLACS are presented. First, fundamental governing equations are detailed. Following, relevant information about the boundary conditions settings is presented and finally a description of the numerical schemes used in FLACS is given.

Governing equations

The governing equations explain the physical aspects of any fluid flow, they are based in the Newton's second law and in the mass and energy conservation principles; to obtain these equations the physical principles should be applied to a suitable model of flow (Yeoh and Yuen, 2009).

The models of flow are traditionally based in the concept of a finite control volume V, in other words, a closed volume within the region of flow which is bounded by a control surface S; and in the concept of infinitesimal fluid element in the flow with a differential volume dV.

For a better understanding, Figure 47 and Figure 48 adapted from Anderson (1995) are presented. Considering a general flow field represented by the arrows, in Figure 47, at the left side a finite control volume fixed in space with the fluid moving through it is represented; at the right side, there is a finite control volume moving with the fluid such that the control volume consists always of the same fluid particles; in both cases the physical principles are applied and the integral form of the governing equations is obtained.

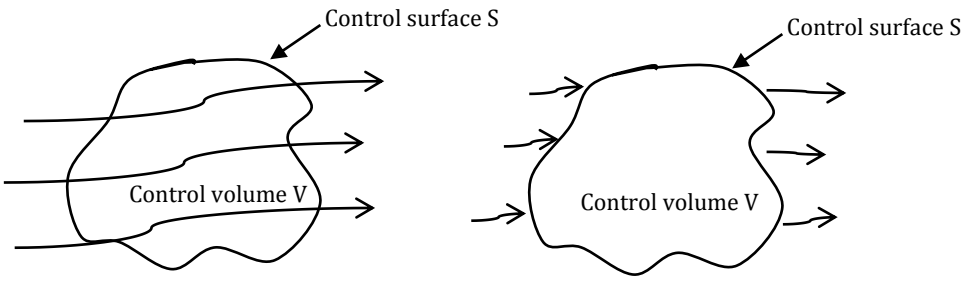

Figure 47 - Finite control volume. Fixed in space (left); moving with de fluid (right)
Source Anderson (1995)

At the left side of Figure 48, an infinitesimal fluid element fixed in space with the fluid moving through it is represented; at the right side of Figure 48, an infinitesimal fluid element moving along a streamline with velocity equals to the local flow velocity is drawn. This infinitesimal fluid is large enough to be treated as a continuous medium (an element with a massive amount of molecules), however it is infinitesimal in the sense of differential calculus; thus, in these cases, the physical principles are applied and the differential form of the governing equations is obtained.

Figure 48 - Infinitesimal fluid, (a) fixed in space (left); (b) Moving along a streamline with velocity V equal to the local flow (right).
Source: Anderson (1995)

From these models the governing equations can be obtained in different forms, they present the same physical meaning, however for CFD application the form of the equations is important; some forms, when implemented in an algorithm in CFD, may cause oscillations or instability in results in special situations. The governing equations derived from the model of a control volume fixed in space with the fluid moving through and from the model of the fluid element fixed in space (Figure 47a and Figure 48a) present a conservative form, that usually provide a smooth and stable algorithm. Anderson (2005) presents a detailed discussion about the suitable forms of the governing equations for CFD.

In the next paragraphs these models are used to present a brief description of the mass conservation, Newton's second law and energy conservation principles with the respective governing equations.

When the principle of mass conservation is applied in an infinitesimal fluid element fixe in space (present in Figure 48a) it can be stated that the mass flow out of the element must equal the time rate of decrease of mass inside the element.

Considering the model flow in Figure 48a, being the density and the velocity functions of space and time and the sides of the element dx, dy and dz, there is a mass flow in this element as showed in Figure 49.

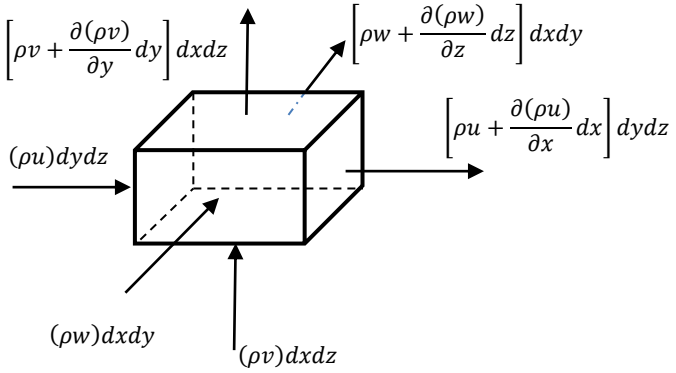

Figure 49 - Infinitesimal element fixed in space and a diagram of the mass fluxes through the faces of the element.
Adapted from Anderson (1995)

Therefore, considering the faces perpendicular to x direction, the mass entering in the left face is $(\rho u)dydz$ and the difference in mass flux between the two faces perpendicular to x direction is $[\partial(\rho u)/\partial x]dx$; thus, denoting the outflow of mass as positive, the net outflow in x direction is given by (Anderson, 1995):

$$\left[\rho u + \frac{\partial(\rho u)}{\partial x} dx\right] dydz - (\rho u)dydz = \frac{\partial(\rho u)}{\partial x} dxdydz \tag{38}$$

Where ρ is the density, u is the component of velocity in x direction.

Similarly, the outflow in y direction and in z direction:

$$\left[\rho v + \frac{\partial(\rho v)}{\partial y} dy\right] dxdz - (\rho v)dxdz = \frac{\partial(\rho v)}{\partial y} dxdydz \tag{39}$$

$$\left[\rho w + \frac{\partial(\rho w)}{\partial z} dz\right] dxdy - (\rho w) dxdy = \frac{\partial(\rho w)}{\partial z} dxdydz \tag{40}$$

Where v and w are the components of velocity in y and z directions respectively. Thus, the total mass flow out the element is:

$$\left[\frac{\partial(\rho u)}{\partial x} + \frac{\partial(\rho v)}{\partial y} + \frac{\partial(\rho w)}{\partial z}\right] dxdydz \tag{41}$$

Still considering Figure 49, since the mass inside the element is $\rho(dxdydz)$, therefore the decrease of mass inside the element is $-\partial\rho/\partial t(dxdydz)$. Thus the conservation of mass principle can be expressed as:

$$\left[\frac{\partial(\rho u)}{\partial x} + \frac{\partial(\rho v)}{\partial y} + \frac{\partial(\rho w)}{\partial z}\right] dxdydz = -\frac{\partial(\rho)}{\partial t} dxdydz \tag{42}$$

Or

$$\frac{\partial(\rho)}{\partial t} + \left[\frac{\partial(\rho u)}{\partial x} + \frac{\partial(\rho v)}{\partial y} + \frac{\partial(\rho w)}{\partial z}\right] = 0 \tag{43}$$

Equation (43) is the partial differential equation form of mass conservation (the continuity equation).

The second physical principle, the principle of conservation of momentum, is based on Newton's second law; considering the infinitesimal moving fluid element model, the Newton's second law states that the sum of the forces acting on the fluid element equals the rate of change of momentum (the product of its mass and the acceleration). Figure 50 from Anderson (1995) is a diagrammatic form to represent the forces regarded in Newton's second law.

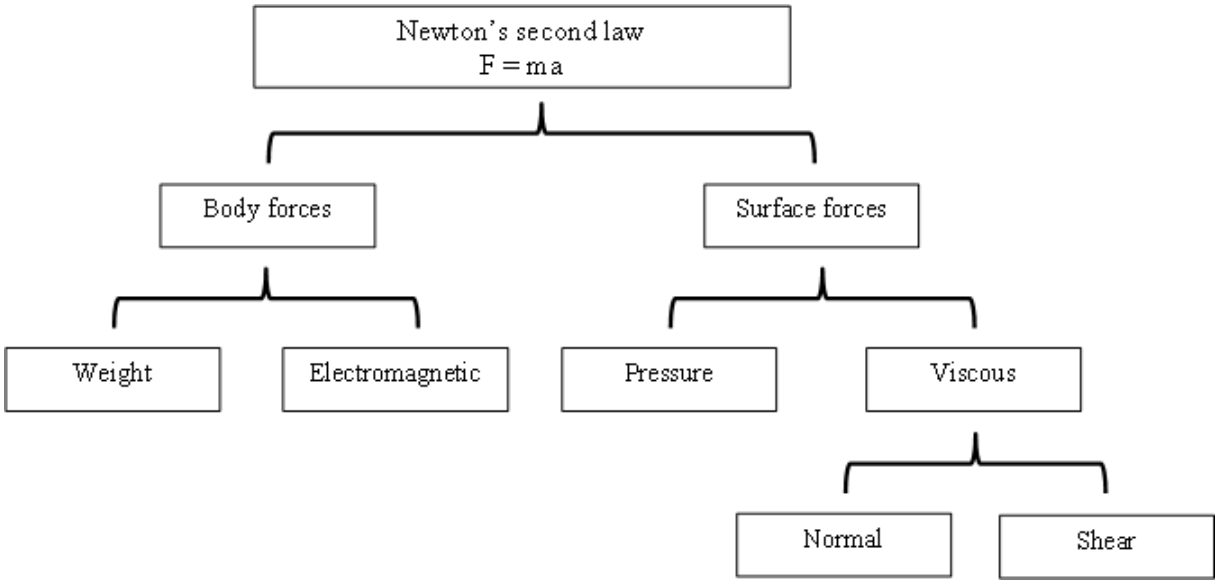

Figure 50 - Newton's second law in diagrammatic form -forces acting in an infinitesimal moving fluid element. Source: Anderson (1995)

The Newton's second law can be applied in each direction; thus, initiating by the x direction, as reported by Yeoh and Yuen (2009), the x compontent of Newton's second law is given by:

$$\sum F_x = ma_x \tag{44}$$

Where F_x is the force in x direction and a_x is the accelaration in x direction.

As presented by Anderson (1995), the time rate of change following a moving fluid element is called substancial derivative and is given by:

$$\frac{D}{Dt} = \frac{\partial}{\partial t} + u\frac{\partial}{\partial x} + v\frac{\partial}{\partial y} + w\frac{\partial}{\partial z} \tag{45}$$

Since the accelaration is the time rate change of u, it can be expressed by:

$$a_x = \frac{Du}{Dt} = \frac{\partial(u)}{\partial t} + \frac{\partial(uu)}{\partial x} + \frac{\partial(vu)}{\partial y} + \frac{\partial(wu)}{\partial z} \tag{46}$$

Remembering that the mass of the element is $\rho(dxdydz)$, the right side of Eq. (44) is:

$$\rho\left[\frac{\partial(u)}{\partial t}+\frac{\partial(uu)}{\partial x}+\frac{\partial(vu)}{\partial y}+\frac{\partial(wu)}{\partial z}\right](dxdydz) \tag{47}$$

The next step consists in evaluating the left side of Eq. (44). As mentioned previously, the forces acting in the fluid element are body forces and surface forces; the next figures from Yeoh and Yuen (2009) show this forces in x direction, the surface forces for the velocity component u that deform the element are due to the normal stress σ_{xx} (Figure 51) and the tangential stresses τ_{yx} and τ_{zx} (Figure 52).

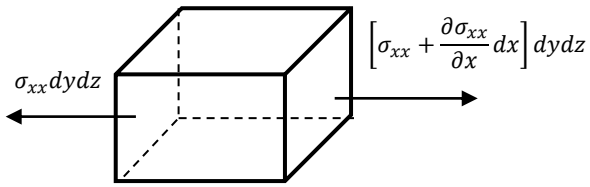

Figure 51 - Normal stresses in *x* direction
Adapted from Yeoh and Yuen (2009)

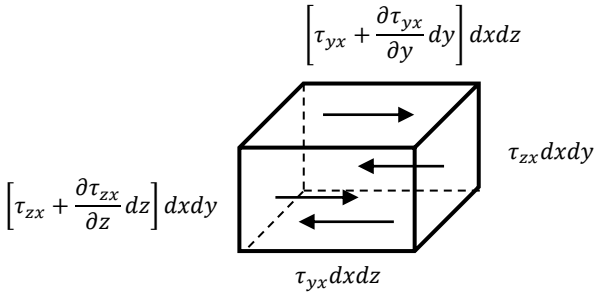

Figure 52 - Tangential stresses in x direction
Adapted from Yeoh and Yuen (2009)

Thus, the total net force due to surface stresses is:

$$\left[\frac{\partial\sigma_{xx}}{\partial x}+\frac{\partial\,\tau_{yx}}{\partial y}+\frac{\partial\tau_{zx}}{\partial z}\right](dxdydz) \tag{48}$$

Combining the surface forces Eq. (48), the body forces and Eq. (47), the momentum equation Eq. (44) becomes:

$$\left[\frac{\partial\sigma_{xx}}{\partial x}+\frac{\partial\,\tau_{yx}}{\partial y}+\frac{\partial\tau_{zx}}{\partial z}\right]+\sum F_x^{body\ forces}=\rho\frac{Du}{Dt} \tag{49}$$

Similarly the y and z components momentum equation can be evaluated:

$$\left[\frac{\partial \sigma_{yy}}{\partial y} + \frac{\partial\, \tau_{xy}}{\partial x} + \frac{\partial \tau_{zy}}{\partial z}\right] + \sum F_y^{body\ forces} = \rho \frac{Dv}{Dt} \tag{50}$$

$$\left[\frac{\partial \sigma_{ww}}{\partial z} + \frac{\partial\, \tau_{yz}}{\partial y} + \frac{\partial \tau_{xz}}{\partial x}\right] + \sum F_z^{body\ forces} = \rho \frac{Dw}{Dt} \tag{51}$$

Finally, there is the third principle in which the governing equations are based: the principle of energy conservation. The first law of thermodynamics states that the energy is conserved; thus, considering the infinitesimal moving fluid element model, the rate of energy exchange is equal to the net rate of heat addition to the element $\Sigma \dot{Q}$, plus the rate of work done on the element $\Sigma \dot{W}$, plus the rate of heat added or removed by a heat source on the element $\dot{Q}_s \Delta V$ (Yeoh and Yuen, 2009).

The rate of energy exchange can be evaluated by the substantial derivative, thus the time rate of energy exchange for a moving fluid element can be given by:

$$\rho \frac{DE}{Dt} dxdydz \tag{52}$$

The rate of work done on the element $\Sigma \dot{W}$ in x direction is equivalent to the product between velocity and surface forces showed in Figure 51 and in Figure 52, thus the net rate of work done in x direction is given by:

$$\left[\frac{\partial (u\sigma_{xx})}{\partial x} + \frac{\partial (u\tau_{yx})}{\partial y} + \frac{\partial (u\tau_{zx})}{\partial z}\right](dxdydz) \tag{53}$$

Similarly, this component can be calculated in y direction and in z direction. Then, the net rate of work done on the fluid element is given by:

$$\begin{aligned}\sum \dot{w} = \Bigg[&\frac{\partial (u\sigma_{xx})}{\partial x} + \frac{\partial (v\sigma_{yy})}{\partial y} + \frac{\partial (w\sigma_{zz})}{\partial z} + \frac{\partial (u\tau_{yx})}{\partial y} + \frac{\partial (u\tau_{zx})}{\partial z} + \frac{\partial (v\tau_{xy})}{\partial x} \\ &+ \frac{\partial (v\tau_{zy})}{\partial z} + \frac{\partial (w\tau_{xz})}{\partial x} + \frac{\partial (w\tau_{yz})}{\partial y}\Bigg](dxdydz)\end{aligned} \tag{54}$$

Still considering the fluid element moving in flow, Yeoh and Yuen (2009) reports that the rate of heat added or removed by a heat source is given by the difference between heat input and the heat loss, thus the rate of heat added or removed by a heat source can be expressed as:

$$\sum \dot{Q} = -\left[\frac{\partial(q_x)}{\partial x} + \frac{\partial(q_y)}{\partial y} + \frac{\partial(q_z)}{\partial z}\right](dxdydz) \tag{55}$$

Where q_x , q_y and q_z are heat fluxes that can be expressed in terms of gradient of temperature and conductivity k:

$$q_x = -k\frac{\partial T}{\partial x} \tag{56}$$

$$q_y = -k\frac{\partial T}{\partial y} \tag{57}$$

$$q_z = -k\frac{\partial T}{\partial z} \tag{58}$$

Finally, combining Eq.(54) to (58), the rate of energy exchange of the fluid element is given by Eq.(59) , which is the equation of conservation of energy:

$$\begin{aligned}\rho\frac{DE}{Dt} = &\left[\frac{\partial}{\partial x}\left(k\frac{\partial T}{\partial x}\right) + \frac{\partial}{\partial y}k\frac{\partial T}{\partial y} + \frac{\partial}{\partial z}k\frac{\partial T}{\partial z}\right] \\ &+ \left[\frac{\partial(u\sigma_{xx})}{\partial x} + \frac{\partial(v\sigma_{yy})}{\partial y} + \frac{\partial(w\sigma_{zz})}{\partial z} + \frac{\partial(u\tau_{yx})}{\partial y} + \frac{\partial(u\tau_{zx})}{\partial z}\right. \\ &\left. + \frac{\partial(v\tau_{xy})}{\partial x} + \frac{\partial(v\tau_{zy})}{\partial z} + \frac{\partial(w\tau_{xz})}{\partial x} + \frac{\partial(w\tau_{yz})}{\partial y}\right] + \dot{Q}_s\end{aligned} \tag{59}$$

The specific energy E of a fluid is usually defined as the sum of kinetic energy and internal energy, and for compressible flows the energy may be expressed in terms of enthalpy.

Concluding, Eq.(43), Eq.(46-48) and Eq. (59) are the governing equations in conservative form that explain the physical aspects of any fluid flow; as mentioned before, these equations can be expressed in many others forms, however the physical meaning remains the same. Originally, the momentum conservation equations were called of Navier-Stokes equations in honour of two researchers that obtained these equations; nowadays, the entire set of governing

equations for viscous flows is often called the Navier-Stokes equations and the set of governing equations for inviscid flows is called of Euler equations (Anderson, 1995).

Boundary conditions

The boundary and initial conditions of the flow dictate the particular solution obtained from the governing equations. For a viscous fluid, the boundary conditions on a surface assumes that the relative velocity between the surface and the fluid immediately at the surface is zero (it is called no-slip condition); then, if the surface is stationary, all the velocity components are equal to zero (Anderson, 1995). Similarly, the temperature of the fluid immediately at the surface is equal to the temperature of the material surface (temperature of wall T_w); if the wall temperature is not known and it is changing due to heat transfer the boundary condition can be provided by the Fourier law of heat condition:

$$\dot{q}_w = -\left(k\frac{\partial T}{\partial n}\right)_w \tag{60}$$

Where $\dot{q}_w$ is the instantaneous heat flux at the wall, n denotes the direction normal to the wall, T is the temperature and k is the conductivity.

When the temperature of the wall reaches the point in which there is no heat transfer to the surface ($\dot{q}_w$ equals zero), by definition, this wall temperature is called adiabatic wall temperature T_{aw} and Eq. (60) gives that:

$$\left(\frac{\partial T}{\partial n}\right)_w = 0 \tag{61}$$

The assumptions above are concerning a viscous flow, for an inviscid flow, in which the there is no friction between the fluid and the wall can be assumed that the flow velocity vector immediately adjacent to the wall must be tangent to the wall; then the boundary condition is be given by:

$$\boldsymbol{V}.n = 0 \tag{62}$$

Numerical schemes

The governing equations of the fundamental physical principles of fluid flow provide values of the flow properties (i.e. temperature, pressure, velocity, etc.) at any of the infinite number of points of the domain, however, they are a coupled system of nonlinear partial differential or integral equations, and hence they are very difficult to solve analytically. CFD tools transform these equations in discretized algebraic forms, which are solved to find the flow field properties at specific discrete points; this process in which the differential or integral equations involving functions (viewed as having an infinite continuum of values throughout some domain) are approximate by analogous expressions which prescribe values at only a finite number of discrete points or volumes in a domain is called the discretization process.

The main discretization methods available at the literature nowadays are the finite difference, finite element, spectral and finite volume (Yeoh and Yuen, 2009). The finite difference method performs the discretization of the partial differential equations, it consists on the application of Taylor series expansions at each nodal point of the grid; the finite element method implies the application of polynomial equations for local elements, this method is not widely used due to the great computational resources required; the spectral method applies the same approach of the previous methods, however global approximations are employed instead of local approximations; and the finite volume method performs the discretization of the integral form of the equations.

Commercial CFD tools apply these methods with some degree of variation according to the applicability; nowadays the majority of the CFD tools perform discretization based on the finite volume method. Anderson (1995) and Yeoh and Yuen (2009) present the basic concepts of the discretization processes, the first study focuses on the finite difference while the later focuses on the finite volume method. Shu (2010) presents a rich discussion about recent development of variations of the finite difference method, finite volume and discontinuous finite element methods. Langtangen et al. (2002) discuss the main aspects of discretization methods applied to solve incompressible viscous flows.

Since the finite volume method is the most applied on the currently available CFD tools, and it is applied on FLACS which is used in this research, following a description of this method is given.

Yeoh and Yuen (2009) show that, for a viscous flow, employing a general variable ϕ to represent the properties of the flow, it is possible to express the governing equations in the general form:

$$\frac{\partial(\rho\phi)}{\partial t}+\frac{\partial(\rho u\phi)}{\partial x}+\frac{\partial(\rho v\phi)}{\partial y}+\frac{\partial(\rho w\phi)}{\partial z} = \frac{\partial}{\partial x}\left[\Gamma_\phi\frac{\partial\phi}{\partial x}\right]+\frac{\partial}{\partial y}\left[\Gamma_\phi\frac{\partial\phi}{\partial y}\right]+\frac{\partial}{\partial z}\left[\Gamma_\phi\frac{\partial\phi}{\partial z}\right]+S_\phi \tag{63}$$

Where Γ_ϕ is the diffusion coefficient and S_ϕ is the source term. This equation represents the physical transport processes occurring in the flow: the rate of the exchange of the variable ϕ (the left size of Eq.(63)) is equivalent to the diffusion term and the source term. By setting the variable ϕ equal to 1, u, v, w, h and selecting suitable values for Γ_ϕ and S_ϕ, the governing equations in an conservative form are obtained; the general form given by Eq. (63) is presented by Anderson (1995) and Arntzen (1998); and the complete description of the steps to obtain the governing equations from the general Eq. (63) are presented by Yeoh and Yuen (2009). In order to perform the discretization of the governing equations, it is useful to consider the integral form of Eq. (63) over a finite control volume:

$$\int_V\frac{\partial(\rho\phi)}{\partial t}dV+\int_V\left\{\frac{\partial(\rho u\phi)}{\partial x}+\frac{\partial(\rho v\phi)}{\partial y}+\frac{\partial(\rho w\phi)}{\partial z}\right\}dV = \int_V\left\{\frac{\partial}{\partial x}\left[\Gamma_\phi\frac{\partial\phi}{\partial x}\right]+\frac{\partial}{\partial y}\left[\Gamma_\phi\frac{\partial\phi}{\partial y}\right]+\frac{\partial}{\partial z}\left[\Gamma_\phi\frac{\partial\phi}{\partial z}\right]\right\}dV+\int_V S_\phi\,dV \tag{64}$$

Applying the Gauss divergence theorem to the volume integral:

$$\int_V\frac{\partial(\rho\phi)}{\partial t}dV+\int_A\{(\rho u\phi)dA^x+(\rho v\phi)dA^y+(\rho w\phi)dA^z\} = \int_A\left\{\left[\Gamma\frac{\partial\phi}{\partial x}\right]dA^x+\left[\Gamma\frac{\partial\phi}{\partial y}\right]dA^y+\left[\Gamma\frac{\partial\phi}{\partial z}\right]dA^z\right\}+\int_V S_\phi\,dV \tag{65}$$

Where dA^x, dA^y and dA^z are the elemental projected area along the x, y and z directions.

As reported previously, the finite volume method discretizes the integral form of the conservation equations; considering the physical domain divided into contiguous small subdomains (control volumes), the property ϕ is calculated at the centroid of these volumes, which depends directly on the fluxes of the control volume faces. Thus, considering a steady flow, Yeoh and Yuen (2009) state that the first term of the left size of Eq. (65) may be disregarded and the other terms can be replaced according the equations above:

$$\int_A \{(\rho u\phi)dA^x + (\rho v\phi)dA^y + (\rho w\phi)dA^z\} = \sum_{i=1}^{N}(\rho u\phi)_i A_i^x + \sum_{j=1}^{N}(\rho v\phi)_j A_j^y + \sum_{k=1}^{N}(\rho w\phi)_k A_k^z \tag{66}$$

$$\int_A \left\{\left[\Gamma\frac{\partial\phi}{\partial x}\right]dA^x + \left[\Gamma\frac{\partial\phi}{\partial y}\right]dA^y + \left[\Gamma\frac{\partial\phi}{\partial z}\right]dA^z\right\} = \sum_{i=1}^{N}\left(\Gamma\frac{\partial\phi}{\partial x}\right)_i A_i^x + \sum_{j=1}^{N}\left(\Gamma\frac{\partial\phi}{\partial y}\right)_j A_j^y + \sum_{k=1}^{N}\left(\Gamma\frac{\partial\phi}{\partial z}\right)_k A_k^z \tag{67}$$

$$\int_V S_\phi\, dV = S_\phi \Delta V \tag{68}$$

For unsteady flows, a similar process can be performed, however an additional integration is required; these flows are out of scope of this research, more details about unsteady flows can be found in Yeoh and Yuen (2009).

The process of replace the terms of Eq. (65) by the equivalent algebraic forms given by Eq. (63-65) is the synthesis of the finite volume method to discretization.

APPENDIX B – TABLES OF THE SENSITIVITY ANALYSIS

Table 21 - Reproducibility of concentration values at height of 0.2 m

		Simulated values of concentration									
Distance from release point [m]		10	15	20	30	40	50	60	70	80	100
	Simulation										
B1	1	3.42	3.53	3.22	2.60	2.12	1.76	1.48	1.27	1.10	0.87
	2	3.42	3.53	3.22	2.60	2.12	1.76	1.48	1.27	1.11	0.87
	3	3.42	3.53	3.22	2.60	2.12	1.76	1.48	1.27	1.11	0.87
	4	3.42	3.53	3.22	2.61	2.12	1.76	1.48	1.27	1.11	0.87
	5	3.42	3.52	3.22	2.60	2.12	1.75	1.48	1.27	1.11	0.87
	6	3.42	3.52	3.21	2.60	2.11	1.76	1.48	1.27	1.10	0.87
B2	1	3.44	1.25	1.49	1.55	1.44	1.31	1.19	1.09	0.99	0.83
	2	3.44	1.25	1.49	1.55	1.44	1.31	1.20	1.09	1.00	0.83
	3	3.45	1.25	1.49	1.55	1.44	1.31	1.20	1.09	1.00	0.83
	4	3.45	1.25	1.49	1.54	1.44	1.31	1.20	1.09	0.99	0.83
	5	3.45	1.26	1.49	1.55	1.44	1.30	1.20	1.09	1.00	0.84
	6	3.44	1.25	1.49	1.55	1.43	1.30	1.20	1.10	0.99	0.83

Table 22 - Reproducibility of concentration values at height of 0.8 m

		Simulated values of concentration				
	Distance from release point [m]	10	15	20	30	40
	Simulation					
B1	1	4.13	3.28	2.73	2.07	1.66
	2	4.13	3.28	2.74	2.08	1.66
	3	4.13	3.28	2.74	2.07	1.66
	4	4.13	3.29	2.74	2.07	1.66
	5	4.13	3.28	2.73	2.07	1.66
	6	4.13	3.28	2.74	2.07	1.65
B2	1	4.33	1.31	1.58	1.55	1.36
	2	4.33	1.31	1.58	1.55	1.36
	3	4.33	1.31	1.58	1.55	1.36
	4	4.33	1.31	1.59	1.55	1.36
	5	4.33	1.31	1.59	1.54	1.36
	6	4.33	1.30	1.58	1.55	1.36

Table 23 - Reproducibility of concentration values at height of 1.5 m

		Simulated values of concentration				
	Distance from release point [m]	10	15	20	30	40
	Simulation					
B1	1	4.50	2.98	2.32	1.69	1.34
	2	4.50	2.98	2.32	1.69	1.35
	3	4.51	2.98	2.32	1.69	1.35
	4	4.51	2.98	2.32	1.69	1.35
	5	4.50	2.98	2.32	1.68	1.35
	6	4.50	2.98	2.32	1.69	1.35
B2	1	4.97	3.38	1.88	1.55	1.28
	2	4.97	3.39	1.88	1.55	1.28
	3	4.97	3.38	1.88	1.55	1.28
	4	4.96	3.39	1.88	1.55	1.28
	5	4.97	3.38	1.88	1.55	1.28
	6	4.97	3.39	1.89	1.56	1.29

Table 24 - Grid variation on B1

Simulation	Distance from release point [m]	10	15	20	30	40	50	60	70	80	100	10	15	20	30	40	10	15	20	30	40
	Height [m]					0.2								0.8					1.5		
B1	original grid	3.42	3.53	3.22	2.60	2.12	1.76	1.48	1.27	1.10	0.87	4.13	3.28	2.73	2.07	1.66	4.50	2.98	2.32	1.69	1.34
L3	grid 10% reduced	3.56	3.66	3.33	2.69	2.18	1.8	1.52	1.3	1.13	0.89	4.30	3.39	2.83	2.13	1.70	4.66	3.06	2.38	1.72	1.37
L4	grid 20% reduced	3.63	3.59	3.26	2.63	2.14	1.77	1.49	1.28	1.11	0.88	4.09	3.28	2.75	2.08	1.67	4.27	2.92	2.30	1.68	1.35
L2	grid 10% increased	3.53	3.8	3.45	2.76	2.23	1.84	1.55	1.32	1.15	0.90	4.55	3.55	2.93	2.19	1.74	5.06	3.22	2.46	1.76	1.39
L1	grid 20% increased	3.42	3.52	3.20	2.58	2.10	1.74	1.47	1.26	1.10	0.87	4.11	3.25	2.71	2.05	1.65	4.43	2.94	2.30	1.67	1.34
W3	grid 10% reduced	3.42	3.53	3.22	2.60	2.12	1.76	1.48	1.27	1.11	0.87	4.13	3.28	2.74	2.07	1.66	4.50	2.98	2.31	1.69	1.35
W4	grid 20% reduced	3.42	3.53	3.22	2.60	2.12	1.76	1.48	1.27	1.11	0.87	4.13	3.28	2.74	2.07	1.66	4.51	2.98	2.32	1.69	1.35
W2	grid 10% increased	3.42	3.53	3.22	2.60	2.12	1.76	1.48	1.27	1.11	0.87	4.13	3.28	2.74	2.07	1.66	4.50	2.98	2.32	1.69	1.35
W1	grid 20% increased	3.44	3.46	3.14	2.54	2.08	1.72	1.46	1.25	1.09	0.86	3.98	3.18	2.66	2.03	1.63	4.23	2.86	2.25	1.65	1.33
H3	grid 10% reduced	3.22	3.41	3.14	2.56	2.10	1.74	1.47	1.26	1.10	0.86	4.07	3.22	2.69	2.04	1.63	4.50	2.96	2.30	1.67	1.33
H4	grid 20% reduced	3.26	3.43	3.15	2.56	2.09	1.74	1.47	1.26	1.10	0.90	4.08	3.23	2.7	2.04	1.64	4.50	2.96	2.30	1.67	1.34
H2	grid 10% increased	3.08	3.34	3.09	2.53	2.07	1.76	1.46	1.25	1.09	0.86	4.03	3.18	2.65	2.00	1.61	4.50	2.95	2.28	1.65	1.31
H1	grid 20% increased	3.09	3.27	3.00	2.43	1.99	1.65	1.39	1.20	1.04	0.82	4.03	3.18	2.64	1.98	1.59	4.55	2.97	2.27	1.61	1.27

Table 25 - Grid variation on B2

Simulation	Distance from release point [m]	10	15	20	30	40	50	60	70	80	100	10	15	20	30	40	10	15	20	30	40
	Height [m]					0.2								0.8					1.5		
B2	original grid	3.44	1.25	1.49	1.55	1.44	1.31	1.19	1.09	0.99	0.83	4.33	1.31	1.58	1.55	1.36	4.97	3.38	1.88	1.55	1.28
L3	grid 10% reduced	3.48	3.70	1.49	1.54	1.43	1.31	1.19	1.09	1.00	0.83	4.34	3.63	1.57	1.54	1.36	4.98	3.42	1.86	1.55	1.28
L4	grid 20% reduced	3.56	3.62	1.39	1.46	1.36	1.25	1.14	1.04	0.95	0.80	4.16	3.51	1.45	1.46	1.30	4.60	3.31	1.72	1.47	1.23
L2	grid 10% increased	3.44	3.78	1.53	1.59	1.47	1.34	1.22	1.11	1.01	0.84	4.52	3.72	1.62	1.59	1.39	5.26	3.53	1.95	1.59	1.31
L1	grid 20% increased	3.53	1.38	1.58	1.60	1.48	1.34	1.22	1.11	1.01	0.84	4.50	1.42	1.67	1.60	1.40	5.15	3.44	1.97	1.60	1.32
W3	grid 10% reduced	3.48	1.23	1.47	1.53	1.42	1.30	1.18	1.08	0.99	0.82	4.32	1.29	1.56	1.53	1.35	4.97	3.37	1.85	1.54	1.27
W4	grid 20% reduced	3.45	1.24	1.48	1.54	1.43	1.30	1.19	1.08	0.99	0.83	4.32	1.30	1.57	1.54	1.35	4.97	3.38	1.86	1.54	1.28
W2	grid 10% increased	3.45	1.23	1.47	1.53	1.42	1.30	1.18	1.08	0.99	0.82	4.32	1.28	1.56	1.53	1.35	4.96	3.37	1.85	1.53	1.27
W1	grid 20% increased	3.44	1.24	1.49	1.54	1.43	1.30	1.19	1.08	0.99	0.83	4.32	1.30	1.57	1.53	1.35	4.97	3.38	1.86	1.54	1.28
H3	grid 10% reduced	2.83	3.30	1.34	1.40	1.30	1.18	1.08	0.98	0.9	0.75	4.04	3.15	1.55	1.43	1.22	4.95	3.31	1.82	1.45	1.17
H4	grid 20% reduced	2.51	2.97	1.45	1.42	1.27	1.13	1.02	0.92	0.83	0.69	4.12	3.35	1.44	1.41	1.23	4.94	3.37	1.71	1.44	1.17
H2	grid 10% increased	3.35	1.24	1.47	1.53	1.42	1.29	1.18	1.08	0.99	0.82	4.30	1.30	1.56	1.53	1.34	4.97	3.37	1.86	1.54	1.27
H1	grid 20% increased	2.83	1.14	1.34	1.40	1.30	1.18	1.07	0.98	0.90	0.75	4.12	1.17	1.43	1.41	1.23	4.94	3.23	1.70	1.43	1.18

Table 26 - Height refinement of the macro grid on B1

Simulation	Distance from release point [m]	10	15	20	30	40	50	60	70	80	100	10	15	20	30	40	10	15	20	30	40
	Height [m]					0.2								0.8					1.5		
B1		3.42	3.53	3.22	2.60	2.12	1.76	1.48	1.27	1.10	0.87	4.13	3.28	2.73	2.07	1.66	4.50	2.98	2.32	1.69	1.34
H3	grid 10% reduced	3.08	3.34	3.09	2.53	2.07	1.76	1.46	1.25	1.09	0.86	4.03	3.18	2.65	2.00	1.61	4.50	2.95	2.28	1.65	1.31
H4	grid 20% reduced	3.09	3.27	3.00	2.43	1.99	1.65	1.39	1.20	1.04	0.82	4.03	3.18	2.64	1.98	1.59	4.55	2.97	2.27	1.61	1.27
H7	grid 30% reduced	2.95	3.26	3.02	2.49	2.04	1.70	1.40	1.34	1.04	0.82	4.00	3.14	2.61	1.98	1.59	4.50	2.94	2.26	1.63	1.30
H8	grid 40% reduced	2.88	3.13	2.90	2.37	1.94	1.62	1.37	1.17	1.02	0.81	3.97	3.11	2.58	1.95	1.57	4.53	2.94	2.26	1.61	1.28
H9	grid 50% reduced	2.73	2.99	2.74	2.23	1.83	1.52	1.28	1.10	0.96	0.76	3.92	3.03	2.52	1.92	1.55	4.48	2.90	2.23	1.61	1.30
H10	grid 60% reduced	3.39	3.52	3.22	2.60	2.12	1.75	1.48	1.26	1.10	0.87	4.13	3.29	2.75	2.08	1.67	4.54	3.00	2.33	1.69	1.35

Table 27 - Height refinement of the macro grid on B2

Simulation	Distance from release point [m]	10	15	20	30	40	50	60	70	80	100	10	15	20	30	40	10	15	20	30	40
	Height [m]					0.2								0.8					1.5		
B1		3.44	3.68	1.49	1.55	1.44	1.31	1.19	1.09	1.00	0.83	4.33	3.63	1.58	1.55	1.36	4.97	3.47	1.88	1.55	1.28
H3	grid 10% reduced	2.83	3.30	1.34	1.40	1.30	1.18	1.08	0.98	0.9	0.75	4.04	3.15	1.55	1.43	1.22	4.95	3.31	1.82	1.45	1.17
H4	grid 20% reduced	2.51	2.97	1.45	1.42	1.27	1.13	1.02	0.92	0.83	0.69	4.12	3.35	1.44	1.41	1.23	4.94	3.37	1.71	1.44	1.17
H7	grid 30% reduced	2.59	3.00	1.42	1.40	1.25	1.12	1.01	0.91	0.83	0.68	4.04	3.16	1.52	1.41	1.21	4.95	3.31	1.78	1.43	1.16
H8	grid 40% reduced	2.60	3.05	1.34	1.37	1.25	1.12	1.01	0.92	0.83	0.69	4.04	3.20	1.44	1.39	1.20	4.96	3.31	1.72	1.42	1.16
H9	grid 50% reduced	2.53	3.00	1.38	1.38	1.24	1.12	1.01	0.91	0.82	0.68	4.01	3.17	1.49	1.39	1.20	4.93	3.29	1.74	1.42	1.15
H10	grid 60% reduced	3.44	3.69	1.49	1.56	1.45	1.32	1.21	1.10	1.01	0.84	4.33	3.64	1.59	1.56	1.37	4.99	3.49	1.89	1.56	1.29

Table 28 - Variation in the simulated values on B1 at height of 0.2 m

Variable		Percentage changes by each variable on B1									
		Distance from the release point [m]									
		10	15	20	30	40	50	60	70	80	100
Ambient temperature	-10%	2.71	2.97	2.73	2.22	1.82	1.51	1.28	1.10	0.96	0.75
	+10%	2.74	2.99	2.75	2.24	1.83	1.52	1.28	1.10	0.96	0.75
Atmospheric pressure	-10%	2.79	3.01	2.76	2.25	1.84	1.54	1.30	1.12	0.98	0.78
	+10%	2.67	2.96	2.73	2.21	1.81	1.49	1.26	1.08	0.93	0.73
Ground roughness	-10%	2.73	2.99	2.74	2.23	1.83	1.52	1.28	1.10	0.96	0.76
	+10%	2.73	2.98	2.73	2.23	1.82	1.51	1.28	1.10	0.95	0.75
Wind speed	-10%	2.85	3.06	2.79	2.25	1.83	1.51	1.27	1.09	0.95	0.75
	+10%	2.61	2.92	2.70	2.21	1.82	1.52	1.29	1.11	0.96	0.76
Spill duration	-10%	2.73	2.99	2.74	2.23	1.83	1.52	1.28	1.10	0.96	0.75
	+10%	2.73	2.99	2.74	2.23	1.83	1.52	1.28	1.10	0.96	0.76
Mass flow	-10%	2.66	2.96	2.72	2.21	1.80	1.49	1.25	1.07	0.93	0.73
	+10%	2.79	3.01	2.76	2.25	1.84	1.54	1.30	1.12	0.98	0.78
Discharge height	-10%	3.33	3.28	2.93	2.32	1.88	1.55	1.31	1.12	0.97	0.77
	+10%	2.15	2.69	2.55	2.13	1.77	1.48	1.25	1.08	0.94	0.74
CFLC	-50%	2.73	2.99	2.74	2.23	1.83	1.52	1.28	1.10	0.96	0.75
	+50%	2.73	2.98	2.74	2.23	1.82	1.52	1.28	1.09	0.96	0.75

Table 29 - Variation in the simulated values on B1 at height of 0.8 m

Variable		Percentage changes by each variable on B1				
		Distance from the release point [m]				
		10	15	20	30	40
Ambient temperature	-10%	3.91	3.02	2.51	1.92	1.55
	+10%	3.93	3.04	2.53	1.93	1.55
Atmospheric pressure	-10%	3.93	3.05	2.54	1.95	1.58
	+10%	3.91	3.02	2.50	1.90	1.52
Ground roughness	-10%	3.92	3.03	2.52	1.92	1.55
	+10%	3.92	3.03	2.52	1.92	1.55
Wind speed	-10%	3.97	3.06	2.54	1.93	1.56
	+10%	3.87	3.00	2.50	1.91	1.54
Spill duration	-10%	3.92	3.03	2.52	1.92	1.55
	+10%	3.92	3.03	2.52	1.92	1.55
Mass flow	-10%	3.91	3.02	2.50	1.89	1.52
	+10%	3.93	3.04	2.54	1.94	1.58
Discharge height	-10%	4.24	3.15	2.59	1.96	1.58
	+10%	3.51	2.87	2.43	1.87	1.52
CFLC	-50%	3.92	3.03	2.52	1.92	1.55
	+50%	3.92	3.03	2.52	1.91	1.55

Table 30 - Variation in the simulated values on B2 at height of 0.2 m

Variable		Percentage changes by each variable on B1									
		Distance from the release point [m]									
		10	15	20	30	40	50	60	70	80	100
Ambient temperature	-10%	2.52	3.00	1.37	1.37	1.24	1.11	1.00	0.91	0.82	0.68
	+10%	2.55	3.03	1.39	1.39	1.25	1.12	1.01	0.91	0.83	0.69
Atmospheric pressure	-10%	2.65	3.09	1.37	1.39	1.27	1.15	1.05	0.96	0.88	0.74
	+10%	2.42	2.94	1.40	1.37	1.22	1.08	0.96	0.86	0.77	0.63
Ground roughness	-10%	2.53	3.01	1.38	1.38	1.25	1.12	1.01	0.91	0.83	0.69
	+10%	2.53	3.01	1.38	1.38	1.24	1.12	1.00	0.91	0.82	0.68
Wind speed	-10%	2.69	3.11	1.39	1.41	1.28	1.16	1.05	0.95	0.87	0.73
	+10%	2.38	2.91	1.38	1.36	1.21	1.08	0.96	0.86	0.78	0.64
Spill duration	-10%	2.53	3.01	1.38	1.38	1.24	1.12	1.01	0.91	0.83	0.68
	+10%	2.53	3.01	1.38	1.38	1.24	1.12	1.01	0.91	0.83	0.68
Mass flow	-10%	2.41	2.93	1.40	1.37	1.22	1.08	0.96	0.86	0.77	0.62
	+10%	2.64	3.08	1.36	1.39	1.27	1.15	1.04	0.95	0.87	0.73
Discharge height	-10%	2.53	3.01	1.38	1.38	1.24	1.12	1.01	0.91	0.83	0.68
	+10%	1.74	2.58	1.46	1.45	1.31	1.17	1.05	0.95	0.87	0.72
CFLC	-50%	2.53	3.01	1.38	1.38	1.24	1.12	1.01	0.91	0.83	0.68
	+50%	-	-	-	-	-	-	-	-	-	-

Table 31 - Variation in the simulated values on B2 at height of 0.8 m

Variable		Percentage changes by each variable on B1				
		Distance from the release point [m]				
		10	15	20	30	40
Ambient temperature	-10%	4.00	3.16	1.48	1.38	1.19
	+10%	4.03	3.19	1.49	1.40	1.20
Atmospheric pressure	-10%	4.06	3.23	1.48	1.41	1.23
	+10%	3.98	3.12	1.49	1.38	1.17
Ground roughness	-10%	4.02	3.17	1.48	1.39	1.20
	+10%	4.01	3.17	1.48	1.39	1.20
Wind speed	-10%	4.08	3.24	1.49	1.42	1.23
	+10%	3.95	3.10	1.48	1.37	1.16
Spill duration	-10%	4.01	3.17	1.48	1.39	1.20
	+10%	4.01	3.17	1.48	1.39	1.20
Mass flow	-10%	3.97	3.11	1.50	1.38	1.16
	+10%	4.06	3.22	1.47	1.41	1.22
Discharge height	-10%	4.01	3.17	1.48	1.39	1.20
	+10%	3.43	2.85	1.56	1.46	1.25
CFLC	-50%	4.01	3.17	1.48	1.40	1.20
	+50%	-	-	-	-	-

Table 32 - Variation in the simulated values on B1 at height of 1.5 m

Variable		Percentage changes by each variable on B1				
		Distance from the release point [m]				
		10	15	20	30	40
Ambient temperature	-10%	4.47	2.90	2.23	1.61	1.29
	+10%	4.50	2.91	2.24	1.62	1.30
Atmospheric pressure	-10%	4.49	2.92	2.26	1.65	1.34
	+10%	4.47	2.89	2.20	1.58	1.25
Ground roughness	-10%	4.48	2.90	2.23	1.62	1.30
	+10%	4.48	2.90	2.23	1.61	1.29
Wind speed	-10%	4.48	2.90	2.23	1.62	1.30
	+10%	4.49	2.90	2.23	1.61	1.29
Spill duration	-10%	4.48	2.90	2.23	1.62	1.30
	+10%	4.48	2.90	2.23	1.62	1.30
Mass flow	-10%	4.47	2.88	2.20	1.57	1.25
	+10%	4.49	2.92	2.25	1.65	1.33
Discharge height	-10%	4.34	2.84	2.21	1.62	1.31
	+10%	4.47	2.91	2.23	1.61	1.28
CFLC	-50%	4.48	2.90	2.23	1.61	1.29
	+50%	4.48	2.90	2.23	1.62	1.30

Table 33 - Variation in the simulated values on B2 at height of 1.5 m

Variable		Percentage changes by each variable on B1				
		Distance from the release point [m]				
		10	15	20	30	40
Ambient temperature	-10%	4.91	3.28	1.73	1.41	1.15
	+10%	4.95	3.31	1.75	1.42	1.16
Atmospheric pressure	-10%	4.94	3.32	1.73	1.44	1.19
	+10%	4.92	3.28	1.75	1.40	1.12
Ground roughness	-10%	4.93	3.30	1.74	1.42	1.15
	+10%	4.93	3.29	1.74	1.41	1.15
Wind speed	-10%	4.93	3.32	1.74	1.44	1.19
	+10%	4.93	3.27	1.74	1.39	1.12
Spill duration	-10%	4.93	3.30	1.74	1.42	1.15
	+10%	4.93	3.30	1.74	1.42	1.15
Mass flow	-10%	4.92	3.27	1.75	1.40	1.11
	+10%	4.94	3.31	1.73	1.43	1.18
Discharge height	-10%	4.93	3.30	1.74	1.42	1.15
	+10%	4.88	3.19	1.84	1.48	1.20
CFLC	-50%	4.93	3.30	1.74	1.42	1.15
	+50%	-	-	-	-	-

APPENDIX C – PRELIMINARY SIMULATIONS FOR THE EXPERIMENTAL DESIGN

In order to define the trials of the field tests, preliminary FLACS simulation jobs were performed to obtain initial information on flows, concentrations and sizing of the LPG clouds expected. Previous simulations were made starting with some flux conditions that were specified elsewhere (Palacios, 2011) when using the same LPG installation to undertake other type of experiments, such as flash fires. Palacios (2011) reported that in most of the flash fire trials the flow became biphasic just a few seconds after the release start. The propane was stored at the tank at around 25ºC and 8500 hPa (in liquid phase) when the jet fires were undertaken. When the propane was released, a vaporization process started reaching fully vapourization at around 0.3 m downstream from the tank during the first seconds of the release. . However, few seconds later, the pipeline cooled and caused the liquefaction of the gas, leading to a biphasic flow. Palacios (2011) stated that the one-phase vapour release was restricted to periods up to 30 s, becoming the flow biphasic after this period. It has to be highlighted that to perform the experiments aimed at the work at hand, a one-phase vapour flow was envisaged for the sake of simplicity in terms of both data acquisition systems and subsequent analysis.

Among the releases performed by Palacios (2011), the trial with data available to compare with that presented the longest vapour release was the trial JFP 005 008, in which the release remained a one-phase vapour flow by 20 s with an outlet orifice of 0.02 m

Considering the same release conditions of the test JFP 005 008, the simulation showed that the jet would touch the ground 15 m apart from the release point and that the maximum distance reached by the cloud with concentrations greater than 1.0% would be about 25 m after 25 s. If the jet was interrupted in the exact moment that the biphasic flow started, the cloud formed would dilute in less than 10 s. Thus, according to simulations, it would be possible to monitor the cloud only by 30 s (20 s of release plus 10 s of the dilution phase).

In order to find better conditions to analyse the dispersion, other simulations apart from the test JFP 005 008 were performed, in which the flow rate was modified and the outlet diameter was set at 40 mm:

- Scenario 1: Considering a mass flow rate equal to the maximum estimated by FLACS given the initials conditions (1.36 $kg.s^{-1}$) by 40 s.

- Scenario 2: Considering) a mass flow rate equal to the maximum reached by Palacios (2011) tests (0.5 $kg.s^{-1}$) by 40 s.

- Scenario 3: Considering a mass flow rate equal to the maximum reached in Palacios (2011) tests (0.5 $kg.s^{-1}$) by 90 s.

The atmospheric conditions were the same for all simulation and are presented in Table 34.

Table 34 - Initial conditions

Parameter	
Ambient temperature [ºC]	25
Ambient pressure [hPa]	0.001
Ground roughness [m]	0.03
Wind speed at 10 m [$m.s^{-1}$]	2
Relative humidity [%]	70

The results were analysed in terms of the distance at which the jet would touch the ground, the maximum distance reached by the cloud with concentrations greater than 1.0% (1/2 LFL) and the total time of cloud dilution, i.e. the duration of the release plus the time that the cloud would take to dilute enough to concentrations less than 1.0%. The results are presented in Table 35.

Table 35 - Preliminary estimated values

JFP 005 008	Jet touchdown distance	m	8
	Max distance (c>0,01)	m	25
	Dilution time	s	30
Scenario 1	Jet touchdown distance	m	9
	Max distance (c>0,01)	m	55
	Dilution time	s	60
Scenario 2	Jet touchdown distance	m	8
	Max distance (c>0,01)	m	45
	Dilution time	s	60
Scenario 3	Jet touchdown distance	m	8
	Max distance (c>0,01)	m	46
	Dilution time	s	130

These trials were simulated without any barrier, then the maximum distances achieved would have to be greater than the distances expected in the field tests with the presence of a fence.

In order to investigate the influence of a fence in these simulations, Scenarios 1 and 2 were repeated considering a fence located at 10.5 m apart from the release point. The results with and without the presence of the fence are presented in Table 36.

Table 36 - Preliminary results with and without barrier

			No fence	With fence
Scenario 1	Jet touchdown distance	m	9	8
	Max distance (c>0,01%)	m	55	50
	Dilution time	s	60	63
Scenario 2	Jet touchdown distance	m	8	8
	Max distance (c>0,01%)	m	45	30
	Dilution time	s	60	70

Given the characteristics of the propane supply system, the safety constraints which recommended clouds as small and short in duration as possible, and given the dimensions of the area available at Can Padró site for the cloud to disperse, the main outcomes of these preliminary simulations were that the field tests should be performed with flow rates up to 1.0 kg/s to get maximum distances of around 50-60 m and maximum dilution times around 60 s.

APPENDIX D – RESULTS OF FIELD TESTS

In this appendix are presented the releases rates, the meteorological data, the wind speed and direction values and the concentrations of trials P25_2 and P25_3. The releases rates presented were averaged by 1 second and the temperatures and pressures used to calculate the release rate are presented simultaneously. The meteorological data consist of measurements of wind speed, temperature, relative humidity and pressure taken by the weather station during the release. The wind speed and direction were taken by the anemometers during the release. Finally, the concentration measures are presented as function of time for each sensor placed in the field tests; the trials present here were taken in a very cloud day with scattered showers; the rain before (not during) the trials created a more stable atmosphere; however, several sensors did not work well due to accumulated water over the sensor output. In the following tables are presented the measured values of all the sensors that worked well during the trials. The concentrations were averaged by 1 second as the release rates.

Table 37 presents the temperature and the pressure at the outlet orifice and the releases rates of trial P25_2 (all values averaged by 1 second). Table 38 presents the meteorological data recorded by the weather station and Table 39 presents wind data recorded by 5 anemometers for trial P25_2. Table 40 presents the concentrations during the trial P25_2.

Table 41 presents the temperature and the pressure at the outlet orifice and the releases rates of trial P25_3 (all values averaged by 1 second). Table 42 presents the meteorological data recorded by the weather station and Table 43 presents the wind data recorded by 5 anemometers for trial P25_3. Table 44 presents the concentrations during the trial P25_3.

Table 37 - Release rate of trial P25_2 averaged by 1 second

Time [s]	Temperature at outlet orifice [ºC]	Pressure at outlet orifice [hPa]	Release rate [kg.s^{-1}]
1	4.68	590	0.38
2	-10.94	1070	0.37
3	-11.97	740	0.34
4	-7.85	480	0.44
5	-1.77	320	0.36
6	2.17	230	0.31
7	4.02	190	0.28
8	4.40	170	0.27
9	3.99	160	0.26
10	3.06	140	0.25
11	2.08	130	0.24
12	0.77	110	0.22
13	-1.92	90	0.20
14	-4.98	0	0.00
15	-10.52	40	0.12
16	-15.03	10	0.04
17	-25.14	30	0.09
18	-26.98	70	0.19
19	-27.56	100	0.22
20	-27.90	110	0.23
21	-27.93	100	0.22
22	-27.91	100	0.22
23	-27.92	90	0.21
24	-27.95	80	0.20
25	-27.76	90	0.21
26	-28.01	100	0.22
27	-27.96	90	0.21
28	-27.99	90	0.21
29	-28.02	90	0.21
30	-28.07	90	0.21
31	-28.09	80	0.20
32	-28.05	80	0.19
33	-28.07	80	0.19
34	-28.10	70	0.19
35	-28.13	70	0.19
36	-28.09	70	0.19
37	-28.05	130	0.25
38	-28.07	90	0.21
39	-28.12	80	0.20
40	-28.15	80	0.20

Table 38 - Meteorological data during trial P25_2

Time [s]	Wind speed [km.h^{-1}]	Temperature [°C]	Relative humidity [%]	Pressure [hPa]
0	2.60	21.40	86.20	993
2	2.10	21.40	86.30	993
4	2.10	21.40	86.30	993
6	2.50	21.40	86.40	993
8	4.10	21.30	86.40	993
10	4.10	21.20	86.50	993
12	3.90	21.20	86.50	993
14	2.60	21.20	86.60	993
16	1.80	21.30	86.70	993
18	2.00	21.30	86.80	993
20	2.60	21.30	86.80	993
22	2.70	21.30	86.90	993
24	2.50	21.20	86.90	993
26	2.40	21.20	87.00	993
28	2.40	21.20	87.00	993
30	2.20	21.20	87.10	993
32	2.00	21.20	87.20	993
34	2.20	21.10	87.20	993
36	2.70	21.00	87.30	993
38	3.20	20.90	87.40	993
40	4.50	20.70	87.50	993
42	3.80	20.60	87.60	993
44	3.30	20.50	87.80	993
46	3.70	20.50	88.00	993
48	4.10	20.50	88.10	993
50	3.60	20.50	88.30	993

Table 39 - Wind speed and direction during trial P25_2

Time [s]	W1A direction [º]	W1A speed [m.s^{-1}]	W2A direction [º]	W2A speed [m.s^{-1}]	W2B direction [º]	W2B speed [m.s^{-1}]	W3A direction [º]	W3A speed [m.s^{-1}]	W3B direction [º]	W3B speed [m.s^{-1}]
0	201	0.12	172	0.35	155	0.24	219	0.36	199	0.28
1	123	0.04	187	0.22	162	0.16	184	0.41	178	0.45
2	123	0.09	140	0.41	150	0.32	131	0.43	129	0.74
3	113	0.13	136	0.68	136	0.23	189	0.47	172	0.75
4	123	0.21	135	0.66	123	0.30	211	0.55	183	0.84
5	108	0.19	135	0.67	116	0.38	196	0.49	168	0.94
6	146	0.06	109	0.81	45	0.31	183	0.36	158	0.76
7	182	0.08	115	0.50	165	0.11	217	0.42	201	0.51
8	157	0.12	143	0.44	109	0.21	200	0.70	184	0.87
9	168	0.23	109	0.44	114	0.23	197	0.81	175	0.75
10	162	0.25	91	0.32	116	0.13	169	0.97	175	0.77
11	139	0.23	63	0.22	116	0.03	176	1.00	155	0.70
12	143	0.29	283	0.16	189	0.42	196	0.60	155	0.48
13	149	0.34	287	0.19	203	0.54	200	0.86	174	0.91
14	149	0.24	246	0.19	180	0.47	190	0.79	154	0.69
15	175	0.35	228	0.40	158	0.48	191	0.67	158	0.38
16	160	0.25	209	0.49	145	0.59	196	0.84	181	0.62
17	158	0.38	203	0.39	129	0.61	189	1.03	160	0.58
18	143	0.40	194	0.20	142	0.44	181	0.85	164	0.38
19	155	0.40	195	0.03	226	0.30	182	0.86	160	0.38
20	140	0.39	100	0.05	266	0.30	197	0.73	173	0.79
21	140	0.35	207	0.15	288	0.22	191	0.65	166	0.53
22	152	0.36	214	0.48	261	0.16	196	0.64	154	0.55

Table 39 - Wind speed and direction during trial P25_2 (cont.)

Time [s]	W1A direction [º]	W1A speed [m.s^{-1}]	W2A direction [º]	W2A speed [m.s^{-1}]	W2B direction [º]	W2B speed [m.s^{-1}]	W3A direction [º]	W3A speed [m.s^{-1}]	W3B direction [º]	W3B speed [m.s^{-1}]
23	145	0.28	229	0.48	237	0.37	211	0.47	174	0.87
24	138	0.29	223	0.55	215	0.42	192	0.78	171	0.66
25	143	0.31	248	0.55	226	0.29	206	0.56	147	0.34
26	133	0.28	235	0.37	214	0.38	183	0.49	188	0.52
27	134	0.22	212	0.31	214	0.36	190	0.46	203	0.58
28	147	0.28	239	0.26	197	0.38	212	0.46	176	0.93
29	151	0.25	224	0.32	184	0.31	174	0.61	163	0.99
30	122	0.31	185	0.29	169	0.38	182	1.16	148	1.02
31	147	0.21	194	0.21	166	0.38	177	0.91	144	0.69
32	151	0.18	205	0.22	158	0.41	181	1.10	153	0.74
33	185	0.20	239	0.27	176	0.24	183	0.81	147	0.50
34	192	0.19	229	0.25	202	0.33	197	0.42	139	0.86
35	166	0.15	263	0.26	207	0.37	201	0.70	133	0.83
36	133	0.21	258	0.09	188	0.36	210	0.55	128	0.85
37	164	0.19	205	0.21	176	0.39	234	0.51	161	0.77
38	198	0.14	205	0.38	199	0.44	224	0.54	167	0.89
39	148	0.12	197	0.40	191	0.44	183	0.53	140	0.67
40	142	0.23	199	0.32	198	0.40	187	0.26	143	0.76
41	122	0.22	205	0.47	173	0.33	203	0.49	193	0.78
42	103	0.26	184	0.39	174	0.28	200	0.70	179	0.79
43	108	0.32	182	0.43	172	0.26	201	0.68	158	0.77
44	126	0.28	169	0.42	191	0.25	201	0.57	142	0.72
45	166	0.23	190	0.43	164	0.34	140	0.84	127	0.89
46	131	0.16	178	0.41	161	0.40	134	0.95	110	1.10

Table 39 - Wind speed and direction during trial P25_2 (cont.)

Time [s]	W1A direction [º]	W1A speed [m.s^{-1}]	W2A direction [º]	W2A speed [m.s^{-1}]	W2B direction [º]	W2B speed [m.s^{-1}]	W3A direction [º]	W3A speed [m.s^{-1}]	W3B direction [º]	W3B speed [m.s^{-1}]
47	140	0.25	166	0.41	156	0.50	160	0.67	114	0.90
48	121	0.37	141	0.35	137	0.55	143	0.74	123	0.87
49	122	0.33	137	0.30	126	0.43	133	0.83	134	0.53
50	127	0.30	151	0.29	137	0.44	131	0.67	119	0.67

Table 40 - Concentrations during the trial P25_2 averaged by 1second

Sensor	1A	1B	1C	3B	3C	4A	4B	5A	5B	5C	6A	6B	6C	7A	7B
y [m]	0.0	0.0	0.0	0.0	0.0	-2.0	-2.0	2.0	2.0	2.0	0.0	0.0	0.0	-2.0	-2.0
x [m]	2.0	2.0	2.0	5.0	5.0	5.0	5.0	9.0	9.0	9.0	9.0	9.0	9.0	9.0	9.0
z [m]	0.1	0.6	1.3	0.6	1.3	0.1	0.6	0.1	0.6	1.3	0.1	0.6	1.3	0.1	0.6
Time [s]															
1	0.05	0.09	0.44	0.07	0.38	0.01	0.10	0.00	0.06	0.14	0.41	0.29	0.30	0.45	0.44
2	0.34	0.18	2.16	0.14	1.05	0.06	0.17	0.00	0.08	0.18	0.40	0.56	0.62	0.35	0.34
3	0.51	0.24	3.41	0.30	2.07	0.07	0.05	0.00	0.08	0.18	0.52	0.86	1.10	0.32	0.32
4	0.46	0.34	3.81	0.43	2.58	0.09	0.07	0.00	0.06	0.13	0.76	1.12	1.71	0.27	0.30
5	0.34	0.25	4.06	0.44	2.96	0.12	0.07	0.00	0.11	0.12	0.91	1.33	1.95	0.16	0.25
6	0.49	0.16	4.23	0.53	3.13	0.13	0.07	0.07	0.22	0.16	0.99	1.44	1.93	0.13	0.18
7	0.49	0.02	4.47	0.58	3.31	0.20	0.06	0.14	0.24	0.19	0.97	1.41	2.01	0.28	0.11
8	0.52	0.00	4.58	0.48	3.39	0.22	0.06	0.13	0.13	0.23	0.91	1.34	2.04	0.36	0.00
9	0.48	0.00	4.53	0.50	3.43	0.21	0.05	0.08	0.17	0.33	1.03	1.40	2.10	0.54	0.06
10	0.39	0.02	4.62	0.51	3.47	0.20	0.05	0.16	0.25	0.31	1.04	1.40	2.10	0.27	0.22
11	0.31	0.08	4.44	0.51	3.46	0.15	0.04	0.11	0.19	0.24	1.04	1.35	2.05	0.19	0.32
12	0.27	0.12	4.51	0.54	3.41	0.10	0.05	0.00	0.07	0.13	1.03	1.41	2.01	0.13	0.22
13	0.05	0.19	4.53	0.57	3.31	0.20	0.06	0.00	0.00	0.08	1.07	1.51	2.01	0.04	0.04
14	0.00	0.08	4.62	0.50	3.28	0.25	0.06	0.00	0.00	0.17	1.12	1.48	2.04	0.06	0.05
15	0.00	0.00	4.55	0.36	3.18	0.21	0.06	0.00	0.06	0.27	1.13	1.51	1.94	0.19	0.17
16	0.00	0.00	4.50	0.54	3.24	0.11	0.06	0.00	0.15	0.25	1.17	1.55	1.96	0.21	0.11
17	0.00	0.00	4.47	0.50	3.16	0.00	0.06	0.00	0.12	0.27	1.12	1.56	1.98	0.29	0.17
18	0.00	0.01	4.24	0.30	3.20	0.00	0.05	0.09	0.10	0.16	1.15	1.57	1.98	0.12	0.36
19	0.00	0.05	4.28	0.34	3.29	0.00	0.04	0.15	0.06	0.14	1.10	1.51	1.97	0.20	0.54
20	0.00	0.05	4.54	0.36	3.34	0.00	0.03	0.12	0.03	0.11	1.02	1.36	1.97	0.33	0.49

Table 40 - Concentrations during the trial P25_2 averaged by 1second (cont.)

Sensor	1A	1B	1C	3B	3C	4A	4B	5A	5B	5C	6A	6B	6C	7A	7B
y [m]	0.0	0.0	0.0	0.0	0.0	-2.0	-2.0	2.0	2.0	2.0	0.0	0.0	0.0	-2.0	-2.0
x [m]	2.0	2.0	2.0	5.0	5.0	5.0	5.0	9.0	9.0	9.0	9.0	9.0	9.0	9.0	9.0
z [m]	0.1	0.6	1.3	0.6	1.3	0.1	0.6	0.1	0.6	1.3	0.1	0.6	1.3	0.1	0.6
21	0.03	0.15	5.21	0.33	3.35	0.00	0.03	0.00	0.01	0.10	0.76	1.31	1.98	0.35	0.35
22	0.37	0.26	5.24	0.34	3.47	0.00	0.03	0.00	0.04	0.15	0.61	1.45	2.00	0.29	0.15
23	0.44	0.27	5.28	0.49	3.54	0.00	0.03	0.00	0.06	0.20	0.72	1.53	2.04	0.41	0.10
24	0.32	0.25	5.41	0.68	3.66	0.01	0.03	0.00	0.06	0.18	0.76	1.62	2.12	0.51	0.22
25	0.26	0.17	5.56	0.41	3.79	0.02	0.02	0.00	0.06	0.17	0.94	1.63	2.22	0.65	0.52
26	0.26	0.09	5.66	0.28	3.93	0.08	0.02	0.00	0.09	0.34	1.05	1.68	2.29	0.57	0.59
27	0.25	0.05	5.77	0.20	4.08	0.13	0.01	0.00	0.20	0.33	0.93	1.68	2.35	0.59	0.55
28	0.17	0.06	6.10	0.48	4.21	0.07	0.01	0.00	0.14	0.21	0.97	1.76	2.42	0.65	0.54
29	0.20	0.14	6.18	0.78	4.24	0.00	0.00	0.00	0.08	0.14	1.24	1.90	2.51	0.61	0.56
30	0.37	0.14	6.30	0.77	4.34	0.00	0.00	0.00	0.05	0.11	1.43	2.01	2.59	0.64	0.54
31	2.25	0.07	6.51	0.73	4.40	0.00	0.00	0.00	0.02	0.10	1.50	2.02	2.63	0.78	0.54
32	1.10	0.08	6.52	0.72	4.49	0.00	0.00	0.00	0.02	0.08	1.54	2.07	2.70	1.00	0.65
33	0.44	0.09	6.39	0.68	4.51	0.00	0.00	0.01	0.02	0.05	1.43	2.20	2.73	0.95	0.64
34	0.36	0.11	6.31	0.74	4.60	0.00	0.00	0.10	0.03	0.08	1.59	2.29	2.77	0.81	0.54
35	0.32	0.14	6.41	0.89	4.70	0.00	0.00	0.24	0.07	0.05	1.69	2.39	2.84	0.87	0.51
36	0.29	0.13	6.59	1.12	4.72	0.00	0.00	0.30	0.10	0.06	1.75	2.44	2.88	0.77	0.51
37	0.36	0.08	6.73	1.19	4.75	0.00	0.00	0.03	0.08	0.11	1.86	2.48	2.85	0.86	0.46
38	0.36	0.15	6.91	1.05	4.80	0.00	0.00	0.02	0.05	0.11	2.00	2.51	2.77	0.70	0.39
39	0.29	0.15	6.91	1.00	4.74	0.03	0.00	0.00	0.05	0.09	2.03	2.55	2.68	0.38	0.30
40	0.25	0.09	7.06	1.23	4.84	0.05	0.00	0.00	0.06	0.07	1.95	2.43	2.59	0.33	0.24
41	0.25	0.15	7.43	1.20	4.94	0.06	0.00	0.02	0.01	0.01	2.01	2.43	2.55	0.42	0.27
42	0.27	0.21	7.42	1.15	4.90	0.10	0.00	0.00	0.00	0.00	1.90	2.47	2.47	0.68	0.35

Table 40 - Concentrations during the trial P25_2 averaged by 1second (cont.)

Sensor	1A	1B	1C	3B	3C	4A	4B	5A	5B	5C	6A	6B	6C	7A	7B
y [m]	**0.0**	**0.0**	**0.0**	**0.0**	**0.0**	**-2.0**	**-2.0**	**2.0**	**2.0**	**2.0**	**0.0**	**0.0**	**0.0**	**-2.0**	**-2.0**
x [m]	**2.0**	**2.0**	**2.0**	**5.0**	**5.0**	**5.0**	**5.0**	**9.0**	**9.0**	**9.0**	**9.0**	**9.0**	**9.0**	**9.0**	**9.0**
z [m]	**0.1**	**0.6**	**1.3**	**0.6**	**1.3**	**0.1**	**0.6**	**0.1**	**0.6**	**1.3**	**0.1**	**0.6**	**1.3**	**0.1**	**0.6**
43	1.56	0.18	7.43	0.86	5.19	0.13	0.00	0.00	0.00	0.05	2.03	2.44	2.33	0.67	0.23
44	2.36	0.19	7.40	0.78	5.13	0.10	0.00	0.18	0.00	0.04	2.05	2.41	2.19	0.57	0.21
45	0.77	0.20	7.35	0.85	4.57	0.06	0.00	0.18	0.00	0.03	2.06	2.28	2.09	0.49	0.31
46	0.33	0.18	4.32	0.82	3.81	0.06	0.00	0.14	0.23	0.07	2.07	2.15	1.79	0.36	0.39
47	0.24	0.12	2.08	0.67	2.50	0.15	0.00	0.16	0.36	0.13	2.03	2.05	1.59	0.24	0.36
48	0.10	0.12	0.56	0.51	1.79	0.09	0.00	0.28	0.42	0.20	1.87	1.91	1.22	0.11	0.35
49	0.27	0.13	0.00	0.13	1.08	0.10	0.00	0.39	0.48	0.42	1.73	1.57	0.79	0.05	0.29
50	0.40	0.11	0.00	0.00	0.67	0.08	0.00	0.40	0.58	0.37	1.40	1.23	0.54	0.07	0.25
Minimum	0.00	0.00	0.44	0.00	0.38	0.00	0.00	0.00	0.00	0.01	0.40	0.29	0.30	0.04	0.00
Maximum	2.36	0.34	7.43	1.23	5.19	0.25	0.17	0.40	0.58	0.42	2.07	2.55	2.88	1.00	0.65
			Values averaged by 1 s												

Table 40 - Concentrations during the trial P25_2 averaged by 1second (cont.)

Sensor	7C	9A	10A	10B	10C	11B	11C	12A	12C	13A	15A	15B	16A	16B
y [m]	-2.0	-3.0	2.0	2.0	2.0	0.0	0.0	-2.0	-2.0	2.0	0.0	0.0	-2.0	-2.0
x [m]	9.0	10.0	11.0	11.0	11.0	11.0	11.0	11.0	11.0	13.0	15.0	15.0	13.0	13.0
z [m]	1.3	0.1	0.1	0.6	1.3	0.6	1.3	0.1	1.3	0.6	0.1	0.6	0.1	0.6
Time [s]														
1	0.08	0.00	0.13	0.18	0.15	0.13	0.00	0.02	0.00	0.00	0.00	0.00	0.08	0.01
2	0.07	0.00	0.00	0.11	0.20	0.27	0.16	0.05	0.00	0.00	0.00	0.04	0.11	0.00
3	0.05	0.01	0.00	0.19	0.25	0.76	0.62	0.05	0.00	0.00	0.04	0.05	0.21	0.01
4	0.02	0.07	0.36	0.32	0.31	1.18	2.85	0.50	0.18	0.00	0.63	0.17	0.55	0.87
5	0.00	0.00	0.29	0.36	0.43	1.36	0.00	0.36	0.39	0.07	0.66	0.17	0.91	1.21
6	0.03	0.00	0.44	0.41	0.39	1.53	0.17	0.23	0.42	0.06	0.51	0.26	1.16	1.26
7	0.00	0.00	0.76	0.39	0.49	1.50	0.98	0.26	0.30	0.23	0.69	0.37	1.24	1.35
8	0.00	0.00	0.82	0.44	0.57	1.49	1.18	0.18	0.24	0.39	0.81	0.40	1.09	1.30
9	0.00	0.00	0.68	0.34	0.44	1.48	1.40	0.06	0.19	0.47	0.67	0.42	1.09	1.28
10	0.02	0.00	0.37	0.32	0.42	1.45	1.40	0.10	0.03	0.49	0.59	0.28	1.15	1.35
11	0.00	0.00	0.01	0.30	0.43	1.41	1.04	0.10	0.00	0.37	0.52	0.27	1.15	1.37
12	0.00	0.00	0.03	0.30	0.36	1.36	1.25	0.00	0.00	0.22	0.63	0.20	1.15	1.28
13	0.00	0.00	0.00	0.27	0.25	1.45	1.75	0.00	0.00	0.16	0.57	0.02	1.05	1.20
14	0.00	0.00	0.00	0.17	0.26	1.46	1.44	0.00	0.00	0.03	0.25	0.00	0.99	1.21
15	0.00	0.00	0.00	0.15	0.39	1.45	1.33	0.00	0.00	0.00	0.25	0.00	1.08	1.24
16	0.00	0.00	0.00	0.36	0.34	1.42	1.71	0.00	0.00	0.00	0.23	0.00	1.08	1.22
17	0.04	0.00	0.00	0.42	0.51	1.44	1.80	0.00	0.00	0.01	0.18	0.05	1.06	1.18
18	0.21	0.00	0.05	0.26	0.47	1.50	1.49	0.05	0.00	0.02	0.47	0.20	1.11	1.20
19	0.25	0.00	0.00	0.14	0.32	1.41	1.54	0.03	0.00	0.01	0.67	0.44	1.17	1.27
20	0.20	0.00	0.00	0.06	0.19	1.06	1.77	0.00	0.10	0.03	0.65	0.54	1.11	1.28

Table 40 - Concentrations during the trial P25_2 averaged by 1second (cont.)

Sensor	7C	9A	10A	10B	10C	11B	11C	12A	12C	13A	15A	15B	16A	16B
y [m]	-2.0	-3.0	2.0	2.0	2.0	0.0	0.0	-2.0	-2.0	2.0	0.0	0.0	-2.0	-2.0
x [m]	9.0	10.0	11.0	11.0	11.0	11.0	11.0	11.0	11.0	13.0	15.0	15.0	13.0	13.0
z [m]	1.3	0.1	0.1	0.6	1.3	0.6	1.3	0.1	1.3	0.6	0.1	0.6	0.1	0.6
21	0.14	0.00	0.00	0.04	0.26	1.03	1.47	0.01	0.17	0.00	0.98	0.48	1.07	1.20
22	0.07	0.00	0.00	0.08	0.53	1.11	1.46	0.20	0.18	0.00	0.89	0.49	0.89	1.04
23	0.04	0.00	0.00	0.12	0.43	1.18	1.56	0.40	0.14	0.00	0.93	0.47	0.68	1.00
24	0.01	0.00	0.10	0.27	0.49	1.30	1.59	0.41	0.00	0.00	1.00	0.49	0.86	1.00
25	0.02	0.00	0.06	0.43	0.36	1.42	1.68	0.38	0.00	0.00	0.93	0.66	0.97	1.04
26	0.05	0.00	0.22	0.52	0.42	1.53	1.78	0.61	0.04	0.00	0.78	0.71	1.10	1.14
27	0.09	0.00	0.08	0.44	0.50	1.56	1.79	0.52	0.18	0.00	0.93	0.79	1.19	1.36
28	0.11	0.00	0.24	0.41	0.52	1.60	1.81	0.80	0.34	0.00	0.82	0.56	1.21	1.41
29	0.12	0.00	0.14	0.40	0.48	1.69	1.78	0.69	0.33	0.00	0.89	0.44	1.25	1.33
30	0.24	0.00	0.01	0.33	0.35	1.83	2.15	0.71	0.20	0.00	0.62	0.26	1.28	1.41
31	0.45	0.00	0.00	0.20	0.21	1.88	2.09	0.68	0.03	0.00	0.72	0.25	1.42	1.09
32	0.42	0.00	0.00	0.21	0.17	1.97	1.94	0.61	0.00	0.00	0.94	0.37	1.57	1.22
33	0.33	0.00	0.00	0.14	0.13	2.04	1.93	0.56	0.00	0.06	1.12	0.51	1.74	1.39
34	0.28	0.00	0.00	0.27	0.16	2.08	2.01	0.59	0.00	0.13	1.18	0.70	1.88	1.57
35	0.25	0.00	0.43	0.63	0.15	2.15	2.02	0.65	0.00	0.00	1.28	0.72	1.94	1.67
36	0.04	0.00	0.75	0.59	0.05	2.36	1.91	0.74	0.00	0.00	1.26	0.49	1.92	1.74
37	0.00	0.00	0.87	0.37	0.00	2.38	2.28	0.66	0.00	0.06	1.45	0.70	1.97	1.77
38	0.00	0.00	0.86	0.29	0.00	2.33	2.12	0.81	0.00	0.35	1.33	0.85	2.06	1.96
39	0.00	0.00	0.80	0.31	0.05	2.31	1.90	1.00	0.00	0.38	1.43	0.93	2.07	1.70
40	0.00	0.00	0.81	0.46	0.00	2.25	2.00	1.13	0.00	0.54	1.53	0.99	1.99	1.51
41	0.00	0.00	0.89	0.71	0.03	2.29	1.92	1.21	0.00	0.87	1.44	0.96	1.92	1.41
42	0.00	0.00	0.98	0.50	0.07	2.22	1.60	1.17	0.00	0.90	1.29	0.87	1.81	1.48

Table 40 - Concentrations during the trial P25_2 averaged by 1second (cont.)

Sensor	7C	9A	10A	10B	10C	11B	11C	12A	12C	13A	15A	15B	16A	16B
y [m]	**-2.0**	**-3.0**	**2.0**	**2.0**	**2.0**	**0.0**	**0.0**	**-2.0**	**-2.0**	**2.0**	**0.0**	**0.0**	**-2.0**	**-2.0**
x [m]	**9.0**	**10.0**	**11.0**	**11.0**	**11.0**	**11.0**	**11.0**	**11.0**	**11.0**	**13.0**	**15.0**	**15.0**	**13.0**	**13.0**
z [m]	**1.3**	**0.1**	**0.1**	**0.6**	**1.3**	**0.6**	**1.3**	**0.1**	**1.3**	**0.6**	**0.1**	**0.6**	**0.1**	**0.6**
43	0.01	0.00	1.00	0.55	0.22	2.03	1.38	1.03	0.00	1.13	1.25	0.87	1.77	1.59
44	0.08	0.00	1.29	0.77	0.34	1.90	1.24	0.95	0.00	1.30	1.36	1.06	1.76	1.42
45	0.11	0.00	1.04	0.75	0.46	1.87	1.25	1.03	0.00	1.34	1.46	0.95	1.54	1.20
46	0.08	0.00	0.85	0.68	0.53	1.86	1.16	0.96	0.00	1.29	1.67	1.02	1.51	0.89
47	0.06	0.00	0.87	0.77	0.68	1.67	0.92	0.83	0.00	1.31	1.55	0.87	1.62	0.96
48	0.08	0.00	1.05	0.78	0.53	1.42	0.55	0.74	0.00	1.32	1.46	0.78	1.34	0.64
49	0.00	0.00	1.12	1.11	0.64	1.09	0.35	0.61	0.00	1.44	1.27	0.71	1.04	0.33
50	0.00	0.00	0.93	0.72	0.57	0.87	0.19	0.45	0.08	1.40	1.01	0.18	0.90	0.11
Minimum	0.00	0.00	0.00	0.04	0.00	0.13	0.00	0.00	0.00	0.00	0.00	0.00	0.08	0.00
Maximum	0.45	0.07	1.29	1.11	0.68	2.38	2.85	1.21	0.42	1.44	1.67	1.06	2.07	1.96
Values averaged by 1 s														

Table 41 - Release rate of trial P25_3 averaged by 1 second

Time [s]	Temperature at outlet orifice [ºC]	Pressure at outlet orifice [hPa]	Release rate [kg.s^{-1}]
1	10.26	740	0.40
2	-12.66	1330	0.39
3	-11.85	880	0.35
4	-7.46	380	0.40
5	-2.45	240	0.34
6	1.84	170	0.28
7	3.23	110	0.23
8	4.44	90	0.20
9	5.07	80	0.18
10	5.46	70	0.17
11	5.58	60	0.16
12	5.52	50	0.15
13	5.17	50	0.15
14	4.75	0	0.00
15	4.19	40	0.09
16	3.23	30	0.12
17	2.49	30	0.12
18	0.93	30	0.12
19	-0.89	30	0.11
20	-4.10	20	0.09
21	-10.30	20	0.09
22	-14.08	20	0.09
23	-22.00	20	0.09
24	-26.70	20	0.09
25	-27.21	20	0.11
26	-27.86	20	0.11
27	-28.13	50	0.15
28	-28.35	40	0.15
29	-28.41	40	0.14
30	-28.34	50	0.15
31	-28.30	40	0.15
32	-28.23	50	0.16
33	-28.18	60	0.17
34	-28.24	60	0.17
35	-28.30	60	0.17
36	-28.32	50	0.16
37	-28.16	60	0.17
38	-28.16	60	0.17
39	-28.26	60	0.17
40	-28.30	80	0.17

Table 42 - Meteorological data during trial P25_3

Time [s]	Wind speed [km.h^{-1}]	Temperature [°C]	Relative humidity [%]	Pressure [hPA]
0	0.00	22.80	88.60	993
2	1.30	23.00	88.90	993
4	1.40	23.00	89.00	993
6	1.70	23.10	89.20	993
8	2.30	23.10	89.10	993
10	3.20	22.80	88.80	993
12	3.40	22.70	88.40	993
14	3.20	22.60	87.90	993
16	2.90	22.50	87.60	993
18	2.80	22.50	87.40	993
20	3.10	22.40	87.30	993
22	3.60	22.40	87.20	993
24	4.30	22.50	87.30	993
26	4.80	22.50	87.40	993
28	4.80	22.40	87.50	993
30	4.10	22.20	87.40	993
32	4.20	22.20	87.30	993
34	4.50	22.20	87.10	993
36	5.00	22.10	87.00	993
38	4.60	22.10	86.90	993
40	4.00	22.10	86.90	993
42	3.90	22.10	86.90	993
44	3.70	22.10	87.00	993
46	3.50	22.10	87.00	993
48	3.60	22.10	87.10	993
50	4.00	22.10	87.10	993

Table 43 - Wind speed and direction during trial P25_3

Time [s]	W1A direction [º]	W1A speed [m.s^{-1}]	W2A direction [º]	W2A speed [m.s^{-1}]	W2B direction [º]	W2B speed [m.s^{-1}]	W3A direction [º]	W3A speed [m.s^{-1}]	W3B direction [º]	W3B speed [m.s^{-1}]
0	179	0.34	270	0.41	266	0.49	275	0.29	226	0.33
1	199	0.32	270	0.53	240	0.54	238	0.46	203	0.64
2	194	0.30	260	0.59	241	0.67	226	0.55	194	0.76
3	188	0.37	250	0.68	234	0.65	225	0.58	204	0.79
4	188	0.35	251	0.57	235	0.69	223	0.67	196	0.77
5	202	0.32	245	0.47	238	0.68	209	0.61	205	0.83
6	223	0.29	243	0.44	243	0.89	230	0.67	203	0.86
7	235	0.26	249	0.55	240	0.86	228	0.80	208	0.91
8	268	0.23	251	0.81	242	0.76	232	1.04	209	1.16
9	260	0.18	248	0.69	233	0.69	228	1.07	211	1.01
10	143	0.09	249	0.74	232	0.65	229	0.95	210	0.90
11	151	0.22	251	0.68	234	0.59	227	0.87	215	0.87
12	135	0.17	251	0.54	237	0.64	222	0.79	208	0.96
13	97	0.15	240	0.41	247	0.61	217	0.77	203	0.91
14	58	0.12	249	0.43	256	0.58	216	0.82	203	0.87
15	78	0.25	248	0.33	261	0.53	213	0.78	203	0.91
16	89	0.12	269	0.27	262	0.46	209	0.77	200	0.81
17	60	0.05	266	0.28	255	0.36	214	0.80	208	0.74
18	268	0.06	260	0.39	233	0.34	224	0.76	220	0.51
19	285	0.07	248	0.47	244	0.41	213	0.62	227	0.49
20	192	0.17	261	0.51	245	0.41	220	0.63	241	0.49
21	189	0.36	269	0.53	240	0.53	221	0.64	259	0.59
22	188	0.27	270	0.51	233	0.58	222	0.69	238	0.77

Table 43 - Wind speed and direction during trial P25_ 3 (cont.)

Time [s]	W1A direction [º]	W1A speed [m.s^{-1}]	W2A direction [º]	W2A speed [m.s^{-1}]	W2B direction [º]	W2B speed [m.s^{-1}]	W3A direction [º]	W3A speed [m.s^{-1}]	W3B direction [º]	W3B speed [m.s^{-1}]
23	195	0.24	265	0.57	237	0.67	225	0.80	213	0.96
24	116	0.16	268	0.74	251	0.7	229	0.90	226	1.20
25	183	0.26	276	0.74	259	0.73	228	0.94	221	1.09
26	172	0.23	284	0.79	283	0.78	227	0.87	233	1.00
27	175	0.23	273	0.91	278	0.8	227	0.90	211	0.87
28	178	0.26	273	0.83	284	0.69	231	0.88	215	0.87
29	122	0.13	271	0.72	254	0.82	237	0.66	222	0.68
30	118	0.12	271	0.63	251	0.79	249	0.56	238	0.37
31	211	0.18	263	0.63	256	0.65	279	0.20	259	0.61
32	208	0.17	258	0.59	252	0.71	321	0.37	280	0.68
33	245	0.13	254	0.64	248	0.76	316	0.54	284	0.39
34	267	0.14	243	0.55	235	0.74	288	0.37	265	0.43
35	277	0.17	251	0.57	254	0.66	199	0.14	277	0.54
36	281	0.27	248	0.76	241	0.92	266	0.39	284	0.51
37	266	0.65	251	0.73	240	0.93	243	0.40	228	0.41
38	274	0.90	249	0.70	252	0.95	232	0.69	204	0.88
39	277	0.88	249	0.80	241	1.03	218	0.74	198	0.92
40	280	0.76	255	0.80	240	1.02	228	0.76	212	0.87
41	0.64	263	0.78	272	0.74	277	0.88	242	0.86	0.64
42	0.67	264	0.67	268	0.75	280	0.76	264	0.79	0.67
43	0.60	271	0.65	259	0.81	282	0.64	261	0.67	0.60
44	0.70	278	0.61	266	0.73	279	0.67	233	0.91	0.70
45	0.71	270	0.55	275	0.82	262	0.6	242	0.86	0.71
46	0.81	269	0.69	276	0.79	267	0.7	256	0.73	0.81

Table 43 - Wind speed and direction during trial P25_ 3 (cont.)

Time [s]	W1A direction [º]	W1A speed [m.s^{-1}]	W2A direction [º]	W2A speed [m.s^{-1}]	W2B direction [º]	W2B speed [m.s^{-1}]	W3A direction [º]	W3A speed [m.s^{-1}]	W3B direction [º]	W3B speed [m.s^{-1}]
47	0.93	272	0.58	273	0.65	269	0.71	232	0.90	0.93
48	0.85	270	0.58	275	0.62	266	0.81	241	0.78	0.85
49	0.68	295	0.52	265	0.6	263	0.93	233	0.63	0.68
50	0.68	294	0.62	266	0.54	265	0.85	265	0.40	0.68

Table 44 - Concentrations of trial P25_3 averaged by 1second

Sensor	1A	1B	1C	3B	3C	4A	4B	5A	5B	5C	6A	6B	6C
y [m]	0.0	0.0	0.0	0.0	0.0	-2.0	-2.0	2.0	2.0	2.0	0.0	0.0	0.0
x [m]	2.0	2.0	2.0	5.0	5.0	5.0	5.0	9.0	9.0	9.0	9.0	9.0	9.0
z [m]	0.1	0.6	1.3	0.6	1.3	0.1	0.6	0.1	0.6	1.3	0.1	0.6	1.3
Time [s]													
1	0.19	0.00	0.21	0.05	0.00	0.45	0.00	0.00	0.00	0.00	0.00	0.00	0.00
2	0.06	0.00	1.64	0.03	0.86	0.47	0.00	0.00	0.00	0.00	0.00	0.00	0.25
3	0.05	0.00	2.76	0.15	1.51	0.62	0.00	0.00	0.00	0.00	0.16	0.22	0.76
4	0.00	0.00	3.36	0.44	2.21	0.69	0.00	0.00	0.00	0.00	0.35	0.63	1.20
5	0.00	0.00	3.72	0.41	2.63	0.65	0.00	0.00	0.00	0.00	0.80	0.91	1.56
6	0.08	0.05	3.86	0.59	2.91	0.69	0.00	0.00	0.00	0.00	0.86	0.92	1.69
7	0.07	0.19	3.80	0.83	3.04	0.67	0.00	0.00	0.00	0.00	0.79	0.90	1.72
8	0.16	0.26	4.19	0.93	3.12	0.80	0.00	0.04	0.00	0.00	0.76	0.89	1.69
9	0.25	0.15	4.21	0.94	3.12	0.89	0.00	0.23	0.00	0.00	0.73	0.88	1.65
10	0.19	0.00	4.31	0.75	3.04	0.94	0.00	0.33	0.00	0.00	0.65	0.92	1.54
11	0.00	0.00	4.39	0.59	2.96	0.95	0.00	0.21	0.00	0.00	0.82	1.02	1.58
12	0.00	0.00	4.33	0.52	2.92	0.77	0.00	0.16	0.00	0.00	0.86	0.89	1.48
13	0.00	0.00	4.20	0.61	2.86	0.52	0.00	0.30	0.00	0.00	0.76	0.69	1.34
14	0.00	0.06	3.76	0.61	2.75	0.28	0.00	0.45	0.02	0.00	0.68	0.58	1.19
15	0.33	0.06	3.65	0.56	2.64	0.28	0.00	0.40	0.09	0.00	0.63	0.56	1.08
16	0.36	0.15	3.88	0.44	2.52	0.31	0.00	0.79	0.00	0.00	0.50	0.47	0.94
17	0.00	0.26	3.75	0.29	2.45	0.17	0.00	0.53	0.00	0.00	0.40	0.36	0.74
18	0.00	0.12	3.65	0.24	2.44	0.00	0.00	0.03	0.00	0.00	0.44	0.40	0.70
19	0.00	0.01	3.58	0.33	2.38	0.00	0.00	0.00	0.00	0.00	0.27	0.36	0.63
20	0.00	0.00	3.50	0.40	2.32	0.15	0.00	0.00	0.00	0.00	0.16	0.27	0.64

Table 44 - Concentrations of trial P25_3 averaged by 1second (cont.)

Sensor	1A	1B	1C	3B	3C	4A	4B	5A	5B	5C	6A	6B	6C
y [m]	0.0	0.0	0.0	0.0	0.0	-2.0	-2.0	2.0	2.0	2.0	0.0	0.0	0.0
x [m]	2.0	2.0	2.0	5.0	5.0	5.0	5.0	9.0	9.0	9.0	9.0	9.0	9.0
z [m]	0.1	0.6	1.3	0.6	1.3	0.1	0.6	0.1	0.6	1.3	0.1	0.6	1.3
21	0.00	0.00	3.27	0.31	1.99	0.35	0.00	0.00	0.00	0.00	0.05	0.16	0.51
22	0.00	0.00	3.49	0.25	1.91	0.23	0.00	0.63	0.00	0.00	0.03	0.00	0.37
23	0.00	0.00	3.79	0.29	2.01	0.05	0.00	0.73	0.00	0.00	0.12	0.00	0.34
24	0.00	0.00	3.64	0.31	2.04	0.26	0.00	0.47	0.00	0.00	0.11	0.06	0.36
25	0.00	0.00	3.57	0.47	2.04	0.33	0.00	0.49	0.00	0.00	0.09	0.04	0.43
26	0.00	0.00	3.61	0.63	2.09	0.47	0.00	0.41	0.00	0.00	0.09	0.02	0.50
27	0.01	0.00	3.73	0.43	2.26	0.51	0.00	0.25	0.00	0.00	0.00	0.02	0.46
28	0.07	0.00	3.99	0.41	2.26	0.65	0.00	0.00	0.00	0.00	0.00	0.10	0.45
29	0.23	0.00	4.46	0.45	2.23	0.75	0.00	0.00	0.00	0.00	0.00	0.16	0.49
30	0.45	0.02	4.48	0.55	2.26	0.72	0.00	0.00	0.00	0.00	0.11	0.24	0.63
31	0.44	0.06	4.56	0.61	2.26	0.65	0.00	0.00	0.00	0.00	0.11	0.31	0.71
32	0.52	0.02	4.82	0.76	2.23	0.65	0.00	0.00	0.00	0.00	0.19	0.31	0.67
33	0.51	0.21	5.00	0.92	2.30	0.73	0.00	0.00	0.00	0.00	0.41	0.28	0.62
34	0.61	0.25	4.93	0.79	2.45	0.46	0.00	0.00	0.00	0.00	0.48	0.26	0.29
35	0.40	0.26	5.07	0.65	2.57	0.00	0.00	0.00	0.00	0.00	0.41	0.28	0.10
36	0.20	0.17	5.12	0.80	2.70	0.00	0.00	0.00	0.00	0.00	0.51	0.31	0.26
37	0.22	0.10	5.33	0.71	2.74	0.00	0.00	0.00	0.00	0.00	0.36	0.34	0.28
38	0.36	0.03	5.89	0.61	2.85	0.00	0.00	0.00	0.00	0.00	0.41	0.26	0.24
39	0.68	0.03	6.57	0.58	3.03	0.00	0.00	0.00	0.00	0.00	0.46	0.13	0.14
40	0.66	0.14	6.80	0.35	3.16	0.07	0.00	0.00	0.00	0.00	0.44	0.00	0.00
41	1.19	0.10	7.08	0.25	3.35	0.60	0.00	0.00	0.00	0.00	0.41	0.00	0.00
42	0.68	0.03	6.57	0.64	3.55	0.83	0.00	0.00	0.00	0.00	0.47	0.00	0.00

Table 44 - Concentrations of trial P25_3 averaged by 1second (cont.)

Sensor	1A	1B	1C	3B	3C	4A	4B	5A	5B	5C	6A	6B	6C
y [m]	**0.0**	**0.0**	**0.0**	**0.0**	**0.0**	**-2.0**	**-2.0**	**2.0**	**2.0**	**2.0**	**0.0**	**0.0**	**0.0**
x [m]	**2.0**	**2.0**	**2.0**	**5.0**	**5.0**	**5.0**	**5.0**	**9.0**	**9.0**	**9.0**	**9.0**	**9.0**	**9.0**
z [m]	**0.1**	**0.6**	**1.3**	**0.6**	**1.3**	**0.1**	**0.6**	**0.1**	**0.6**	**1.3**	**0.1**	**0.6**	**1.3**
43	0.68	0.06	6.63	0.68	3.66	0.92	0.03	0.00	0.00	0.00	0.45	0.24	0.23
44	0.67	0.09	6.69	0.37	3.79	1.00	0.08	0.00	0.00	0.00	0.56	0.50	0.55
45	0.66	0.11	6.75	0.28	0.14	0.91	0.05	0.00	0.00	0.00	0.77	0.75	0.81
46	0.66	0.14	6.80	0.93	4.03	0.77	0.05	0.15	0.00	0.00	1.06	1.04	0.70
47	0.79	0.13	6.80	1.32	4.23	0.54	0.07	0.04	0.00	0.00	1.35	0.83	0.45
48	0.93	0.12	6.89	1.11	4.23	0.42	0.37	0.51	0.00	0.00	1.31	0.66	0.21
49	1.06	0.11	6.99	0.65	3.44	0.07	0.18	0.18	0.00	0.00	1.07	0.59	0.05
50	1.19	0.10	7.08	0.14	2.89	0.02	0.17	0.00	0.00	0.00	1.00	0.25	0.00
Minimum	0.00	0.00	0.21	0.03	0.00	0.00	0.00	0.00	0.00	0.00	0.00	0.00	0.00
Maximum	1.19	0.26	7.08	1.32	4.23	1.00	0.37	0.79	0.09	0.00	1.35	1.04	1.72
Values averaged by 1 s													

Table 44 - Concentrations of trial P25_3 averaged by 1second (cont.)

Sensor	7A	7B	7C	9A	10B	11B	11C	12A	12C	13A	15A	16A	16B
y [m]	-2.0	-2.0	-2.0	-3.0	2.0	0.0	0.0	-2.0	-2.0	2.0	-2.0	0.0	0.0
x [m]	9.0	9.0	9.0	10.0	11.0	11.0	11.0	11.0	11.0	13.0	13.0	15.0	15.0
z [m]	0.1	0.6	1.3	0.1	0.6	0.6	1.3	0.1	1.3	0.6	0.1	0.1	0.6
Time [s]													
1	0.01	0.00	0.00	0.10	0.00	0.00	0.70	0.01	0.38	0.00	0.05	0.00	0.00
2	0.00	0.00	0.00	0.01	0.00	0.07	0.10	0.01	0.06	0.00	0.05	0.00	0.00
3	0.06	0.00	0.11	0.00	0.00	0.47	0.08	0.01	0.00	0.00	0.07	0.00	0.00
4	0.48	0.00	0.18	0.00	0.00	0.73	0.17	0.01	0.00	0.00	0.65	0.33	0.43
5	0.43	0.00	0.18	0.06	0.00	1.00	0.48	0.01	0.00	0.00	0.81	0.65	0.70
6	0.40	0.00	0.39	0.19	0.00	1.16	0.90	0.01	0.01	0.00	1.04	0.80	1.00
7	0.47	0.00	0.51	0.14	0.00	1.25	1.13	0.01	0.05	0.11	1.18	0.95	1.08
8	0.58	0.00	0.56	0.14	0.00	1.25	1.28	0.01	0.11	0.26	1.26	0.84	1.23
9	0.63	0.00	0.71	0.11	0.00	1.27	1.37	0.01	0.30	0.30	1.23	0.92	1.23
10	0.64	0.25	0.72	0.04	0.00	1.15	1.45	0.01	0.14	0.18	1.23	0.87	1.19
11	0.50	0.10	0.71	0.04	0.00	1.04	1.44	0.01	0.12	0.20	1.22	0.74	1.14
12	0.34	0.16	0.60	0.00	0.00	1.03	1.30	0.01	0.20	0.33	1.10	0.63	1.05
13	0.42	0.05	0.55	0.00	0.00	0.98	1.33	0.01	0.23	0.43	0.97	0.57	1.00
14	0.39	0.11	0.55	0.00	0.03	0.91	1.18	0.01	0.19	0.37	0.98	0.53	0.96
15	0.50	0.09	0.63	0.13	0.18	0.86	1.45	0.01	0.21	0.26	0.89	0.35	0.73
16	0.51	0.05	0.65	0.36	0.29	0.88	1.18	0.01	0.21	0.00	0.79	0.38	0.84
17	0.51	0.06	0.60	0.00	0.44	0.88	1.14	0.01	0.17	0.00	0.69	0.38	0.79
18	0.56	0.12	0.48	0.01	0.51	0.83	1.08	0.01	0.28	0.00	0.66	0.28	0.69
19	0.64	0.17	0.51	0.07	0.60	0.77	1.00	0.01	0.25	0.00	0.63	0.26	0.59
20	0.56	0.25	0.42	0.16	0.20	0.70	0.99	0.01	0.58	0.00	0.49	0.20	0.57

Table 44 - Concentrations of trial P25_3 averaged by 1second (cont.)

Sensor	7A	7B	7C	9A	10B	11B	11C	12A	12C	13A	15A	16A	16B
y [m]	-2.0	-2.0	-2.0	-3.0	2.0	0.0	0.0	-2.0	-2.0	2.0	-2.0	0.0	0.0
x [m]	9.0	9.0	9.0	10.0	11.0	11.0	11.0	11.0	11.0	13.0	13.0	15.0	15.0
z [m]	0.1	0.6	1.3	0.1	0.6	0.6	1.3	0.1	1.3	0.6	0.1	0.1	0.6
21	0.56	0.06	0.35	0.14	0.00	0.61	0.99	0.01	0.32	0.00	0.47	0.00	0.45
22	0.38	0.00	0.26	0.00	0.00	0.44	0.89	0.01	0.09	0.00	0.29	0.00	0.18
23	0.37	0.00	0.15	0.00	0.00	0.42	0.76	0.01	0.00	0.00	0.20	0.00	0.11
24	0.37	0.00	0.08	0.00	0.00	0.41	0.86	0.01	0.00	0.00	0.21	0.00	0.00
25	0.15	0.00	0.14	0.00	0.00	0.36	0.70	0.01	0.00	0.00	0.10	0.00	0.00
26	0.00	0.00	0.26	0.00	0.00	0.33	0.61	0.01	0.00	0.00	0.00	0.00	0.00
27	0.10	0.03	0.21	0.00	0.00	0.38	0.49	0.01	0.00	0.00	0.00	0.00	0.00
28	0.00	0.12	0.21	0.00	0.00	0.45	0.33	0.01	0.00	0.00	0.00	0.00	0.00
29	0.02	0.00	0.07	0.00	0.00	0.46	0.18	0.01	0.14	0.00	0.00	0.00	0.00
30	0.22	0.00	0.00	0.00	0.00	0.42	0.35	0.01	0.24	0.00	0.00	0.00	0.00
31	0.12	0.00	0.06	0.00	0.00	0.41	0.24	0.01	0.16	0.00	0.00	0.00	0.00
32	0.09	0.00	0.21	0.00	0.00	0.23	0.00	0.01	0.00	0.00	0.00	0.00	0.00
33	0.10	0.00	0.25	0.00	0.00	0.30	0.26	0.01	0.00	0.00	0.02	0.00	0.00
34	0.40	0.00	0.14	0.29	0.00	0.26	0.51	0.01	0.00	0.00	0.09	0.00	0.01
35	0.59	0.00	0.19	0.33	0.00	0.11	0.58	0.01	0.13	0.00	0.17	0.00	0.15
36	0.23	0.00	0.05	0.25	0.00	0.00	0.57	0.01	0.03	0.00	0.20	0.00	0.16
37	0.13	0.00	0.35	0.20	0.00	0.00	0.57	0.00	0.00	0.00	0.13	0.00	0.07
38	0.28	0.12	0.54	0.15	0.00	0.03	0.72	0.01	0.00	0.00	0.20	0.00	0.02
39	0.39	0.23	0.57	0.06	0.00	0.22	1.07	0.00	0.00	0.00	0.55	0.00	0.00
40	0.41	0.22	0.55	0.02	0.00	0.10	0.87	0.00	0.00	0.00	0.75	0.00	0.13
41	0.41	0.20	0.53	0.00	0.00	0.04	1.10	0.00	0.00	0.00	0.90	0.00	0.31
42	0.38	0.20	0.53	0.00	0.00	0.00	1.08	0.00	0.00	0.00	0.99	0.00	0.59

Table 44 - Concentrations of trial P25_3 averaged by 1second (cont.)

Sensor	7A	7B	7C	9A	10B	11B	11C	12A	12C	13A	15A	16A	16B
y [m]	**-2.0**	**-2.0**	**-2.0**	**-3.0**	**2.0**	**0.0**	**0.0**	**-2.0**	**-2.0**	**2.0**	**-2.0**	**0.0**	**0.0**
x [m]	**9.0**	**9.0**	**9.0**	**10.0**	**11.0**	**11.0**	**11.0**	**11.0**	**11.0**	**13.0**	**13.0**	**15.0**	**15.0**
z [m]	**0.1**	**0.6**	**1.3**	**0.1**	**0.6**	**0.6**	**1.3**	**0.1**	**1.3**	**0.6**	**0.1**	**0.1**	**0.6**
43	0.35	0.19	0.57	0.00	0.00	0.00	1.13	0.00	0.00	0.00	1.09	0.00	0.61
44	0.32	0.19	0.62	0.00	0. 00	0.08	0.98	0.00	0.00	0.00	1.24	0.00	0.97
45	0.29	0.18	0.67	0.00	0.00	0.22	0.92	0.00	0.00	0.00	1.40	0.00	1.13
46	0.36	0.18	0.71	0.00	0.00	0.32	0.62	0.00	0.00	0.00	1.44	0.00	1.15
47	0.43	0.25	0.82	0.00	0.00	0.43	0.81	0.00	0.00	0.00	1.30	0.00	1.11
48	0.49	0.32	0.93	0.00	0.00	0.44	0.56	0.00	0.00	0.00	1.39	0.00	1.24
49	0.56	0.40	1.04	0.00	0.00	0.35	0.59	0.00	0.00	0.00	1.57	0.00	1.47
50	0.56	0.47	1.15	0.00	0.08	0.12	0.59	0.00	0.00	0.00	1.43	0.00	1.46
Minimum	0.00	0.00	0.00	0.00	0.00	0.00	0.00	0.00	0.00	0.00	0.00	0.00	0.00
Maximum	0.64	0.47	1.15	0.36	0.60	1.27	1.45	0.01	0.58	0.43	1.57	0.95	1.47
Values averaged by 1 s													